

Naval Surface Warfare Center

Carderock Division

West Bethesda, MD 20817-5700

NSWCCD-65-TR-1998/11+CR June 1997

Survivability, Structures, and Materials Directorate

Technical Report

The Analysis and Design of Tee-Joints for Composite Hull Structures

by

Jack Bish and Keith T. Kedward

Department of Mechanical and Environmental Engineering

University of California at Santa Barbara

Santa Barbara, CA 93106-5070

19990115 041



Approved for public release; distribution is unlimited.



DEPARTMENT OF THE NAVY

NAVAL SURFACE WARFARE CENTER, CARDEROCK DIVISION
9500 MACARTHUR BOULEVARD
WEST BETHESDA MD 20817-5700

9078
Ser 65-76
12 Nov 98

From: Commander, Naval Surface Warfare Center, Carderock Division
To: Chief of Naval Research (ONR 332)


Subj: SEABORNE STRUCTURAL MATERIALS PROJECT

Ref: (a) Program Element 62234N for FY95-97.
(b) Contract No. N61533-95-C-0021.

Encl: (1) NSWCCD-65-TR-1998/11+CR, *The Analysis and Design of Tee-Joints for Composite Hull Structures*

1. Reference (a) directed the Naval Surface Warfare Center, Carderock Division (NSWCCD) to improve the Navy's ability to predict and prevent out-of-plane, matrix-dominated failure modes in composite structural details through an improved material properties database/design and validated design tools and rules of thumb. Funding for academic support was provided by reference (b). Enclosure (1) describes parametric design studies of multi-material, composite tee joints along with potential simplified design tools for this class of joints.

2. Comments or questions may be referred to Ms. Karin L. Gipple, Code 6552; telephone (301) 227-5041; e-mail, gipple@dt.navy.mil.


J. E. BEACH
By direction

Subj: SEABORNE STRUCTURAL MATERIALS PROJECT

Copy to:

COMNAVSEASYS COM WASHINGTON DC
[PMS450 (K. Harris) (5),
PMS500 (Camponeschi), SEA 03 (Will),
SEA 03P1 (Kadala),]

CNR ARLINGTON VA [ONR 332 (Kelly),
ONR 334, ONR 334 (Barsoum, Rajapakse)]

PEOSUB WASHINGTON DC

DTIC FORT BELVOIR VA

Dr. Keith T. Kedward
Department of Mechanical and Environmental
Engineering
University of California at Santa Barbara
Santa Barbara, CA 93106-5070

Dr. Jack Gillespie
Composite Manufacturing Science Lab
University of Delaware
Newark, DE 19716

NAVSURFWARCEN CARDEROCKDIV
BETHESDA MD [Codes 0119 (Messick), 3442 (TIC),
60 (w/o encl), 65, 65R (2), 65 (files, w/o encl), 651,
652, 653, 653 (Kihl), 654, 655, 6551 (Bartlett),
6551 (Potter), 6551 (Nguyen), 6552 (Bonanni),
6552 (Charette), 6552 (Cross), 6552 (Gipple) (10),
6552 (Hoyns), 6552 (Loup), 6552 (Palmer),
6552 (Rasmussen), 6552 (Telegadas), 6553 (Crane),
6553 (Coffin), 6553 (Williams)]

REPORT DOCUMENTATION PAGE

Form Approved
OMB No. 0704-0188

Public reporting burden for this collection of information is estimated to average 1 hour per response, including the time for reviewing instructions, searching existing data sources, gathering and maintaining the data needed, and completing and reviewing the collection of information. Send comments regarding this burden estimate or any other aspect of this collection of information, including suggestions for reducing this burden, to Washington Headquarters services, Directorate for Information Operations and Reports, 1215 Jefferson Davis Highway, Suite 1204, Arlington, VA 22202-4302, and to the Office of Management and Budget, Paperwork Reduction Project (0704-0188), Washington, DC 20503.

1. AGENCY USE ONLY (Leave blank)		2. REPORT DATE June 1997		3. REPORT TYPE AND DATES COVERED Final	
4. TITLE AND SUBTITLE The Analysis and Design of Tee-Joints for Composite Hull Structures				5. FUNDING NUMBERS PE 62234N Contract No. N61533-95-C-0021	
6. AUTHOR(S) Jack Bish and Keith T. Kedward (University of California at Santa Barbara)					
7. PERFORMING ORGANIZATION NAME(S) AND ADDRESS(ES) Naval Surface Warfare Center Carderock Division 9500 MacArthur Boulevard West Bethesda, MD 20817-5700				8. PERFORMING ORGANIZATION REPORT NUMBER NSWCCD-65-TR-1998/11+CR	
9. SPONSORING/MONITORING AGENCY NAME(S) AND ADDRESS(ES) Chief of Naval Research (ONR 332) Ballston Centre Tower One 800 North Quincy Street Arlington, VA 22217-5660				10. SPONSORING/MONITORING AGENCY REPORT NUMBER	
11. SUPPLEMENTARY NOTES					
12a. DISTRIBUTION/AVAILABILITY STATEMENT Approved for public release; distribution is unlimited.				12b. DISTRIBUTION CODE	
13. ABSTRACT (Maximum 200 words) The design of polymer matrix composite joints is strongly influenced by the presence of out-of-plane or through-the-thickness stresses. These stresses can be critical, since out-of-plane interlaminar tension and shear strengths, as well as moduli, are strongly influenced by the low strength and stiffness of the polymer matrix constituents, as well as the fiber matrix interface. To aid in the design of these structures, this research develops a methodology for predicting structural adequacy of composites in the presence of through-the-thickness loadings. Specifically, this work details guidelines for the design of resin fillet tee-joints for use in marine applications. A combination of finite element analyses and approximate analytical formulations are used to create these practically oriented design guidelines. A parametric study, using finite element models, was conducted examining the effects of changing various material and geometric variables on the stresses and failure modes of the tee-joint structure. The tee-joint structure was sectioned in order to facilitate the creation of analytical approximations to predict the failure stresses in the various sections. This approach offers the added benefit of developing insight that guides the designer towards the most appropriate joint configuration for a specific application.					
14. SUBJECT TERMS marine structures composite materials tee-joints finite element models				15. NUMBER OF PAGES 119	
				16. PRICE CODE	
17. SECURITY CLASSIFICATION OF REPORT UNCLASSIFIED	18. SECURITY CLASSIFICATION OF THIS PAGE UNCLASSIFIED	19. SECURITY CLASSIFICATION OF ABSTRACT UNCLASSIFIED	20. LIMITATION OF ABSTRACT SAR		

NSN 7540-01-280-5500

Standard Form 298 (Rev. 2-89)
Prescribed by ANSI Std. Z39-18
298-102

Table of Contents

1.0 Introduction.....	1
1.1 Tee-Joints.....	1
2.0 Literature Review.....	4
2.1 Tee-Joints.....	4
2.2 Curved Section.....	7
2.3 Double Lap Joints.....	9
2.4 Single Lap Joints.....	11
3.0 Material Properties.....	13
3.1 Fiber Orientation.....	13
3.2 Laminate Properties.....	14
3.3 Adhesive Properties.....	15
4.0 Tee-Joint.....	17
4.1 Gap Length.....	18
4.2 Resin Filler.....	23
4.3 Rm/t Ratio.....	24
4.4 Span Length.....	29
4.5 Baseplate Thickness.....	39
4.6 Horizontal Overlamine Length.....	41
4.7 Tapers.....	44
5.0 Tee-Joint Sections.....	50
5.1 Section A: Double Lap.....	50
5.2 Section B: Vertical Doubler.....	61
5.3 Section C: Curved Region.....	65
5.4 Section D: Interior Horizontal Overlamine.....	82
5.5 Section E: Exterior Horizontal Overlamine.....	89
6.0 Experimental Evaluation.....	93
7.0 Design Guidelines.....	94
8.0 Conclusions and Recommendations.....	106
9.0 References.....	109

Administrative Information

The Structures and Materials Department (Code 65) of the Survivability, Structures and Materials Directorate at the Naval Surface Warfare Center, Carderock Division (NSWCCD) was tasked to improve the Navy's ability to predict and prevent out-of-plane, matrix-dominated failure modes in composite structural details through an improved material properties database/design and validated design tools and rules of thumb. The work was funded as part of the FY95-97 Materials, Electronics, and Computer Technology Program (Program Element 62234N). The work described in this report was performed under subcontract to the University of Delaware (Contract No. N61533-95-C-0021) by the Department of Mechanical and Environmental Engineering, University of California at Santa Barbara.

1.0 Introduction

The University of California at Santa Barbara (UCSB) effort has focused on several issues in composite structural design and methodologies for predicting structural adequacies in the presence of through-the-thickness loadings. This program consists of extensive literature reviews of such subjects as tee-joints, adhesive joints and bolted joints. It also has focused on two joint configurations. First, tee-joints have been studied through a combined numerical parametric study and analytical approximations with the intention of creating a series of design guidelines. Second, bolted composite joint have been experimentally and numerically examined in order to create design guidelines and illustrate the differences caused by using different materials such as fiberglass, predominately used in the marine industry, and carbon fiber composites, predominately used in aerospace applications. This report details the tee-joint portion of the program. The following is a brief introduction to the various problems examined in this work.

1.1 Tee-Joints

Tee-joints are a form of connection where the two joined members are perpendicular to each other as illustrated in Figure 1.1. These joints occur in many areas of structural design, for instance in marine structures bulkhead to hull connections and at the intersection of interior and exterior bulkheads.

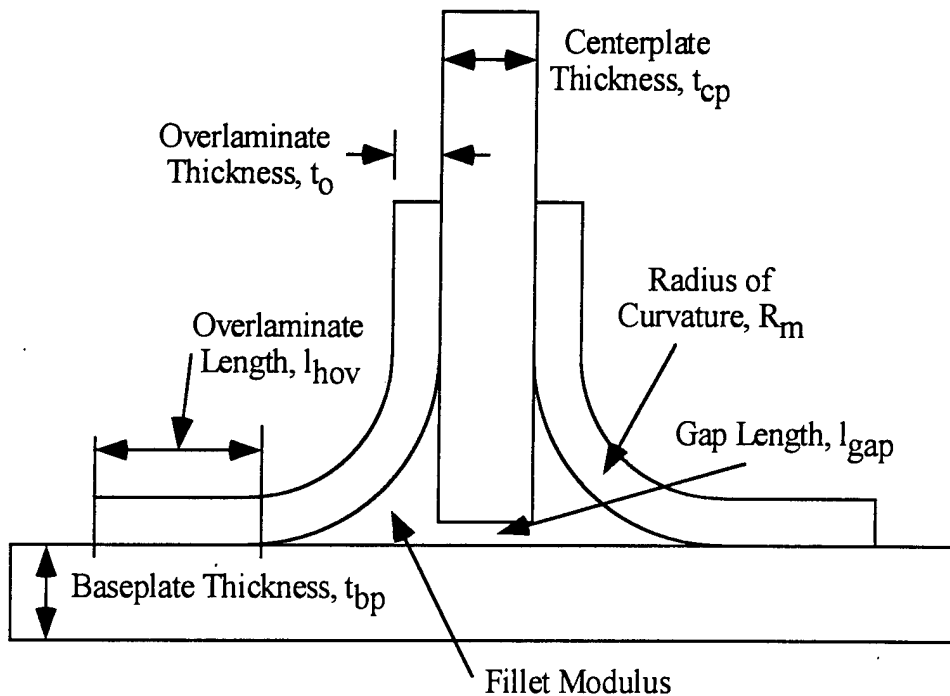


Figure 1.1: Tee-joint geometry with key design variables.

Previously reported research on this type of joint has mainly focused on finite element analysis of specific geometries with verification from limited experimental programs. An analytical approach appears to have been rarely attempted. Four reasons for this omission are given by Hawkins et al. [1993]:

- i) There is a lack of continuity of the reinforcing fibers across the joint due to the fact that typically the boundary angles can only be fabricated following the cure of the parent laminates.
- ii) The strength of the connections depends upon the relatively low tensile and shear strengths of the adhesive and in the through-the-thickness direction of the laminates,
- iii) There are no continuous fibers extending through successive plies to arrest cracks or delaminations from propagating rapidly through the various members.
- iv) The tendency of the boundary angles to peel and delaminate under load emphasizes the irregularities and imperfections of the laminate, compared with ductile characteristics of homogenous metallic materials.

Although, these factors illustrate the difficulty in analytically modeling the entire joint as a complete structure, insight into the joint structure can be gained by examining the contributing pieces of the structure.

The tee-joint configuration can be broken down into various sections as shown in Figure 1.2. Each of these individual sections can then be examined to gain an insight into the behavior of the complete structure.

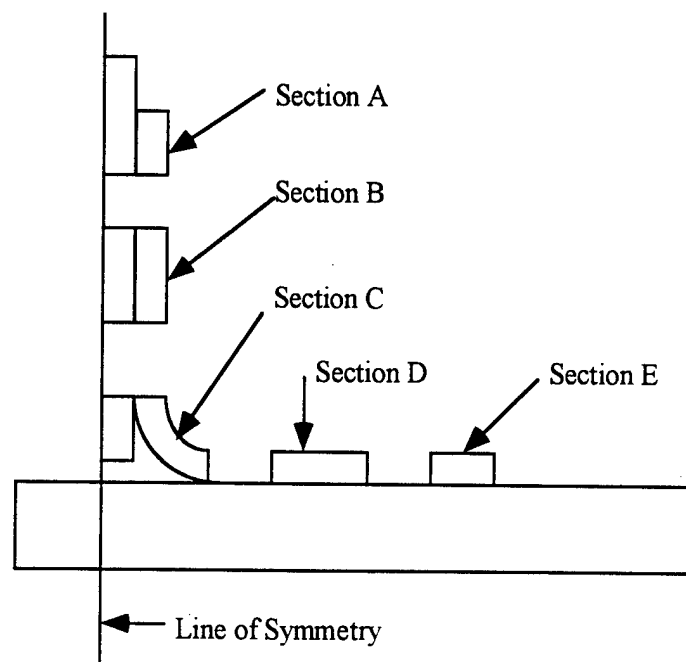


Figure 1.2: An illustration of the sectioned tee-joint. The section titles are as follows: Section A double lap, Section B vertical doubler, Section C curved region, Section D interior horizontal overlaminate and Section E exterior horizontal overlaminate.

The characterization of each section will begin with classical approaches, such as closed form elasticity solutions, from which simplified expressions will be generated. Verification of these simplified expressions will be conducted through the use of finite element analysis.

Finite element analysis will also be used to determine the relative importance of each section of the tee-joint as a function of various design parameters and for size determinations.

The parametric, finite element study will examine the effects of several geometric and material variables on the tee-joint structure and the subsequent failure modes. Typically in this kind of structure with a complex geometry, failure occurs in the out-of-plane direction due to the relatively low through-the-thickness strength of bi-directionally reinforced polymer composite laminates in this material direction. These failure modes are seen in various areas such as curved sections, and the termination points of doubler regions comprising a typical tee-joint structure. The variables examined are gap length, resin modulus, R_m/t ratio, span length, baseplate thickness, overlamine length and the inclusion of tapers. The geometric parameters are explained in detail in the following sections.

The objective of this study is to produce a set of design guidelines which will give the designer insight into the failure modes of a tee-joint based upon several geometric and material properties. This study does not preclude the use of finite element studies, but will allow the designer to make intelligent design choices before using computer modeling. Thus, the number of design iterations and amount of computer time necessary for the design of composite tee-joints may be reduced.

2.0 Literature Review

2.1 Tee-Joints

Currently, tee-joints used in marine construction are designed by either extensive finite element analysis or broad guidelines that do not lend themselves to optimizing the joint or produce significant insight into the rationale for their various design rules. To improve the design process, the tee-joint is sectioned such that geometries and loading conditions seen in other problems are constructed, as illustrated in Figure 1.2. Strength of material approaches are then used to derive simple expressions which closely determine the critical stresses in the various sections of the tee-joint. These individual sections are then analyzed with finite element methods to determine the validity of the derived expressions and to determine the applicability in the complete tee-joint structure. The included literature review begins by examining previous work on tee-joints and also includes reviews of literature relevant to the analysis of the various sections.

A series of papers examining the behavior of composite tee-joints has been written by R. A. Sheno and others from the University of Southampton, Department of Ship Science. The first in the series, Sheno and Violette [1990], details an experimental test series conducted on fiberglass tee-joints. The test series examines five different geometries under compressive loading applied at the top of the centerplate. The geometries include three different fillet radii, a foam pad and a triangular foam insert. The foam pad and triangular foam insert are placed at the base of the joint and replace the curved beam regions by straight sections. Unfortunately, the tests described in this paper, Sheno and Violette [1990], use only one sample per configuration which calls into question the validity of the work. In fact, in two of the tests, a lateral displacement was observed which caused the crosshead of the test machine to pivot, resulting in an applied moment. But, the following conclusions are reached based upon the results of the conducted tests. First, the finite element results closely approximate the experimental results. Also, an analytical tool, based upon beam theory and implemented as a comprehensive group of computer algorithms, closely approximates the behavior of the joints. The described analytical methodology is not given, but the comment is made that the model needs to be improved by reducing the number of approximations and increasing the simplicity so that the model can be used in practical engineering situations.

The next journal article in this series, Sheno and Hawkins [1992], details an experimental investigation into tee-joints using a baseline model designed according to current naval design compared to several specimens in which the geometry is altered to determine the effects on tee-joint strength and stiffness. The article begins with a discussion of current naval practices focusing on the lack of design requirements or modeling procedures. The paper continues with a discussion on the inability of traditional analytical methods to model this system. This inability is caused by several factors including the discontinuous nature of the lay-up within the boundary angles (overlaminates), the presence of imperfections caused during manufacture and the variations in material properties from one section to another. To alleviate the problems caused by the lack of rigorous design guidelines, the authors propose to carry out a set of

experiments to identify the variables which most critically influence tee-joint design. The variables which are geometric in nature are shown in Figure 2.1.1.

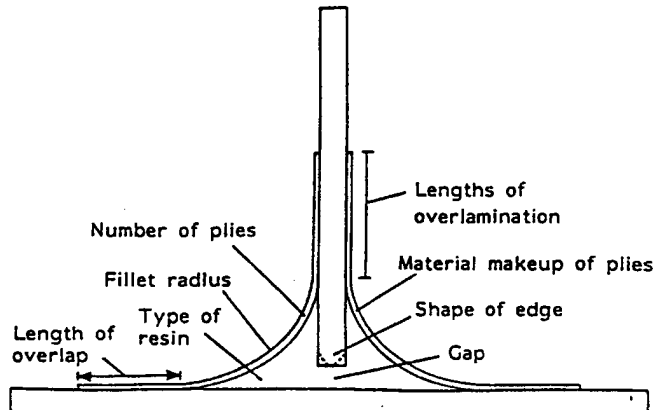


Figure 2.1.1: Tee joint design variables, Shenoi and Hawkins [1992].

The major non-geometric parameter examined was the use of compliant matrix materials to help alleviate the peel stress magnitude at the resin overlamine interface.

As stated earlier, the test series presented in the paper, Shenoi and Hawkins [1992], consists of seven joint configurations used to determine the effects of varying geometry and resins. The first two specimens are baseline tests constructed according to current naval standards. One of these samples used polyester resin while the other used a more compliant urethane-acrylate resin mix for the resin fillet region. The other five configurations were designed to test the effects of altering the fillet radius, the gap thickness, and tapering the edge of the web. Four samples of each configuration were tested with a load applied at 45° to the horizontal at the top of the centerplate. The following observations were made about the effects of altering the various parameters:

- i) Increasing the gap between the center and baseplates allowed greater deflections for a given load (100%) and a greater load potential (50%).
- ii) Tapering the edge of the center plate or web reduced the stiffness by a small amount (10%) while increasing the failure load (>50%).
- iii) The addition of an overlamine with no change in the fillet radius increased stiffness (50%) and failure load (100%).
- iv) Increasing the radius of the fillet resulted in a higher failure load (150%), by decreasing the magnitude of the out-of-plane stress in the curved region, but did not change the stiffness of the specimen.

The numbers in parentheses are the percentage changes between tests specimens where the variable of interest was altered as given in the article. These numbers are only a relative change dependent upon the amount each variable was altered between the configurations.

A finite element analysis examined the configurations used in the experimental phase of the study. In this study, the tee-joint was modeled using a coarse mesh with two elements across the resin fillet and the thickness of the boundary elements and one element

in the center and baseplates. An example of the mesh and the resulting stress contours is shown in Figure 2.1.2. It can be seen that this mesh is coarse and omits important factors including the bond line between the overlaminates and the center and baseplates. The results of the numerical study were not successful in modeling the loads and deflection of the actual tee-joints. This fact was assumed to be caused by the inadequate and incomplete nature of the material data. Corrections to these values result in accurate finite element predictions as compared to the experimental evaluation.

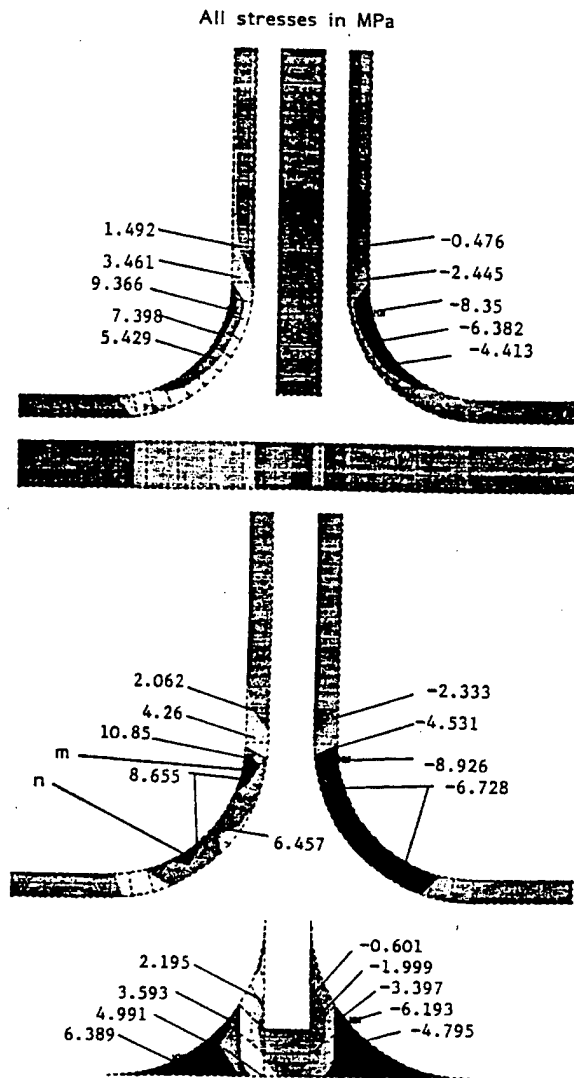


Figure 2.1.2: Sample stress contour plot from Shenoi and Hawkins [1992].

Using the results of the finite element analysis in conjunction with the results of the experimental series, a few more configurations were examined. From these data, a study of strength and stiffness efficiency was conducted. The desired efficiency was defined as the ability of a design configuration to withstand as large a load and as high a deflection with as low internal stresses as possible. The authors found that the most efficient tee-

joint design is one using a large radius flexible resin fillet with an overlamine of minimal thickness, just sufficient to withstand the membrane tensile loads.

The third paper in this series is Hawkins et al. [1993]. This paper is similar to and follows the previous paper Sheno et al. [1992]. The major difference is in the introduction and discussion of the topic. Further works in this topic by these authors include an examination of the fatigue characteristics of FRP tee-joints, Sheno et al. [1995], and a treatise on the aspects of out-of-plane joints in marine structures, Junhou and Sheno [1996] which includes work by Sheno and others on tee-joints.

The effects of fatigue on FRP tee-joints is examined in Sheno et al. [1995]. The fatigue test series focused on two joint types previously examined in other papers by the authors. These joints were chosen because they represented the two extremes of joint behavior, one joint was similar to those used in standards, such as Lloyd's standard for commercial applications, with a thick overlamine while the other was composed of a thin overlamine over a large radius epoxy fillet as introduced in Sheno and Hawkins [1992]. The tests were carried out with a load at an angle of 45° to the horizontal, as this load mode was assumed to most closely simulate the combined moments and forces experienced by tee-joints in service. The failure mechanisms under the fatigue loading conditions were found to be similar to those found in the static tests. Failure was seen to occur by a delamination in the boundary angle and a debond of the fillet from the boundary angle which also led to a crack in the fillet. This failure mode was consistent with stress patterns found with finite element analysis predictions.

2.2 Curved Section

The curved section of the tee-joint structure, Section C, is a critical portion of the design due to the out-of-plane stresses that are applied to the overlamine in this region. The stress distribution in curved regions has been looked at by many authors. Isotropic elasticity solutions to this problem are given in a text by Timoshenko and Goodier [1970]. Further complexities are added in a text by Lekhnitskii [1981] which details the solution to curved sections subjected to moments and point loads at the ends for cylindrically orthotropic materials. The following section is a brief literature review discussing current articles on curved composite shells.

Ko [1988] presents a derivation starting with the exact expressions for anisotropic curved beams subjected to end forces and end moments as described by Lekhnitskii [1981] and resulting in simplified relations for the delamination stress and its radial location. These derivations are accomplished by assuming that the curved bars are thin. This assumption results in two simple relations, for the two loading conditions mentioned earlier, which are not dependent upon the anisotropy of the material being examined.

In an article by Kedward et al. [1989], the importance of the design of curved regions in composite structures is discussed. The paper begins with examples from the aerospace community where designs either failed or had to be redesigned due to the development of out-of-plane stresses in curved regions. Further discussion includes the

presentation of simplified expressions for the radial stresses in curved bars, as derived by Ko [1988], and expressions for hygrothermal loading conditions. A finite element analysis is also included which verifies these simplified relations.

Four other papers are also reviewed, Lu et al. [1994], McRobbie et al. [1995] Cui et al. [1995] and Cui et al. [1996] which examine the problem of out-of-plane stresses developing in curved sections. These papers move away from the idea of simplified relations as used in this study, but illustrate current work in this area of interest.

Lu et al. [1994] examines a curved beam, or C-specimen, with cylindrical material orthotropy under pure bending in the presence of a crack. In most practical situations using polymer composite materials, the curved bar would be assumed to have failed with the presence of a crack. The crack would be caused by the initial delamination of the bar because of the radial stress developed in this region. The paper discusses the effects of the crack and characterizes the analytical solution with regards to a few material and geometric parameters.

In McRobbie et al. [1995], a similar problem is investigated with the significant difference being the use of single and double skinned materials. These samples consist of filament wound shells around a resin impregnated core. As in the previous articles, this article begins with an analytical discussion of the problem. But, in this paper, the authors report that the use of finite element methods are avoided due to relative magnitudes of the through-the-thickness stresses and the in-plane stresses. This difference in magnitude would require excessive mesh refinement due to the least-squares approximation of the equilibrium equations present in finite element programs, according to McRobbie et al. [1995]. The analytical methods are verified by a series of tests.

The effects of combined stress on the through-the-thickness failure of carbon epoxy composites is examined in Cui et al. [1995]. The creation of the combined stress state is accomplished by using waisted C-specimens. These specimens result in a test section where the specimen is under tension or compression combined with interlaminar shear and tension. As before, the article begins with an analytical examination of the problem. Next, the paper describes a series of tests conducted to determine the effects of the combined stress state on the delamination strength of the curved region. From these tests, the following conclusions are drawn. First, the tangential stress has a significant effect on the delamination strength under the through-thickness tension. Also, as the tangential stress changes from tension to compression, the delamination strength drops significantly. This drop is associated with fiber buckling under compressive loads. Finally, the study found that the interlaminar shear affects the delamination strength when the tangential stress is tensile and a shear failure is dominant, but this property has little effect when the tangential stress is compressive and a cleavage failure occurs.

Another paper, Cui et al. [1996], details the use of another form of curved beam specimen to find the interlaminar tensile strength (ILTS) of glass/polyester laminates. This type of specimen consists of a four point beam test where the beam has a curved section

between the interior rollers, see Figure 2.2.1. For this test specimen, there are three different possible failure modes. First, the delamination failure caused by the through-the-thickness tensile stress in the curved region. This is the desired failure mode. Second, surface fiber fracture caused by the circumferential stress in the curved region. The third failure mode is the interlaminar shear crack within the straight portion of the curved four point beam test specimen. Cui et al. [1996] detail a set of equations dependent upon the specimen's material properties which is used to construct a geometry which guarantees tension induced delamination in the curved portion of the specimen. An experimental test series confirmed the validity of this specimen and the test results were comparable to other test methods for finding a laminate's ILTS. The authors conclude that the main advantage of this type of specimen is its simplicity in preparation and test set-up.

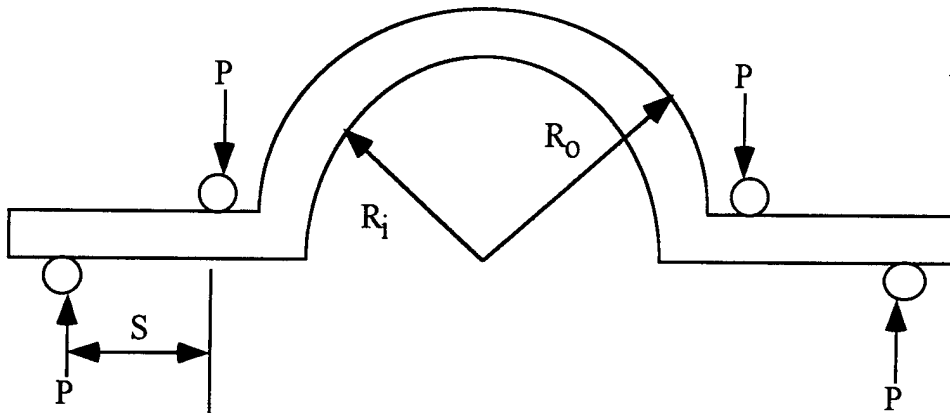


Figure 2.2.1: Four-point curved beam specimen as examined in Cui et al. [1996].

2.3 Double Lap Joints

Lap joints are a common form of joint where the transferred load is parallel to the direction of the joint, see Figure 2.4. There are various forms of lap joints, two of which are shown in the following figure. The double lap joint corresponds to Section A of the divided tee-joint structure illustrated in Figure 1.2. In this case, the geometry of the tee-joint section characterizes the beginning portion of the double lap joint where the peak peel and shear values occur and then decrease to a lower bound. In the double lap joint, the stress values would begin to increase after this point as the load was again transferred through shear mechanisms to the inner adherend. A brief literature review on this type of joint is included below and this portion of the tee-joint structure is examined in more detail in Section 5.1.

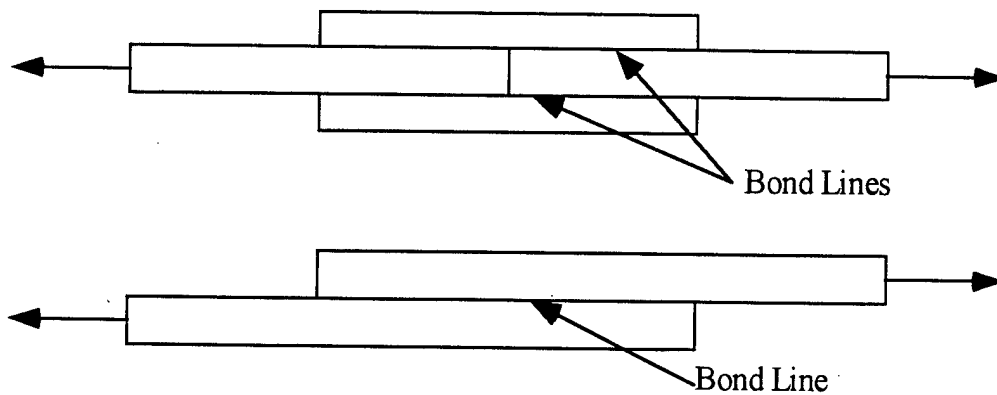


Figure 2.4: Double and single lap joints.

The stress profiles and critical stresses in double lap joints have been examined by many authors in various journal articles. A brief review of this literature is included here focusing on two papers used in the theoretical section of this work. The first work, Hart-Smith [1974], details a derivation in which the adhesive undergoes purely plastic shear deformation near the termination of the outer adherends. Various other parameters are discussed in this work, including a correction factor to account for the increased flexibility of polymer matrix composite adherends. But use of this correction factor, a lower effective peel modulus based upon material and geometric parameters, does not result in more accurate stress profiles. The presented derivation results in a simple expression for the peel stress profile and the maximum peel stress in double lap joints. This expression is independent of the applied load and assumes the adhesive is undergoing perfectly plastic shear deformation at the termination of the outer adherends. This is usually the case of interest, since, in most configurations the adhesive deforms plastically prior to failure. The amount or length of plastic shear deformation necessary for this derivation to be accurate is not mentioned in this work. The author concludes that the tip thickness is the dominant effect of the adherends on the stress profile and the peak peel stress.

Oplinger¹ details a finite difference formulation of the double lap joint problem which is used in the creation of a computer program for the calculation of peel and shear stresses in double lap joints of various configurations. The derivation begins by examining the shear stress and shear stress gradient between the adherend and adhesive. This derived expression is used in conjunction with the equilibrium equations for the system and a beam on elastic foundation model which includes the effects of bond shear stress. The resulting equation is differenced and used in the included computer program. The reference details the abilities of the program and includes examples illustrating the output for various joint types and material properties. Allowance is made for non-linear adhesives by using an equivalent bi-linear curve as an approximation for the continuous stress-strain curve.

¹ Oplinger, D.W., "Program <TJOINTNL> to Obtain Finite Difference Solutions for Bond Stresses in Double Lap/Strap Joints," Private Communication, May, 1995.

2.4 Single Lap Joints

The single lap joint illustrated in Figure 2.4 corresponds to Section E of the divided tee-joint illustrated in Figure 1.2. This correspondence is more pronounced when the tee-joint structure is constrained by rollers placed a set distance from the termination of the horizontal overlaminates as compared to the case where the bottom of the baseplate is held fixed, see Section 4. In the case with rollers, there can be considerable flexure in the baseplate of the tee-joint. This effect is also seen in the adherends of a single lap joint. In other cases where the tee-joint structure is constrained along the bottom of the baseplate, this effect is lessened. A brief literature review on this type of joint is included below and this portion of the tee-joint structure is examined in more detail in Section 5.5.

Many authors have examined the stresses in adhesively bonded single lap joints. In most cases, the presented work builds upon the seminal work of Goland and Reissner [1944]. This paper examines the problem in two parts, the determination of the loads at the ends of the joint and the determination of the stresses in the joint due to the applied loads. Solutions are obtained for the limiting cases where either the cement layer is so thin that its effects on the joint flexibility can be neglected or where the joint flexibility is mainly due to the adhesive layer. For these cases, expressions are obtained for the shear and peel stresses in the adhesive layer. The derivations presented in this work have been examined in detail in other literature, Hart-Smith [1973], Tsai and Morton [1994a] etc., with the intent of improving the methods for analyzing this type of joint. Some of these articles are reviewed herein.

Hart-Smith [1973] presents analyses of the influence of various factors on the strength of adhesive bonded single lap joints. This study builds on the earlier work by Goland and Reissner [1944] through the addition of various factors, including adhesive plasticity, stiffness imbalance between the adherends and the effects of composite adherends. The analyses predict three different failure modes. The first is that of failure of the adherend just outside the joint due to the in-plane stresses resulting from the direct load stresses and the bending stresses from the eccentricity in the load path. The second failure mode is that of the adhesive layer in shear. This mode is rare in structural applications due to the perfectly plastic response of the adhesive layer. This observation is demonstrated in this work where the elastic-plastic response of the adhesive is added to the analytical model. The third failure mode is due to adhesive peel stress. This mode can be seen as failure of the bond layer or failure of the adherend due to the low interlaminar tensile strength of many polymer matrix composite systems. The effects of adherend imbalance is also discussed and joint efficiency is examined. The author presents various models for finding the critical stresses in the joint, depending upon the various parameters used and gives insights into the construction of more efficient structural single lap joints.

Oplinger [1994] presents an extensive study of this problem detailing the previous works by Goland and Reissner [1944], Hart-Smith [1973] and others. This article continues the modification of the earlier models, but neglects various effects which can be of interest, depending upon the types of material used. This analysis does not take into account the adherend transverse shear deformation which can have a sizable effect on the

peel and shear stresses. As discussed in Section 5.1 and mentioned in the literature, due to the anisotropic behavior of polymeric composite materials the adherend transverse shear deformation can be large in this type of joint and others. A simple correction is suggested by the author which reduces the bond shear modulus and results in good agreement with finite element models. The method presented in this work is a consistent model which takes into account various factors including bond shear strains, but neglects others such as the bond thickness deformation. The model is an analytically simple beam model, similar to that presented by Goland and Reissner [1944], which incorporates classical beams for the adherends and a thickness-wise uniform distribution of stresses in the bond layer. The predictions generated by the Oplinger model have been shown to compare favorably to finite element models by Tsai and Morton [1994b].

3.0 Material Properties

The material systems examined in this program are typical of those currently considered for marine structures. Although the applicability of the model is to a large range of materials, this research will use various E-glass/vinylester laminates, most specifically in the form of a $[0^\circ / 90^\circ]$ fiber orientation, and vinylester fillers. This choice of material differs from that adopted for investigation in most of the existing literature on the design of composite joints where the focus is typically on aerospace applications involving carbon fiber/epoxy laminates. This difference is due to the specific requirements associated with the design of marine structures. Unlike aerospace engineering, where the prime consideration is performance and the driving consideration is a high specific stiffness and/or strength, marine hull structures tend to be driven by durability and economic considerations.

3.1 Fiber Orientation

In the tee-joint structure, the material properties depend upon the fiber orientations in the various sections. In the baseplate and horizontal overlaminates, when using a $[0^\circ / 90^\circ]$ E-glass laminate, the fibers are aligned along the length and width of the tee-joint, as illustrated in Figure 3.1.1. This results in the lower strength material properties being aligned perpendicular to the pull off load applied in the following finite element and simplified analytical models. Due to this weakness, the peel stress generated at the termination of the horizontal overlaminate becomes a concern to the designer. In the centerplate and vertical overlaminates, the fibers are aligned along the height and width of the tee-joint. This alignment results in an area of concern at the termination of the vertical overlaminate.

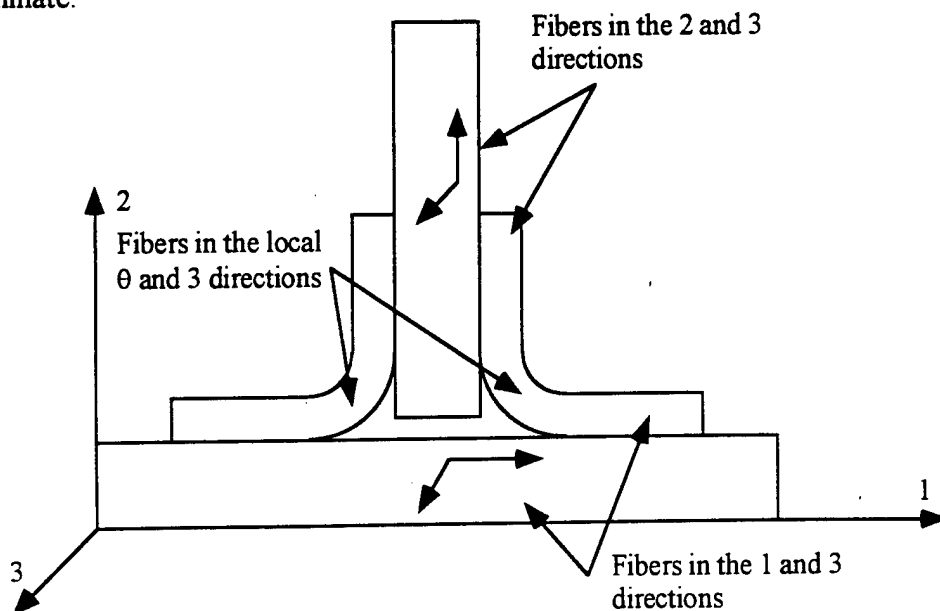


Figure 3.1.1: Fiber orientations in the various tee-joint sections.

In the curved region of the tee-joint structure, the fibers are aligned in the circumferential direction along the bend and through the width of the structure. This configuration results in an out-of-plane, radial stress generated in the curved region which is another potential failure zone.

These weaknesses are generic to most polymeric composite systems where the out-of-plane strength is significantly lower than the in-plane values. If the tee-joint design used other PMC's, such as carbon graphite/epoxy or E-glass/vinylester laminates, then the fibers would lay in the same planes as illustrated in the previous figure, as long as the laminate orientation was the same. There are methods to increase the out-of-plane strengths of these composite systems, such as textile composites which include a three dimensional lay-up and/or through thickness reinforcement, but these are predominantly used in the aerospace industry and are not of direct relevance to the current research.

3.2 Laminate Properties

The exact lamina properties are not readily available for this material, but the laminate properties and stacking sequence have been documented in other work, Ellis [1996], Wisnom [1996]. In Ellis [1996], the material properties are representative of an E-glass/resin system with a 60% fiber volume with a $[0^\circ / 90^\circ]_{12}$ stacking sequence. This sequence is a laminate composed of twelve layers of 0° , and twelve layers of 90° in a symmetric lay-up. This type of laminate can also be created by using a $0^\circ / 90^\circ$ weave cloth without any ply rotation. The material properties for this laminate are given in Table 3.1 along with the material properties for a uni-directional E-glass laminate. A similar material is examined by Wisnom [1996] and the properties are included for a comparison. Other materials are used in this study and the material properties are noted in the individual sections, as necessary, but the $[0^\circ/90^\circ]$ E-glass laminate given in Ellis [1996] is used predominately throughout this study.

Table 3.1: Material properties for use in various predictions, Mallick [1993], Ellis [1996], and Wisnom [1996].

Material Property	Uni-Directional E-Glass	$0^\circ/90^\circ$ E-Glass Laminate (Ellis)	$0^\circ/90^\circ$ Glass Laminate (Wisnom)
E_1	39 GPa	20.7 GPa	29.9 GPa
E_2	4.8 GPa	20.7 GPa	29.9 GPa
E_3	4.8 GPa	10.35 GPa	15.4 GPa
ν_{12}	.3	.2	.156
ν_{23}	.2	.3	.375
ν_{13}	.2	.3	.375
G_{12}	4.8 GPa	5.52 GPa	4.34 GPa
G_{23}	3 GPa	4.14 GPa	4.83 GPa
G_{13}	3 GPa	4.14 GPa	4.83 GPa

The material properties used by Wisnom [1996] are given as a comparison to the values given in Ellis [1996]. In the Wisnom [1996] study, there is no specification for the type of fiber used and the properties are given for a glass/epoxy composite. There are two types of glass fibers commonly used in structural applications, E-glass and S-glass. Of the two fiber types, E-glass is more widely used while the more expensive S-glass is only used where strength and stiffness requirements warrant the extra cost. A comparison of E-glass and S-glass properties is given in Table 3.2 along with material properties for a graphite/epoxy system. The higher elastic modulus values seen in Table 3.1 from the Wisnom study could be caused by the use of S-glass, instead of E-glass, as the fiber type is not documented.

Table 3.2: Comparison of E-glass, S-glass and T-300 carbon fiber properties, Mallick [1993].

Material	Tensile Modulus	Tensile Strength	Poisson's Ratio	Strain to Failure	Cost (\$/kg)
E-glass	72.4 GPa	3.45 GPa	.2	4.8 %	1.75 - 2.7
S-glass	86.8 GPa	4.30 GPa	.22	5.0 %	6.6 - 11
T-300 carbon	231 GPa	3.65 GPa	.2	1.4	-

Wisnom [1996] also states that no data was available for the through thickness Poisson's ratio, so an estimated value is used. This estimated value is also used to find the through thickness shear modulus. The lack of specific material data is often seen in the literature and is a definite handicap when modeling this and other composite systems.

3.3 Adhesive and Filler Properties

There are a wide range of resin materials which can be used in the construction of the fillet area of tee-joints. A few of these resins are epoxies, polyesters, vinylesters and urethane-acrylate. The material choice is based upon a variety of physical properties, such as environmental degradation, creep, fatigue life, and impact and shock loads. Shenoi and Hawkins [1992] uses both polyesters and a mix of polyesters and urethane-acrylate resin for a filler, while stating that, due to the brittle nature of polyester resin systems, a stress concentrating effect can occur at the interface with the reinforcing fibers. Vinylesters and epoxies both have larger ultimate elongations than the more brittle polyester resins, alleviating this concern. Table 3.3 illustrates a range of filler materials and various material properties. Similar values are presented in Mallick [1993].

Currently, the material of choice for marine structures is a vinylester resin system. This is due to various parameters, as briefly mentioned above, and explained here in more detail.

- i) Environmental degradation - exposure to wet environments is inherent in any marine structure.

- ii) Creep - important for decks and platforms where equipment loads are present.
- iii) Fatigue life - wave-structure interaction and rotating machinery are two possible fatigue loads in marine structures.
- iv) Impact and shock loads - caused by underwater explosions and hitting floating obstacles at high speeds.

Table 3.3: Material properties for various resin systems.

Resin	Tensile Modulus	Tensile Strength	Strain to Failure	Cost (\$/kg)
Polyesters				
Atlas P 2020	4.07 GPa	48.3 MPa	0.91	1.45
Atlas 80-6044	6.28 GPa	77.3 MPa	0.86	1.47
CoRezyn 9595	3.93 GPa	71.1 MPa	2.0	1.87
Vinylester				
Derakane 411-45	3.38 GPa	76-83 MPa	5-6	3.17
Epoxy				
Epon 828	7-3.6 GPa	48.-90 MPa	2-9	22-33

In the following sections, other materials are examined in a parametric study, but the baseline tee-joint is constructed with properties taken from a typical vinylester resin.

4.0 Tee-Joint

The tee-joint structure will be studied as an assemblage composed of various sections which are generic in structural design problems. But, before the individual sections are examined, the complete tee-joint structure will be investigated by altering various design variables as seen in Figure 1.1. The design variables examined in this study include:

- i) The gap between the center and baseplates varies from a butt-joint with a gap equivalent to a bond line to a gap of the same order as the radius of the curved overlamine.
- ii) The R_m/t ratio values vary over the range of practical values and include the "optimum" design suggested by Sheno and Hawkins [1992].
- iii) The elastic modulus, E_a , of the filler material extends from low modulus epoxies to vinylesters and polyesters.
- iv) The boundary conditions vary from a baseplate with a fixed bottom layer to rollers a set distance from the end of the overlaminates.
- v) The length of the horizontal overlaminates varies from 25.4 to 50.8 mm.
- vi) The thickness of the baseplate varies from being equivalent to the thickness of the centerplate to 4 times that value.
- vii) The span length between the rollers which constrain the tee-joint varies from 0 to 101.6 mm.

Table 4.1 also presents the altered variables and the range of values considered for each variable.

Table 4.1: Geometric and material variables examined in Section 4 and the range of values used.

Variable	Range of Values
Gap Length (presented as a ratio of the mean radius of the curved region to the gap length, R_m/L_{gap})	.127 mm - a bond line to 20 mm
Overlamine Thickness	1.5875 mm to 12.7 mm
Filler Modulus	690 MPa - low modulus epoxy to 6792 MPa - high modulus polyester
Span Length (measured from the termination of the horizontal overlamine to the constraining roller)	0 mm to 101.6 mm
Length of Horizontal Overlamine	25.4 mm to 50.8 mm
Baseplate Thickness	12.7 mm to 50.8 mm
Tapers	15° to 90° (no taper)

This investigation will examine the stress distribution in the tee-joint as a function of an individual design variable. These stress profiles will allow the designer to evaluate

the critical section depending upon how the tee-joint is loaded and the various geometric parameters. This section will also help illustrate where the critical sections of the tee-joint structure are located.

Finite element methods are used to determine the stress profiles. The model is comprised of 8-noded, plane strain elements. An illustration of this model is given in Figure 4.0.1. This model is also used in the examination of the individual sections of the divided tee-joint. All the models examined in this study are subjected to vertical, symmetric pull-off loads parallel to the centerplate of the tee-joint and applied along the mid-plane of the centerplate. The boundary conditions change from a baseplate with a fixed base in the initial sections to rollers located a set distance from the termination of the horizontal overlaminates in the subsequent sections. The boundary conditions are explained in each individual section.

4.1 Gap Length

The first design variable to be examined is the gap length between the center and base plates, see Figure 1.1. A tee-joint without overlaminates and with a gap length equal to the bond line thickness is called a butt-joint, as shown in Figure 4.1.1. The butt-joint failure is caused by attempting to transfer the load from one member to another by involving the weakest through-thickness material direction. In some cases, butt joints are also designed to have overlaminates to help disperse the load from directly under the centerplate by transferring load by shear mechanisms, see Figure 4.1.1. This method also results in failure due to the load distribution through the stiffest load path available, the gap region between the base and centerplates. Delamination still occurs in the baseplate and the additional load paths created by the overlaminates are not usually used effectively.

To transfer the stress more efficiently, the stiffness of the butt-joint's center - baseplate connection must be decreased to allow load transfer throughout the entire structure. One means of accomplishing this goal is to use a larger gap between the joined members. To a first order the condition can be approximated by simply modeling the stiffness of this region in the same fashion as a tensile member where

$$k = \frac{E_a A}{L_{gap}} \quad (1)$$

This neglects the other load paths created by the addition of overlaminates, but gives an estimation of the effects of changing the gap length. In this equation, E_a is the modulus of the adhesive filler, A is the cross sectional area of the bond line and L_{gap} is the gap length.

ABAQUS

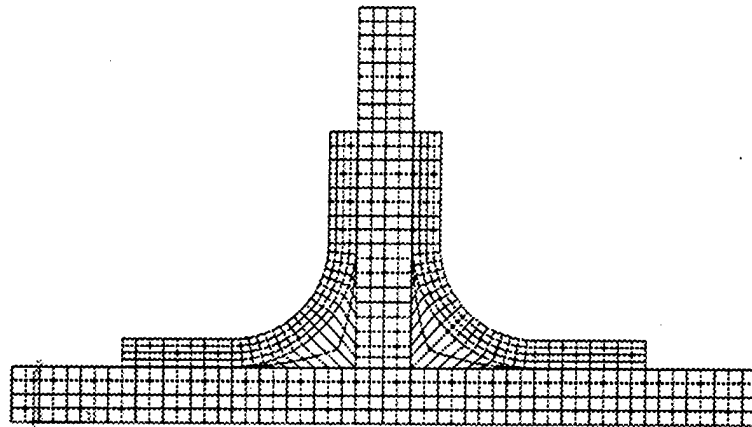


Figure 4.0.1: Example of the finite element model mesh used in examining the load path in the tee-joint structure.

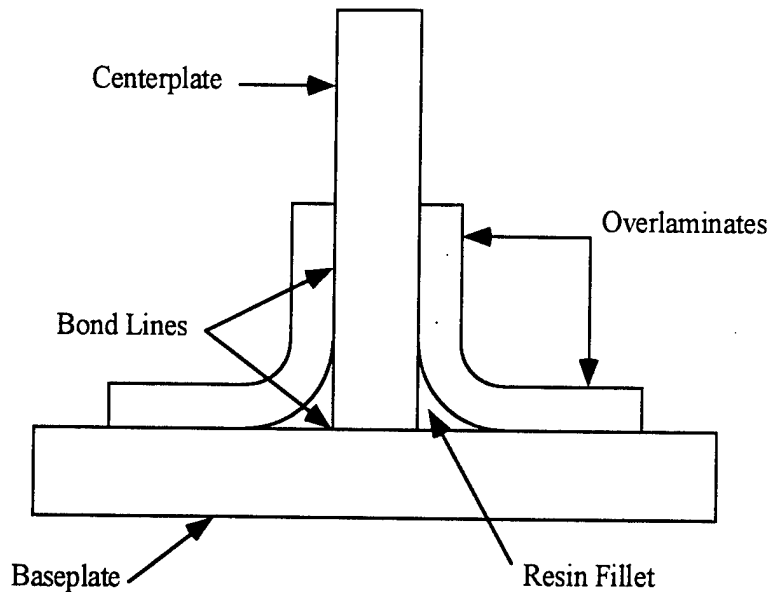


Figure 4.1.1: A typical butt joint with overlaminates. The bond lines are on the order of .127 mm or .005 in.

To study the effects of increasing the gap length, finite element models with a range of gap lengths were created while the remainder of the model was held constant. These models consist of a tee-joint composed of the $0^\circ / 90^\circ$ laminate with the properties shown in Table 3.1. The geometry is held constant, except for the gap length, with a R_m/t ratio of 4, a baseplate that is held fixed along the bottom and the structure is subjected to a vertical pull off load parallel to the center plate, as noted in the previous section. The filler in these models is a vinylester with a modulus of approximately 3.4 GPa. This generic tee-joint which is used as a control throughout the variations examined in this section is illustrated in Figure 4.1.2.

The stresses presented in subsequent graphs are normalized by the far field stress. This reference stress, σ_0 , is measured in the top portion of the centerplate above the vertical overlaminates and below the load application point such that the stress is uniform throughout the member. The load is applied at the middle of the centerplate and the model is constrained such that the nodes along the top of the centerplate have the same vertical displacement. Unless otherwise mentioned, the generic joint and the others examined below all have a load of 100 N acting over an area of 12.7 mm for a reference stress, σ_0 , of 7.874 N/mm per unit depth.

To aid in the visualization of the joint and stress profiles presented in the previous and subsequent graphs, an illustration is included which shows the scale of the tee-joint along the baseplate, Figure 4.1.3. In the graphs of the stress profiles, the ends of the horizontal overlaminates are at about .15 and .85, the curved regions end at about .3 and .7 and the centerplate is in the region from .46 to .54.

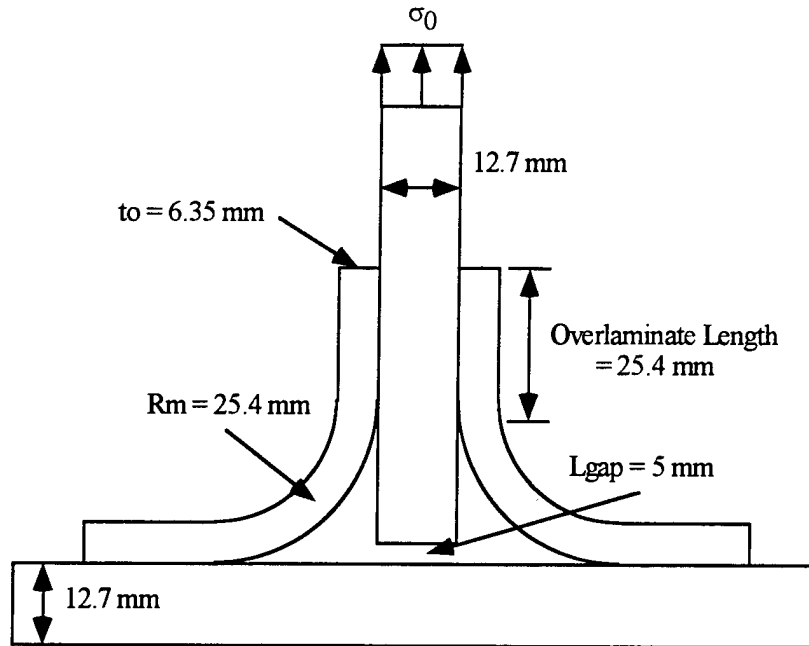


Figure 4.1.2: Generic tee-joint with the baseline dimensions used throughout section 4.0.

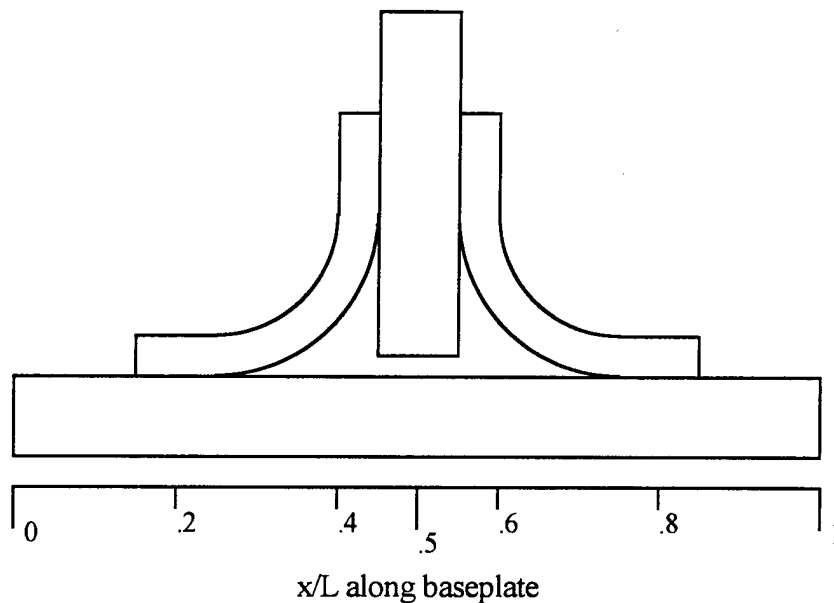


Figure 4.1.3: Illustration of the relative position of various geometric features as measured along the baseplate as a function of x/L .

A variety of gap lengths are examined. To facilitate the visualization of the size of the gap length as compared to the size of the entire structure, the graph is presented using a ratio, R_m/L_{gap} , to show the effects of increasing the gap length. R_m is the mean radius of the curved region of the overlaminate and L_{gap} is the gap length. Three of these curves are presented in Figure 4.1.4. In this study, the mean radius is held constant while the gap length is altered to achieve the various R_m/L_{gap} ratios presented on the following graph.

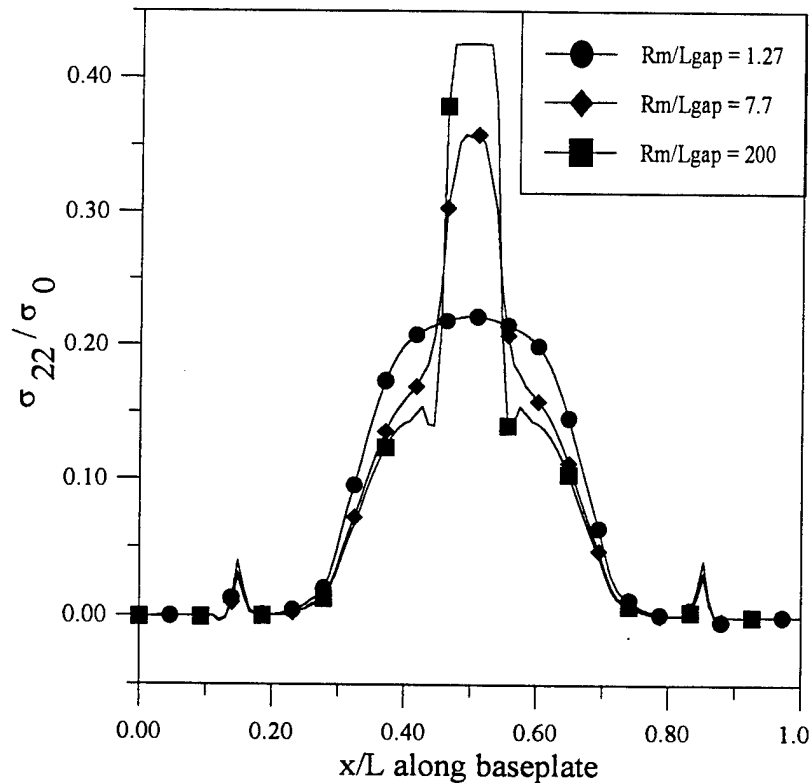


Figure 4.1.4: An illustration of the stress profile along the top layer of the baseplate as a function of the gap length.

The stress profile presented in this and subsequent graphs is measured along the length of the baseplate and is computed for the line of nodes at the top of the baseplate. The ABAQUS finite element package outputs the average stress at each node through an element print command. The element which contains the desired node is specified and the program automatically determines the nodal stresses. For the included stress profiles, which are measured along the baseplate, the examined nodes are in the baseplate. A different stress would be found if the nodes were assumed to be in the adjacent, adhesive element. Later in this work, other stress profiles are examined and the method for determining these will be discussed as is necessary.

It can be seen in Figure 4.1.4 that as the gap length decreases, thereby increasing Rm/L_{gap} , the load is dispersed throughout the fillet region and not concentrated in the gap region. The case where $Rm/L_{gap} = 200$ is equivalent to a butt joint with an overlamine. In this case, the majority of the load is transferred through the bond line between centerplate and the baseplate. This results in an out-of-plane stress on the baseplate with a magnitude of approximately 45% of the remote stress. Due to the lower strength of composite systems in this direction, this becomes an area of concern which can limit the load carrying capacity of the tee-joint. As the Rm/L_{gap} ratio is reduced, the load in the out-of-plane direction is decreased. There will still be an appreciable out-of-plane stress in this area, but the problem can be decreased by increasing the gap length.

As the gap length is increased, decreasing the out-of-plane stress in the baseplate, care must be taken because as the gap length is increased, so is the flexibility of the structure. However, the change in displacement of the tee-joint is relatively small. Table 4.2 shows the displacement of a node within the centerplate as a function of the R_m/L_{gap} ratio. The node is chosen at a location where the load and displacement is uniform.

Table 4.2: Change in vertical displacement with a varying R_m/L_{gap} ratio.

R_m/L_{gap}	Vertical Displacement
200	0.3115 mm
25.4	0.3117 mm
7.7	0.312 mm
5.08	0.3124 mm
2.54	0.3145 mm
1.27	0.3207 mm

From this table, it can be seen that the relative change in flexibility of the tee-joint is not greatly affected by altering the gap length. The largest change is approximately 3% over the large range of parameters examined.

4.2 Resin Filler

Another method which can be used to spread the load throughout the tee-joint structure is to use a lower modulus filler, see Equation (1). This change of material can result in various changes from different moduli, Poisson's ratios, strengths and ultimate elongations. There can also be a wide range of values for each filler material depending upon manufacturing variables. In this study, the material values are taken from the literature and Mallick [1993], and assumed constant. The key property examined is the elastic modulus of the filler material.

As the modulus of the filler is reduced, the stiffness of the overall structure is also reduced allowing the load to be distributed over a range of load paths. These effects are illustrated in Figure 4.2.1. In this graph, the model consists of a R_m/t of 4 and a gap length of 5 mm corresponding to a R_m/L_{gap} ratio of 5.08. The moduli shown on this graph correspond to low modulus epoxy, vinylester and high modulus polyester materials. The materials cover a wide range of properties and also have different strengths, ultimate elongations and costs. As mentioned earlier in Section 3, the materials also differ in other properties such as environmental effects, fatigue life and stress strain behavior. These properties affect the behavior of the tee-joint, but are not considered in this study.

From this graph, it can be seen that decreasing the modulus of the filler material can cause a modest redistribution of the stress to include the overlamine portions of the structure. Although the stress is redistributed, the peak levels do not change much, approximately 15%, even with a tenfold change in the modulus of the filler material.

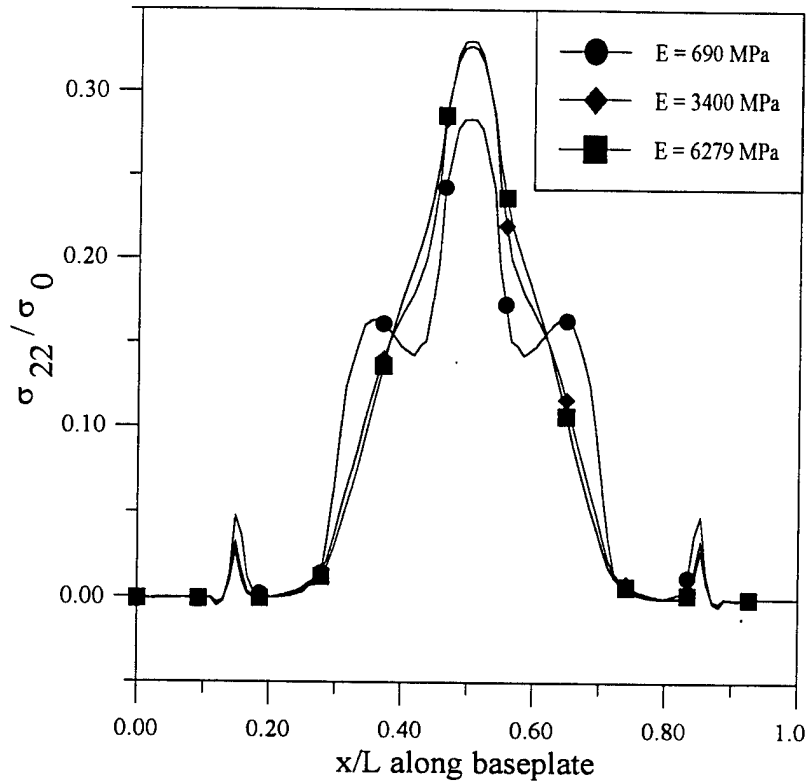


Figure 4.2.1: An illustration of the stress profile along the top layer of the baseplate as a function of the filler material elastic modulus.

The main change is in the shape of the profile. As the modulus decreases, the stress is transferred to the overlamine regions. This distribution can change the location of the critical portion of the tee-joint structure. In the models with a higher modulus filler, one of the critical concerns is the peel stress generated between the centerplate and the vertical overlaminates. This can be seen in Figure 4.2.2. This portion of the divided tee-joint structure is addressed in Section 4.1. As the modulus of the filler decreases, another potentially, critical portion arises in the curved portion of the overlamine, as illustrated in Figure 4.2.3. This problem is examined in Section 4.3.

4.3 Rm/t Ratio

Altering the Rm/t ratio of the overlamine portion of the tee-joint will also cause a redistribution of the stress profile as measured at the top of the baseplate. By increasing or decreasing the overlamine thickness, the stiffness of the curved region will change. This change alters the percentage of the total load carried by the overlamine and the gap sections. A simple, first order model of the stiffness of the curved regions can be derived by energy methods. This model begins by defining a curved member with a load, P , applied at one end and a corresponding moment, M , at the other, as illustrated in Figure 4.3.1.

$$M = PRm(1 - \cos\theta) \quad (2)$$

ABAQUS

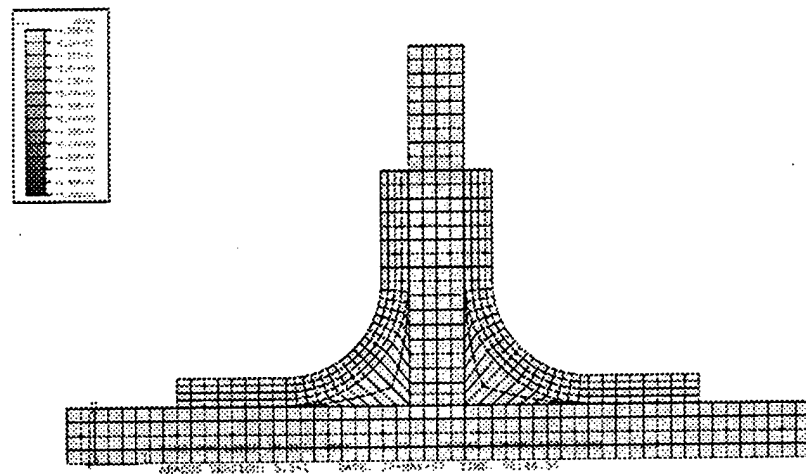


Figure 4.2.2: Horizontal stress contour with $E = 6279 \text{ MPa}$, and the geometry shown in Figure 4.1.2.

ABAQUS

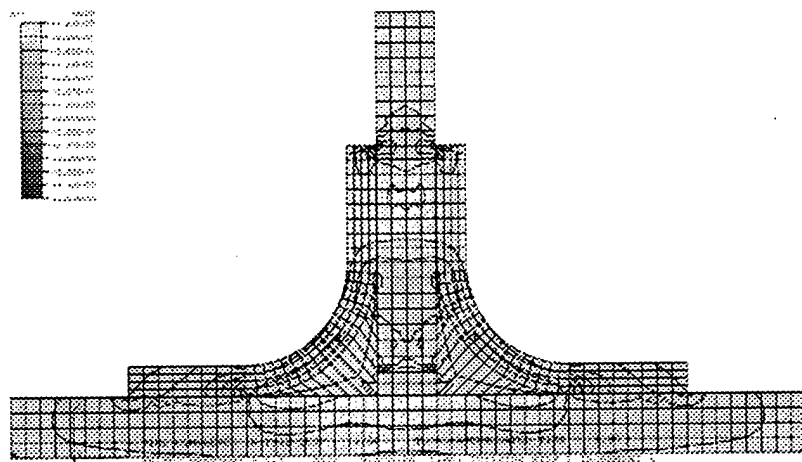


Figure 4.2.3: Horizontal stress contour plot with $E = 690 \text{ MPa}$ and the geometry shown in Figure 4.1.2.

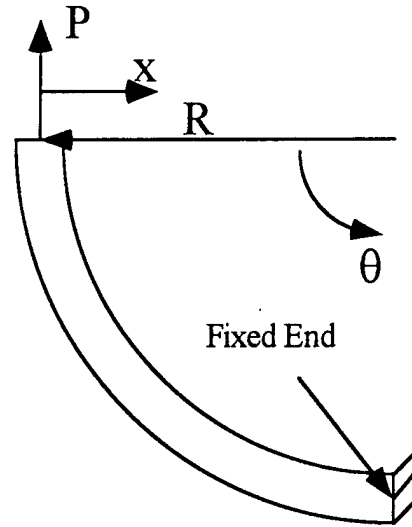


Figure 4.3.1: Illustration showing the configuration used in the following derivation.

where θ is measured along the beam and equal to 0 at the load application point. The energy in the system is defined as

$$= \int_0^{\frac{\pi}{2}} \frac{M^2}{2EI} R d\theta \quad (3)$$

The deflection of the system is found by differentiating the energy with respect to the load.

$$= \frac{\partial U}{\partial P} \quad (4)$$

The stiffness is then defined as

$$k = \frac{P}{\delta} \quad (5)$$

This results in an expression for the stiffness given by

$$k = \frac{Eb}{3 \frac{Rm^3}{t^3} [3\pi - 8]} \quad (6)$$

From this expression, it can be seen that, as the Rm/t value increases, the stiffness of the curved regions will decrease causing the majority of the load to pass through the gap region of the tee-joint. This observation is illustrated in Figure 4.3.2.

In this study, the outer radius is held constant while the thickness of the overlamine is altered to create the desired Rm/t values. From this graph and the previous expression, it can be observed that as the Rm/t value decreases the stress profile as measured along the top of the overlamine will change. As this change occurs, the critical section of the tee-joint structure will also change.

From the graphs of the stress profiles, Figures 4.1.3, 4.2.1 and 4.3.2, the behavior of the Sheno joint can be analyzed, Sheno and Hawkins [1992]. In this joint, a high modulus filler and a high Rm/t ratio result in a structure where the majority of the load is

transferred through the filler region. This design does not need an overlamine as a load carrying member and the main reason for including the overlamine is for blast and fire protection. The large gap size used in this design results in lower out-of-plane stress in the base plate. But, without an overlamine to provide added stiffness to the structure, this type of tee-joint is flexible when compared to similar tee-joints with thicker overlaminates.

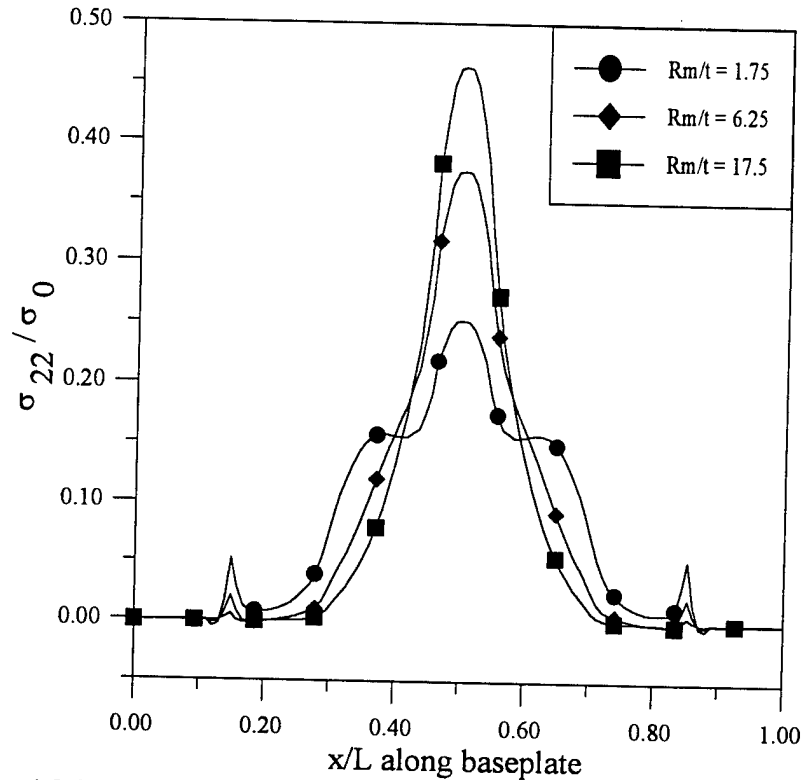


Figure 4.3.2: An illustration of the stress profile along the top layer of the baseplate as a function of the R_m/t ratio of the overlamine.

In the previous sections 4.1 through 4.3, the boundary condition used in the finite element model was to constrain the bottom of the baseplate. This condition approximates the case where the baseplate is either much stiffer than the tee-joint or much thicker than that used in the previous finite element models. A more practical boundary condition, especially in the case of smaller tee-joints used in test programs, is to place the constraint on the top portion of the baseplate a set distance away from the end of the overlamine. This configuration is illustrated in Figure 4.3.3. The effects of this type of boundary condition and various design parameters on a tee-joint in this configuration are examined in the subsequent sections. First, graphs will be shown illustrating the effects of increasing the span of the test specimen. Further parameters examined include the effects of increasing the thickness of the baseplate as compared to the centerplate, and altering the length of the horizontal overlaminates.

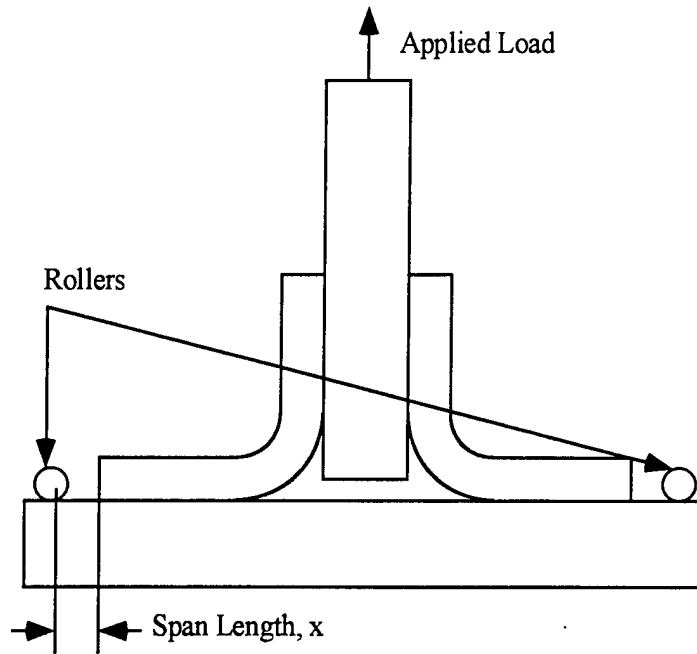


Figure 4.3.3: A tee-joint in a test jig constrained with rollers a set distance from the end of the horizontal overlaminates.

4.4 Span Length

To examine the effects of altering the model's boundary conditions, a symmetrical finite element model is used. The accuracy of the symmetrical model as compared to the model of an entire tee-joint is illustrated in Figure 4.4.1. The profiles in this graph are from test cases where the model is constrained at the bottom of the baseplate and have been examined in the previous sections. From this graph, it can be seen that the models predict similar stresses with only small variations along the length of the baseplate.

These small variations are due to the method the ABAQUS finite element program uses when the symmetry and orientation commands are used. In the previous models which consisted of a finite element mesh of the entire tee-joint, the orientation command was used to define the local coordinate system for the curved portion of the tee-joint. This function is necessary to input the material properties of the material in the curved region, since the fibers bend along the curve in the circumferential direction. This software command also causes the stresses in the curved region to be output in a local, cylindrical coordinate system. This form of output is useful because the stresses are in the critical direction which outlines the weaknesses of this type of composite system in a curved orientation, the out-of-plane or radial direction. The symmetry command causes the program to recognize a line of symmetry for a specified finite element mesh. To do this operation, the program converts the entire model to the global coordinate system and outputs the stresses in this frame of reference. Thus, in one model, the entire joint is in the global coordinate system while the other has a local, cylindrical coordinate system in the curved sections and the rest of the joint is in the global, Cartesian coordinate system.

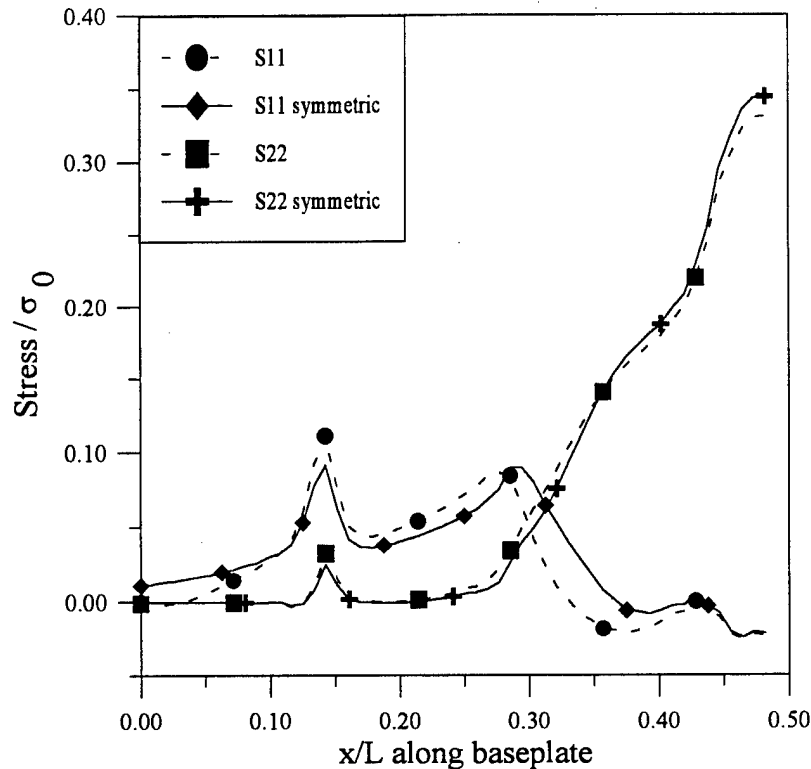
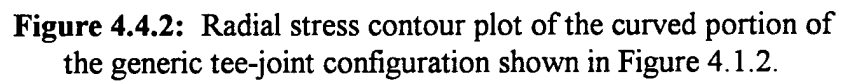


Figure 4.4.1: Comparison of the stress profiles along the baseplate for the original model and the symmetric finite element model.

An anomaly is seen in the ABAQUS output of the non-symmetric model between the curved region and the horizontal overlamine. This error can be seen in a stress contour plot of the radial stresses in the curved portion of the joint which is shown in Figure 4.4.2. The free surface in this section, the left face of the curved segment in the previous figure, can carry no stress in the radial direction; but, in Figure 4.4.2, there are radial stresses on this surface near the interface of the curved region and the horizontal overlamine. The cause of these stresses is the change in coordinate system between the two sections of the tee-joint, no other change occurs which can account for the anomalous stresses. This discrepancy is a problem within the ABAQUS program, but the magnitudes are small in a localized area and do not cause significant differences in the parametric study of the tee-joint structure.

A graph, Figure 4.4.3, is included to aid in the visualization of the symmetric tee-joint model and the presented stress profiles. In the stress profile graphs, the middle of the centerplate is at $x/L = 1$. This line is both the application point of the vertical pull off load and the line of symmetry for the finite element model. For the dimensions of the generic model, as illustrated in Figure 4.1.2, the horizontal overlamine ends at .66, the curved region ends at .8 and the centerplate ends at .96.



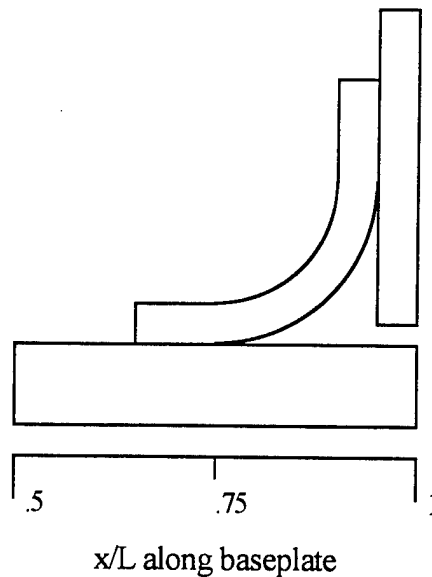


Figure 4.4.3: Illustration of the relative position of various geometric features as measured along the baseplate as a function of x/L for the symmetric tee-joint.

Figure 4.4.4 illustrates the effects of altering the span length. In this study, the boundary conditions are assumed to be rollers with the dimensions of one element. The profiles shown in the figure are only of the portion of the baseplate under the tee-joint.

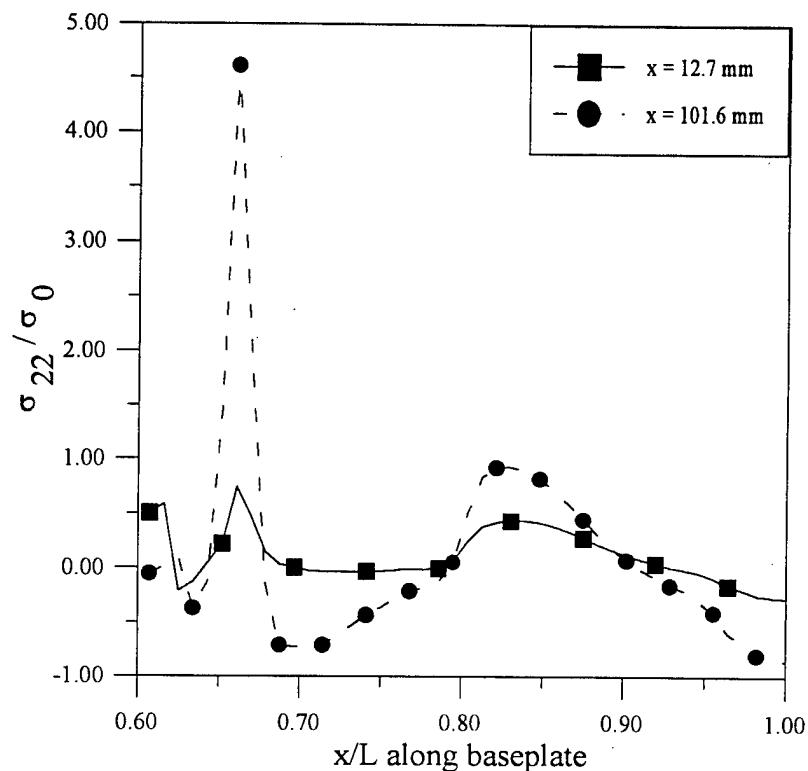


Figure 4.4.4: Peel stress along the baseplate as a function of the span length where the start of the constraint is positioned a set length, x , from the end of the overlaminates

In Figure 4.4.4, new areas of concern for the designer are shown. Here, the critical area is the end of the horizontal overlamine where large peel stresses are generated due to the bending of the baseplate. As the span length increases, the magnitude of the peel stress at the end of the overlamine also increases. This portion of the tee-joint structure is examined in Section 4.5. Figure 4.4.5 is included to illustrate the stresses with a few intermediate span lengths.

A vertical stress contour plot of the model with the rollers located 12.7 mm from the end of the overlamine is included due to the differences between this case and those seen earlier. In Figure, 4.4.6, the bending of the baseplate and the constraint caused by the tee-joint structure cause a compressive zone to form in the fillet region. This is not seen in earlier models. This zone can also be seen in the previous two figures where as the span length increases, so does the magnitude of the compressive stresses in the gap region. In this configuration, as seen in the previous figure, the maximum compressive stress generated in the gap region is approximately half of the far field, reference stress. The compressive region extends from the centerplate through the gap region and into the baseplate.

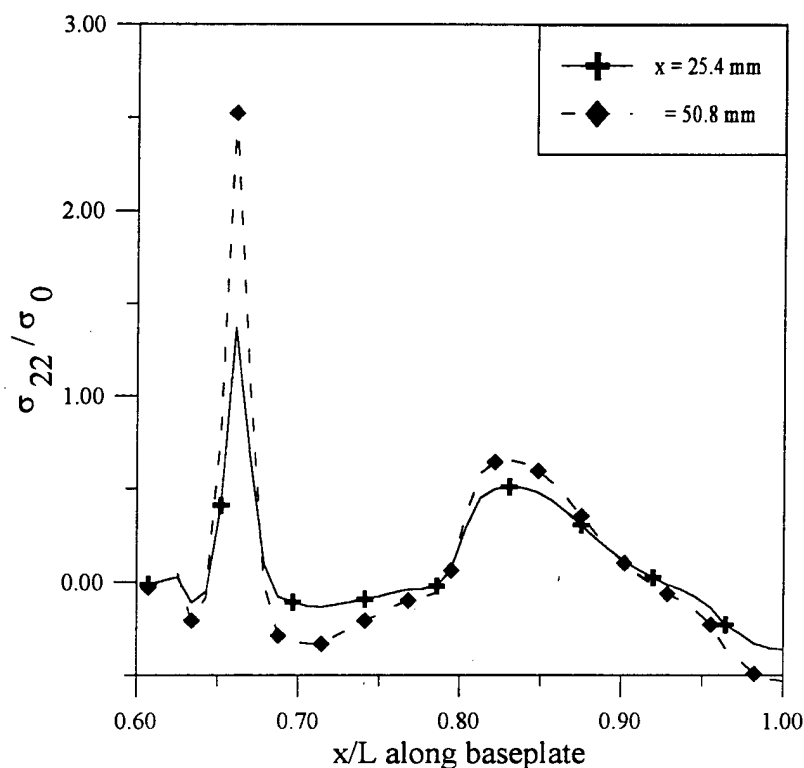


Figure 4.4.5: Peel stress along the baseplate as a function of the span length where the start of the constraint is positioned a set length, x , from the end of the overlamine. In these profiles, the generic tee-joint described above is used.

ABAQUS

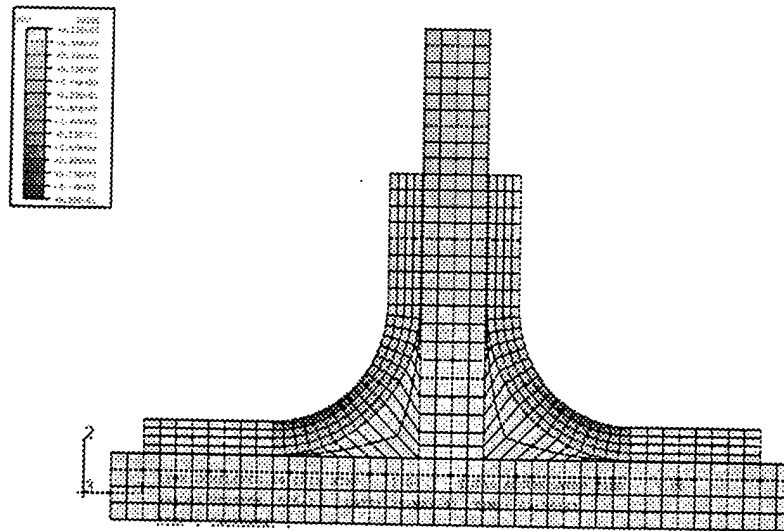


Figure 4.4.6: Vertical stress contour plot for the model with constraints 12.7 mm from the end of the horizontal overlaminate, and the geometry of the generic tee-joint shown previously.

The compressive zone is formed by the flexure of the tee-joint structure due to the applied pull-off load. In a beam, the curvature caused by the applied load would be uniform and can easily be computed using strength of material approaches. The addition of the tee-joint structure increases the stiffness of the beam in a localized area under the centerplate which resists the bending of the beam. The baseplate, literally, has to push the tee-joint structure which results in a compressive region. This effect is also dependent upon the tee-joint configuration and will be affected by other variables, such as the overlamine thickness, which alter the stiffness of the structure. The change in the curvature of the tee-joint can be seen in the Figure 4.4.7. In Figure 4.4.7, the curvature of the baseplate can be seen to change under the centerplate due to the increased flexural rigidity in this area of the tee-joint. This change is the cause of the compressive region.

The critical areas within this tee-joint configuration are the curved section and the end of the overlaminates, as mentioned before. Typically, the concern in the curved region is due to the radial stress which is an out-of-plane stress, but in this tee-joint there is also a large stress concentration in the in-plane direction. This concentration is especially important in designs using materials which are only slightly orthotropic in strength. In this case, where the in-plane and out-of-plane strengths only differ by a relatively small margin when compared to other polymer composite systems, this region can be a possible failure site. While in more orthotropic materials, the failure will occur in other locations which have lower out-of-plane stresses due to the lower material strength as compared to the in-plane strength in these directions. The radial and circumferential stress contour plots for the curved section are included in Figures, 4.4.8 and 4.4.9 to help illustrate this observation.

The magnitude of the circumferential stress is decreased for the range of parameters considered by altering the modulus of the filler material. In Section 4.2, an examination was made of the effects of changing the filler modulus. Further effects are noticed when examining the generic tee-joint with the new boundary conditions. In this case, using the higher modulus resin mentioned in Section 4.2 caused a decrease in the circumferential stress while leaving the radial stress unchanged. But, this change resulted in higher compressive stresses in the gap region. Using the lower modulus material prevented the formation of the compressive region, but caused a higher stress level in the curved section. As mentioned earlier, the low modulus resin materials result in a more compliant tee-joint which allows the load to disperse throughout the structure, and reduces the effect of the tee-joint on the curvature of the baseplate.

The change in filler modulus results in a large change in the vertical displacement of the structure, see Table 4.3. The vertical displacement is measured in the same manner as in Section 4.1. Here, there is a change of 14% over the range of filler moduli examined with the greatest change occurring between the cases with the lowest moduli.

ABAQUS

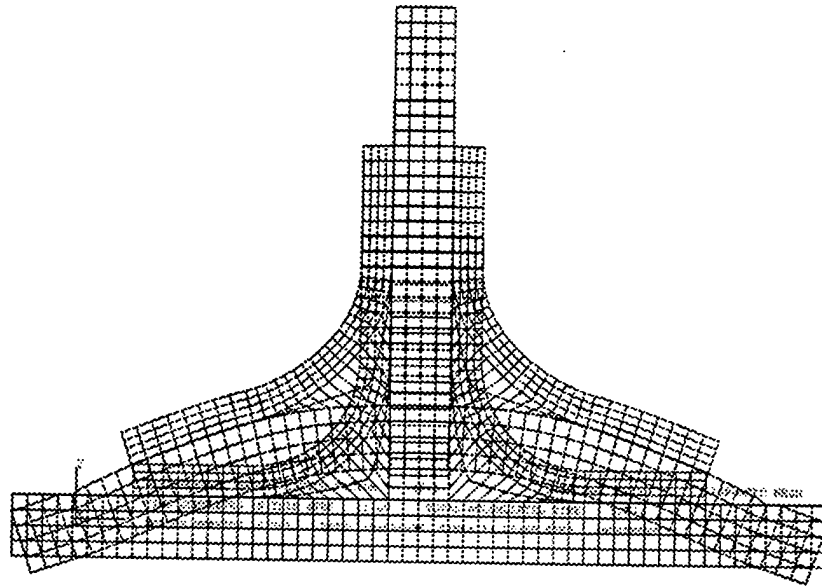


Figure 4.4.7: A comparison of the tee-joint geometry before and after loading. The displacement is magnified to aid in the visualization.

ABAQUS

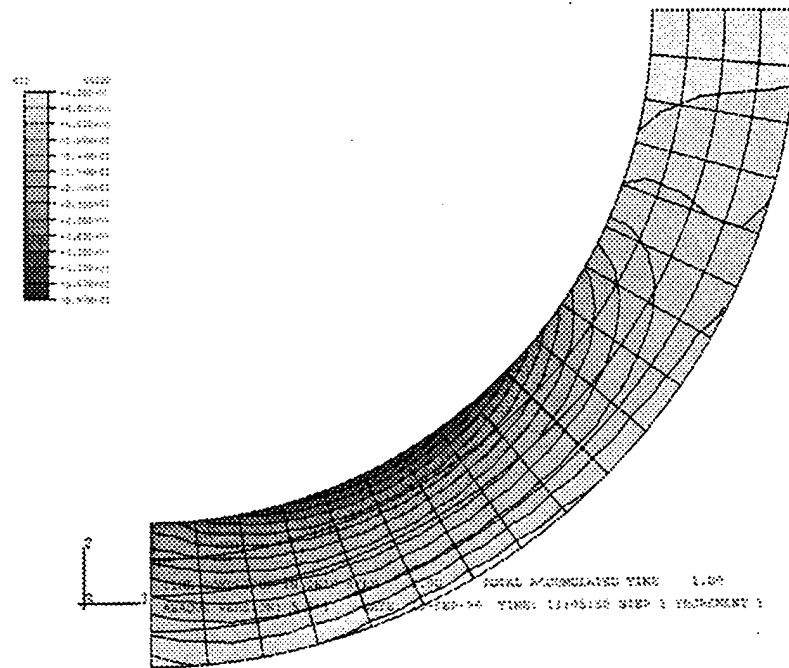


Figure 4.4.8: The circumferential stress contour plot of the curved section of the generic tee-joint with rollers located 12.7 mm from the end of the horizontal overlaminates.

ABAQUS

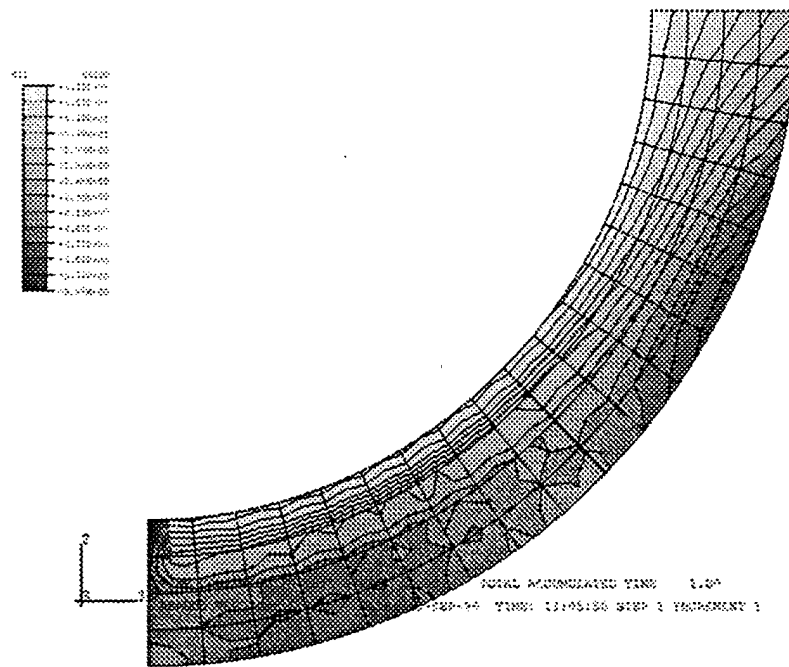


Figure 4.4.9: The radial stress contour plot of the curved section of the generic tee-joint with rollers located 12.7 mm from the end of the horizontal overlaminates.

Table 4.3: Change in vertical displacement with varying filler modulus.

Filler Modulus	Vertical Displacement
690 MPa	0.3522 mm
2000 MPa	0.3224 mm
3400 MPa	0.3124 mm
5000 MPa	0.3068 mm
6279 MPa	0.304 mm

4.5 Baseplate Thickness

The effects of altering the boundary conditions and span length of the tee-joint discussed in the previous section can be alleviated by increasing the thickness of the baseplate. The model examined earlier had a relatively thin baseplate, 12.7 mm, which deflected under the applied load causing a curvature in the baseplate which was constrained by the addition of the tee-joint structure. This constraint resulted in large peel stresses at the end of the horizontal overlamine. In a test program with specimens with similar dimensions, this would represent a potential out-of-plane failure mechanism. Figure 4.5.1 illustrates the effects of increasing the baseplate thickness.

From Figure 4.5.1, it can be seen that an increase in baseplate thickness can decrease the peel stresses at the end of the horizontal overlamine. The model used in the previous section generated large peel stresses due to excessive bending in the baseplate. An increase in the baseplate thickness of 6.35 mm resulted in a reduction in peel of approximately 60%.

In figure 4.5.1, an increase in the vertical stress is also seen at approximately $x/L = .85$. This concentration is due to high radial stresses in the curved section of the tee-joint. In this case, where the baseplate thickness is altered, the opening moment applied to the curved region of the joint also changes. With thinner baseplates, the curvature of the baseplate is more pronounced and there is a larger opening moment applied to the curved region. The moment decreases as the flexural stiffness or thickness of the baseplate increases. In tee-joints with thinner baseplates, this becomes a region of concern. But, as the thickness of the baseplate increases, the importance of this area decreases as the stress concentrations in other regions increase. In Section 4.4, this concentration also occurred, as seen in Figures 4.4.4 and 4.4.5, due to the changes in curvature as the span length is altered, but was small in comparison to the peel at the end of the horizontal overlamine which was the area of major concern.

The configurations with thicker baseplates are likely to appear in floor to hull connections where the baseplate member will not undergo appreciable bending. This case approaches the behavior seen in earlier models where the tee-joint is constrained along the bottom of the baseplate. An illustration of this comparison is given in Figure 4.5.2. In this figure, the model with a $t_{bp} = 50.8$ mm and rollers located 12.7 mm from the end of the overlamine is compared to a similar model with a baseplate that is constrained along the bottom.

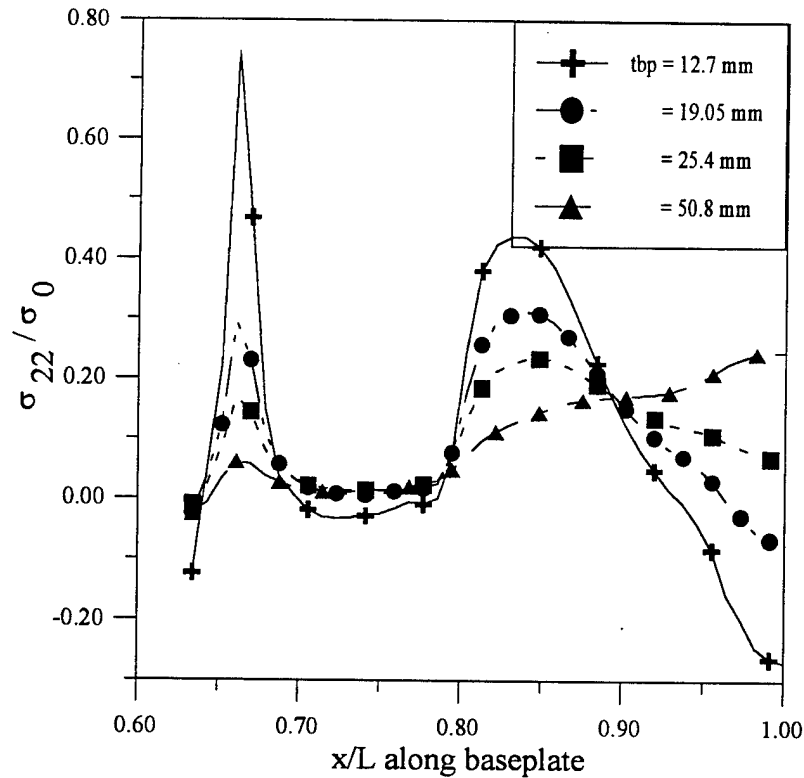


Figure 4.5.1: Normalized peel stress along the top of the baseplate as a function of the thickness of the baseplate, t_{bp} . The model used in this figure is shown in Figure 4.1.2.

It can be seen from this figure that, as the baseplate thickness increases, the importance of the type of boundary condition decreases. Also, the flexibility added by constraining the tee-joint by rollers allows the load to be carried throughout the entire structure. Unlike some of the earlier cases where the load is primarily transferred directly through the fillet region, the current model with rollers and a thick baseplate allow the load to be transferred through the overlaminates. This redistribution is shown in Figure 4.5.3, a contour plot of the generic tee-joint with a thick baseplate, $t_{bp} = 50.8$ mm. Here, the critical regions are peel stresses in the horizontal and vertical overlaminates and the out-of-plane stress in the curved section.

In the model with a thin baseplate, $t_{bp} = 12.7$ mm, there are also compressive vertical stresses in the gap region, as seen in Figure 4.4.6, but these stresses do not occur in the tee-joint with a thick baseplate. In a tee-joint with a slight increase in baseplate thickness, $t_{bp} = 19.05$ mm, there is still a compressive zone, but its magnitude is only a small fraction of the reference stress, approximately 10%, which is a substantial reduction from the previous case with $t_{bp} = 12.7$ mm.

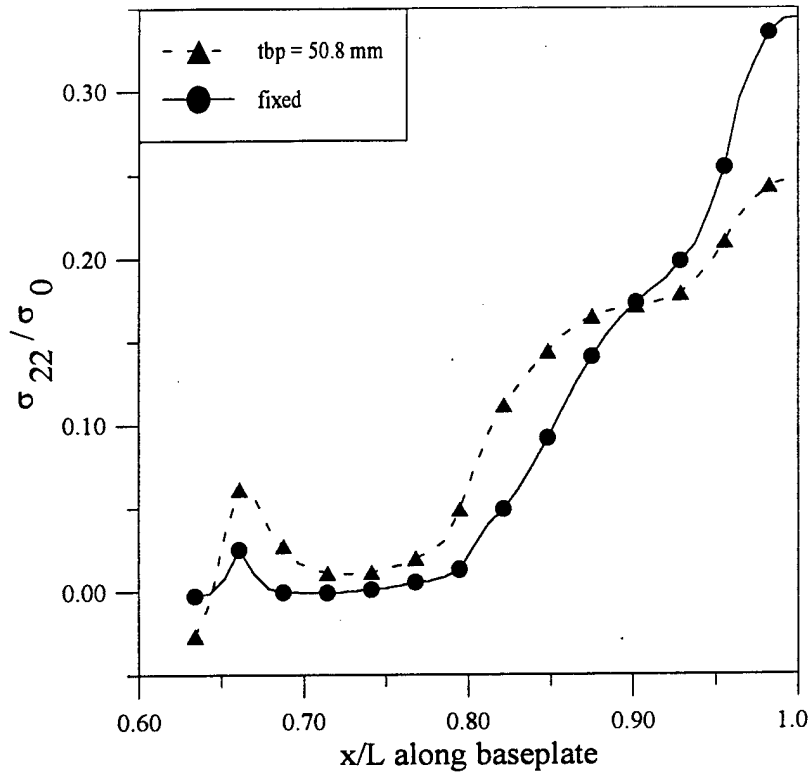


Figure 4.5.2: Normalized peel stress for two models one with rollers located 12.7 mm from the end of the horizontal overlaminate and a $t_{bp} = 50.8$ mm, and the other with a $t_{bp} = 12.7$ mm fixed along the bottom. Both models are otherwise identical.

4.6 Horizontal Overlamine Length

Models with increasing horizontal overlamine length, l_{hov} , are used to examine the effects of altering this parameter. The model used is the generic model with a baseplate thickness of 12.7 mm. While this is not the “optimum” case, it will be of interest to see how the longer overlaminates effect the peel stresses along the baseplate in this case. Three models are run with a l_{hov} of 25.4 mm, 38.1 mm and 50.8 mm and are illustrated in figure 4.6.1. In this figure, the end of the overlaminates correspond to the peaks inherent in each curve shown on the figure and the case with $l_{hov} = 25.4$ mm corresponds to the generic case shown in Figure 4.4.3. From this figure, it can be seen that increasing l_{hov} decreases the peel stress generated at the end of the overlamine. But, with this geometric configuration, this change also increases the compression in the gap region which increases the risk of causing crushing in this area.

As in the previous sections, there is a stress concentration at approximately $x/L = .85$ in Figure 4.6.1. This peak corresponds to a large stress in the curved region of the tee-joint. In all of the configurations illustrated in Figure 4.6.1 including the baseline generic geometry, the critical area is the curved portion of the tee-joint. This result is shown in the contour plot given in Figure 4.4.6. As the length of the horizontal overlamine increases, this problem becomes more pronounced due to the increase in joint flexibility.

ABAQUS

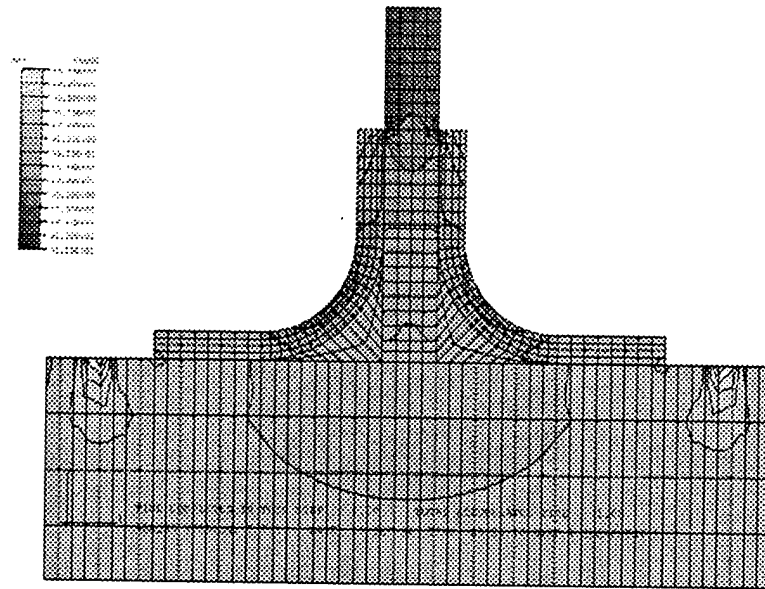


Figure 4.5.3: Vertical contour plot of model with $t_{bp} = 50.8$ mm.

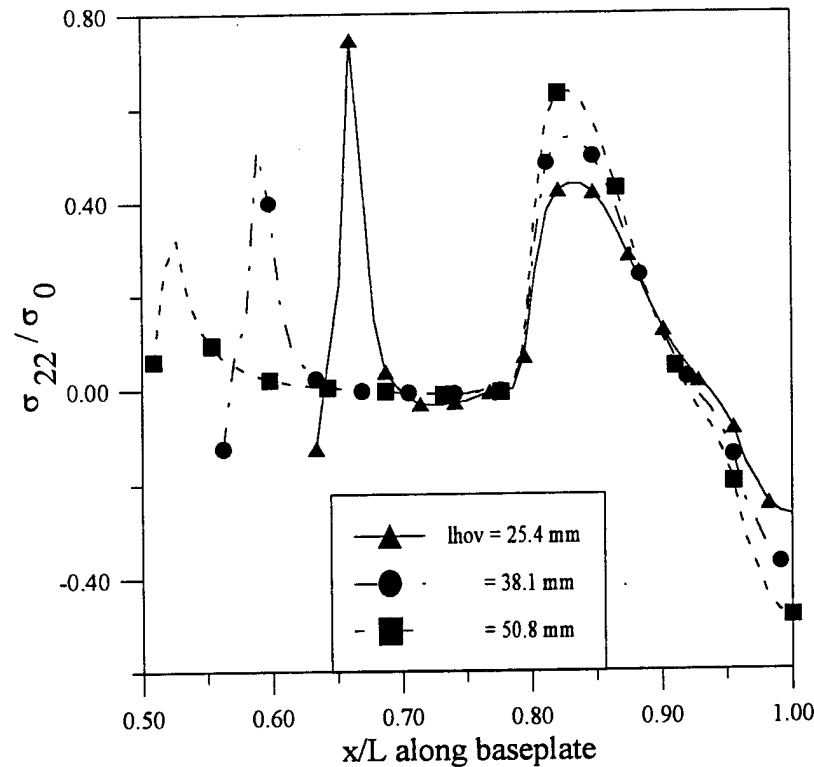


Figure 4.6.1: Effects of changing overlaminate length on the normalized peel stress for the generic model with $t_{bp} = 12.7$ mm and rollers located 12.7 mm from the end of the overlaminate.

To increase the length of the horizontal overlaminates, the span length of the model also has to be increased. This change results in a larger curvature and a larger opening moment applied to the curved region. Another effect occurs as the curvature of the joint increases, this change is a higher level of compression in the gap area of the fillet region.

Even though the span length increases, the peel stresses at the end of the horizontal overlaminate decrease. In section 4.4, the opposite was seen to occur. The difference between the two cases is due to the greater length of overlaminate available to transfer the load generated between the baseplate and overlaminates by the curvature of the baseplate.

Figure 4.6.2 shows that increasing the baseplate thickness reduces the peel stresses at the overlaminate end and the compressive zone in the gap region. Commentary on this point has also been discussed in Section 4.5 and again implies the importance of well proportioned tee-joints in the design of marine structures. From Figure 4.6.1 and 4.6.2, it can be seen that as the horizontal overlaminate length is increased the peel at the termination of the doubler region is decreased, but the stresses in the curved region and the compressive zone in the gap region are increased. Depending upon the properties of the constituent materials, either of these areas can become critical. The configuration with a thicker baseplate, shown in Figure 4.6.2, has lower peak values for the peel stresses

when compared to the earlier, generic case. This decrease is due to the thicker baseplate and the corresponding reduction in curvature of the tee-joint structure.

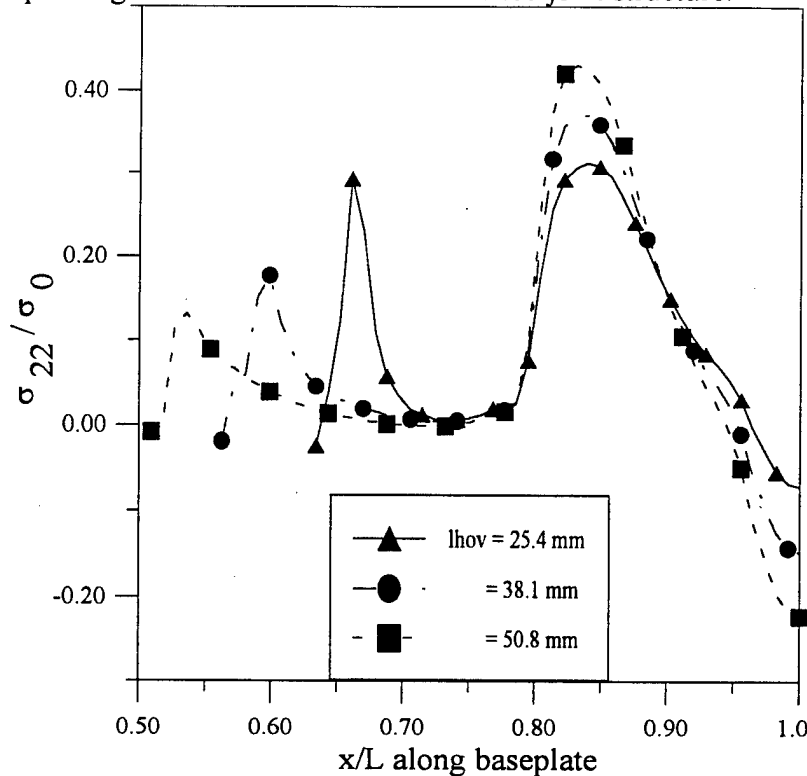


Figure 4.6.2: Effects of changing overlaminate length on the normalized peel stress for the generic model with $t_{bp} = 19.05$ mm.

4.7 Tapers

A method to decrease the high peel stresses that develop at the termination point of doubler regions is to introduce a taper. This feature has been frequently used in aerospace and marine structures. In fact, the current design guidelines for marine tee-joints recommends the inclusion of a taper at the ends of both the horizontal and vertical overlaminates. The taper will decrease the peel stress generated in these regions and will decrease the significance of these areas as possible failure sites. This feature has not been added to the previously examined tee-joints for several reasons. First, the basic response of the tee-joint changes considerably with the addition of tapers. By examining tee-joints without this type of structure the basic response can be examined to gain insight into the response of a tee-joint to a pull off load. Also, the main parameters which govern the failure mechanisms and strength of the tee-joint can be more easily identified without the tapers reducing the stress concentrations in some of the critical tee-joint sections. In some cases, the use of tapers may also be prohibited due to space for long gradual tapers and/or manufacturing limitations, economic considerations and other design constraints. The effects of using this effective refinement will be briefly examined in this section.

One of the effects of the addition of tapers is to decrease the stress concentration in the centerplate directly above the termination of the vertical overlaminates. This concentration appears in many of the tee-joint configurations presented previously and is

illustrated in Figure 4.7.1. The effects of tapers on this form of stress concentration has been addressed in a paper, Malvar and Bish [1995] which examines grip effects during the tensile testing of composite rebar. In the case of tee-joints, this effect is not critical, but is decreased along with the higher peel stresses with the addition of a taper.

The addition of tapers can also effect the tee-joint by increasing the overlamine and span length. As stated earlier, this change can result in a larger tee-joint curvature causing larger compressive stresses in the gap region, higher stresses in the curved section while decreasing the peel stress at the end of the horizontal overlamine. To prevent these changes, the tapers examined in this section will be of limited length and taper angle. While this might not illustrate the most effective taper, it does allow a comparison between tee-joints with and without tapers and an evaluation of the trends which occur with the addition of tapers. In the literature, suggested taper angles are between 10 degrees and 15 degrees for carbon or graphite/epoxy materials.

Two tapers are examined. The first, Type 1, begins at the tangency point of the curved region and results in a taper angle of approximately 15° , as measured from the center and baseplates. The second, Type 2, begins 12.7 mm from the tangency point of the curved region and slopes to the horizontal overlamine at an angle of approximately 27° . The tapers end with a thickness of two bond line thicknesses or .254 mm. An illustration of the two tapers is included in Figure 4.7.2. A third taper is also examined with an angle of 45° , but is not shown in this figure.

Figure 4.7.3 illustrates the change in stresses along the top of the baseplate caused by the addition of tapers. Addition of the tapers to the end of the overlaminates results in a decrease of the peak, peel stress generated at the end of the horizontal overlamine. There is also a corresponding decrease in the peel stresses at the termination point of the vertical overlaminates. The critical section for tee-joints designed with either of these types of taper would most probably be the curved region. Both of the tapers are successful in damping out the large peel stresses generated at the termination of the doubler regions. As expected, the more gradual Type 1 taper angle causes the largest decrease in peel stress, as seen in Figure 4.7.3. This result corresponds well with literature where the most efficient joint has been documented to have a taper angle between 10° and 15° .²

² Kedward, K.T., Private Communications, 1997.

ABAQUS

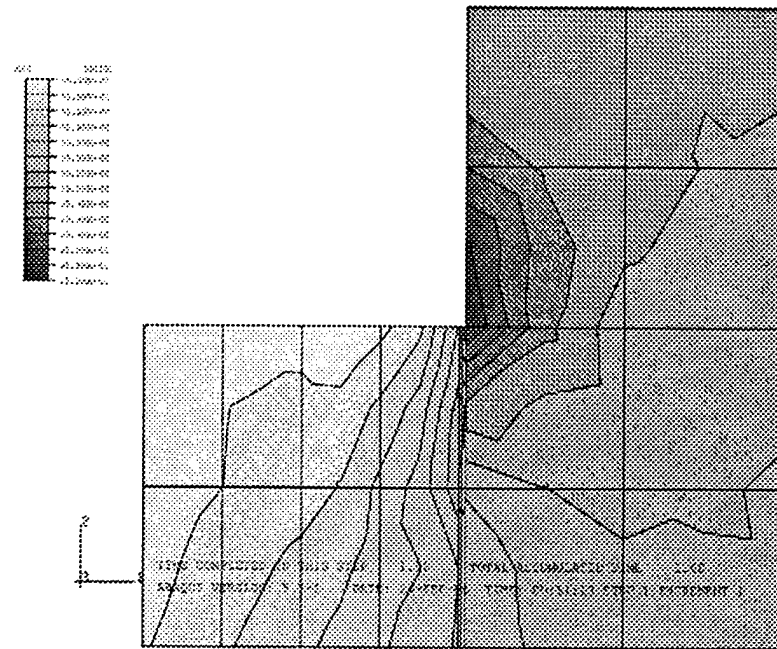


Figure 4.7.1: Vertical stress contour plot of the region of the centerplate near the end of the vertical overlamine. The geometry is the generic joint with a baseplate thickness of 50.8 mm.

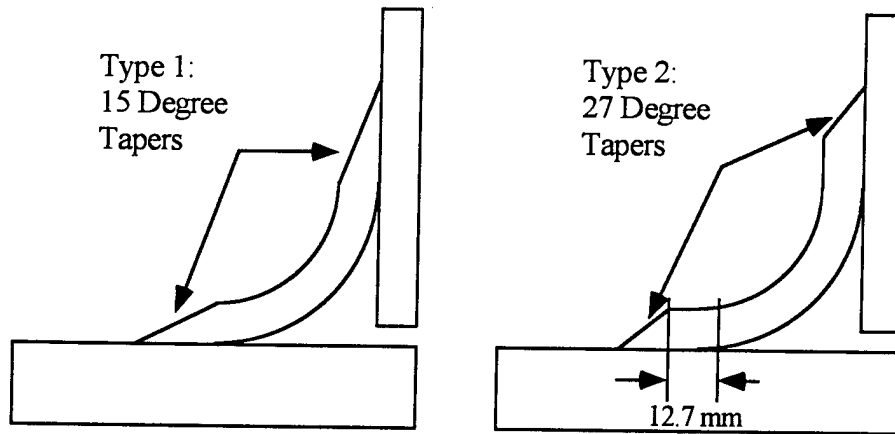


Figure 4.7.2: An illustration of the two types of taper examined in this section.

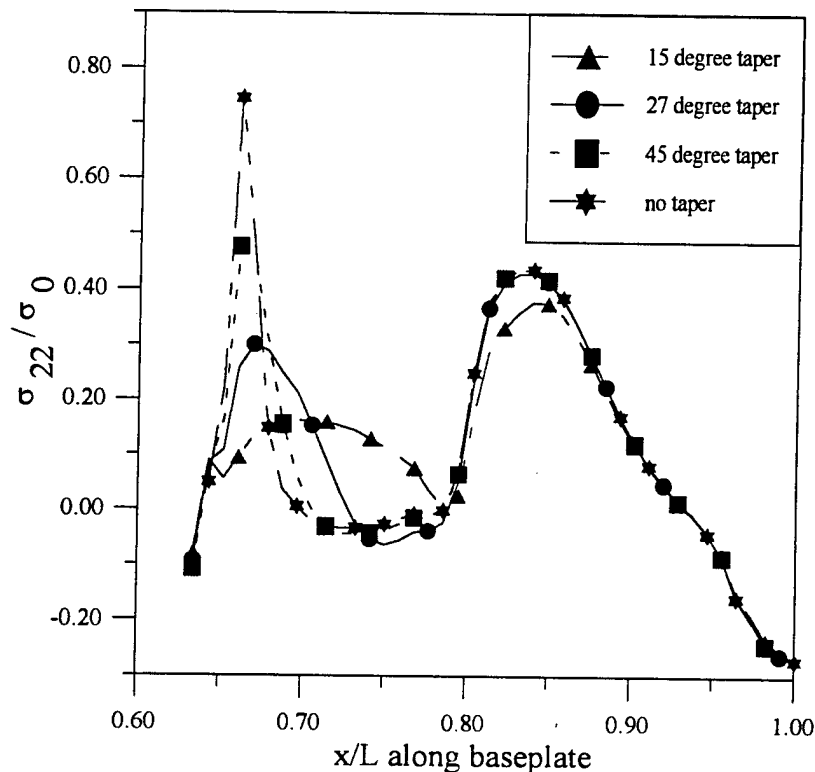


Figure 4.7.3: Peel stress profile along the baseplate for three different configurations, the generic joint, and the generic joint with all of the tapers mentioned previously.

It should also be noted that for this material a large decrease in the peak peel stress is observed for tapers with steeper angles. From Figure 4.7.3, it can be seen that even this limited taper results in a large percentage decrease in the peak peel stress. With a taper of 27°, there is a 60% decrease in the peak peel stress. Another taper with an angle of 45° results in a 36% decrease in the peak peel stress. These results illustrate that even a limited, steep taper results in a significant reduction in peel stress.

Similar affects from the addition of tapers are seen in the overlamine along the centerplate. These effects are illustrated in Figure 4.7.4.

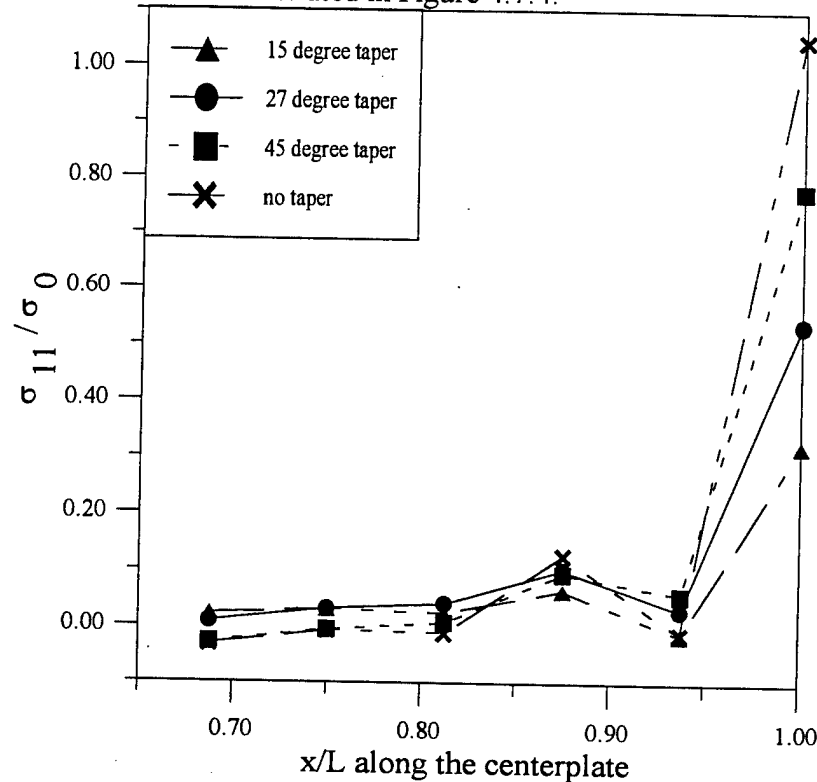


Figure 4.7.4: Peel stress profile along the centerplate for three different configurations, the generic joint, and the generic joint with all of the tapers mentioned previously.

Here, as in the cases along the baseplate, even a relatively steep taper has a large effect on the measured peel stress. A taper with an angle of 27° results in a peel reduction of approximately 50%.

This section has shown the importance of tapers and that the performance of tapers is different for various polymeric composite systems. In the E-glass systems investigated in this work, even a steep taper angle results in a drastic reduction in peel stress. This response is also seen, to a different extent, in carbon/epoxy systems, see Figure 4.7.5 which details the same tee-joint geometry and loading conditions, but uses a typical [0° / 90°] graphite/epoxy laminate.

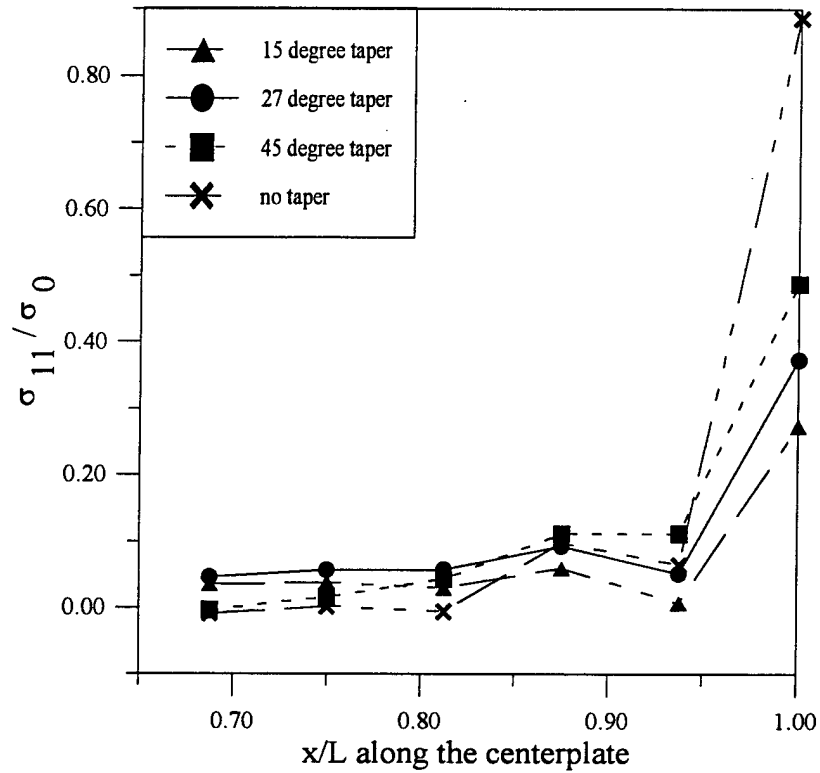


Figure 4.7.5: Peel stress profile along the centerplate as shown in Figure 4.7.4, but with a carbon/epoxy laminate.

5.0 Tee-Joint Sections

In this section, the various segments of the tee-joint, as shown in Figure 1.2, are examined.

5.1 Section A: Double Lap

The configuration of the top portion of the tee-joint designated Section A in Figure 1.2 is similar to a double lap joint. This type of joint is frequently seen in composite structures. The major weakness in this type of joint is caused by the transfer of load from one member to another through shear mechanisms during which large peel stresses are created. Peel stress is an out-of-plane load which in this case tends to pull the overlamine off the centerplate or causes a delamination of either member adjacent to the interface.

One method of approximating the response of this type of joint under tensile loading conditions, as seen in this section of the tee-joint, is by using beam on elastic foundation analysis as detailed by Hetenyi [1946], Hart-Smith [1974], Oplinger [1995] and others. By making various assumptions, a simplified expression for the maximum peel stress can be derived based upon geometric and material parameters. The derivation is as follows starting with equilibrium equations for the system shown in Figure 5.1.1.

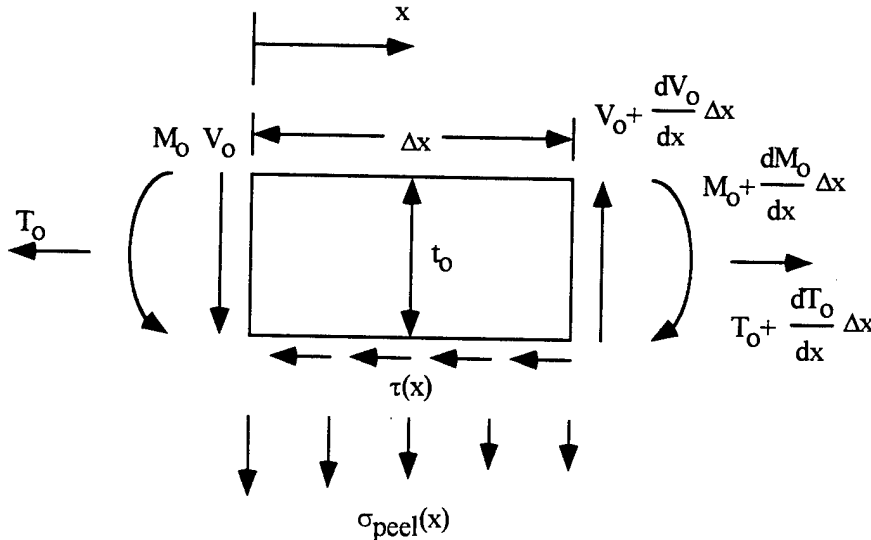


Figure 5.1.1: Free body diagram of a double lap joint.

These equations are

$$\frac{dM_o}{dx} = V_o - \frac{\tau_o t_o}{2} \quad (7)$$

for moment equilibrium and

$$\frac{dV_o}{dx} = \sigma_o \quad (8)$$

for normal equilibrium and

$$\frac{dT_0}{dx} = \tau_0 \quad (9)$$

for axial equilibrium where τ_0 is the shear profile along the joint and t_0 is the thickness of the outer adherend. The characteristic equation for the outer member based upon plate bending is

$$\frac{d^2 w_o}{dx^2} = -\frac{M}{D_0}, \quad (10)$$

where D_0 is the plate bending stiffness for an isotropic material. In using this isotropic expression to model an anisotropic material, the modulus and the Poisson's ratio used are the longitudinal modulus of the composite and ν_{13} . The assumed elastic adhesive peel stress is defined as

$$\sigma_o = E_a \frac{w_o}{t_a} \quad (11)$$

where E_a is the adhesive modulus and t_a is the bond line thickness. Combining the previous equations, (7) through (11), results in the following differential equation for an element of the outer adherend.

$$D_0 \frac{d^4 w_o}{dx^4} - \frac{E_a}{t_a} w_o = \frac{d\tau_0}{dx} \frac{t_0}{2} \quad (12)$$

This equation can be solved using different means depending upon various assumptions. First, the Volkersen shear stress profile can be used to determine the slope of the shear stress in the adhesive layer. This assumption results in a solution dependent upon the loading of the joint. A second approximate method is to assume that the adhesive is undergoing perfectly plastic shear deformation in which case the right hand side of Equation (12) is zero. A third method of approximating the peel stress is by modeling the shear deformation in the adherends which is especially a concern for composite adherends with low transverse shear moduli. These methods are investigated in the following sections.

5.1.1 Volkersen Shear Stress Distribution

Using the first method with a Volkersen shear stress profile to determine an expression for the peel stress in the joint, the solution to Equation (12) is as follows. The homogeneous solution has the form

$$w_o = e^{-mx} [C1 \cos(mx) + C2 \sin(mx)] \quad (13)$$

where

$$m^4 = \frac{E_a}{4D_0 t_a}. \quad (14)$$

The particular solution is found assuming a Volkersen shear profile, Volkersen [1938],

$$\sigma_o(x) = \frac{P}{l} \frac{\lambda l}{k \sinh(\lambda l)} [(k-1) \cosh(\lambda(l-x)) + \cosh(\lambda x)]. \quad (15)$$

The constants in Equation (15) are defined as follows

$$\lambda^2 = \frac{Ga}{ta} \left[\frac{1}{E_o t_o} + \frac{1}{E_i t_i} \right], \quad (16)$$

$$k = \frac{E_o t_o + E_i t_i}{E_i t_i}, \quad (17)$$

and l is the length of the joint. Using these expressions, Equation (12) becomes

$$D_o \frac{d^4 w_o}{dx^4} - \frac{E_a}{t_a} w_o = A [-(k-1) \sinh(\lambda(l-x)) + \sinh(\lambda x)] \quad (18)$$

where

$$A = \frac{P \lambda^2 t_o}{2k \sinh \lambda l}. \quad (19)$$

The particular solution for this equation has the following form.

$$w(x) = \frac{A}{C} [-(k-1) \sinh(\lambda(l-x)) + \sinh(\lambda x)] \quad (20)$$

where

$$C = \left(D_o \lambda^4 + \frac{E_a}{t_a} \right). \quad (21)$$

Equations (13) and (20) can be combined to give the total solution to the differential equation. The other constants are found by setting the bending moment and shear stress equal to zero at the free end of the joint. This derivation results in the following expression for the peel stress achieved in the double lap joint region with the assumptions mentioned above.

$$\sigma_o(x) = \frac{E_a}{t_a} \left[C1(e^{-mx} \cos(mx)) + C2(e^{-mx} \sin(mx)) - \frac{A}{C}(k-1) \sinh(\lambda(l-x)) \right] \quad (22)$$

where the constants are defined as follows

$$C1 = \frac{\frac{t_o}{2D_o} \tau_o - \frac{A}{C}(k-1) \lambda^3 \cosh(\lambda l) - \frac{A}{C} \lambda^3 - C2(2m^3)}{2m^3} \quad (23)$$

and

$$C2 = \frac{-\frac{A}{C} \lambda^2 \sinh(\lambda l)}{2m^2}. \quad (24)$$

The maximum peel stress in the joint is at $x = 0$. Substituting this value into Equation (22) results in the following relation.

$$\sigma_{peel, \max} = \frac{E_a}{t_a} \left(C1 - \frac{A}{C}(k-1) \sinh(\lambda l) \right) \quad (25)$$

This expression can be simplified by substituting in Equations (19), (21) and (23).

$$\sigma_{peel, \max} = \frac{E_a t_o P \lambda (k-1)}{2 t_a k} \left[\frac{1}{2 D_o m^3} - \frac{\lambda}{\left(D_o \lambda^4 + \frac{E_a}{t_a} \right)} \left(\frac{\lambda^3}{2 m^3} + 1 - \frac{\lambda^2}{2 m^2} \right) \right] \quad (26)$$

This equation for the maximum peel stress has been simplified and is in terms of material and geometric constants. The simplification is accomplished by using the relations that hyperbolic cosine and sine are approximately equivalent at arguments larger than 2 which will occur in all practical tee-joints and by dropping lower order terms. The argument of

the hyperbolic functions is λl where λ is defined in Equation (16) and l is the length of the joint. In the generic tee-joint detailed above, λl is equal to approximately 10 and variations through a wide range of values both in geometric and material constants still result in this argument being larger than 2.

5.1.2 Plastic Shear Deformation in the Adhesive

The second approximate method, as mentioned earlier, assumes that the adhesive layer in the joint is undergoing perfectly plastic shear deformation. This simplification causes the right hand side of Equation (12) to be equal to zero and the result is the particular solution as seen in Equation (13). This process is detailed in Hart-Smith [1974] for aerospace structures composed of carbon/epoxy laminates and results in the following solution

$$_{peel}(x) = \tau_p t_o m e^{-mx} \cos(mx) \quad (27)$$

which has a maximum at the free surface where $x = 0$. The maximum is found using the following relation.

$$_{peel,max} = \tau_p t_o m \quad (28)$$

In these equations, τ_p is the adhesive plastic cut off shear stress.

Although this method is documented, the usefulness of the solution depends on factors which are not discussed in the reference, Hart-Smith [1974]. There is no mention of the length of plastic deformation necessary and the expressions are load independent. This independence causes problems in that the designer must determine whether or not the adhesive is undergoing plastic deformations to decide which equation is applicable. Also, the adhesive plastic cut off shear stress is usually not well characterized. An approximate value can be found by transforming the stresses using the Von Mises criterion for distortion energy for the isotropic adhesive layer. This transformation is as follows

$$_y = \cos 45 \sqrt{[(\sigma_1 - \sigma_2)^2 + (\sigma_2 - \sigma_3)^2 + (\sigma_3 - \sigma_1)^2]} \quad (29)$$

In this equation, $\sigma_1 = \tau$, $\sigma_2 = -\tau$, and $\sigma_3 = 0$. Substitution leads to

$$_y = \frac{1}{\sqrt{2}} \sqrt{6\tau^2} \quad (30)$$

where σ_y and τ_y are the yield stresses of the adhesive material. From this relation, the adhesive plastic cut off shear stress can be found, as a rough approximation, to be about 58% of the axial value,

$$_y = \frac{\sigma_y}{\sqrt{3}} \quad (31)$$

5.1.3 Transverse Shear Deformation of the Adherend

In another approximate method of modeling a double lap joint, or Section A of the divided tee-joint, the shear deformation of the adherend must be examined. This need is dictated by the large anisotropy of many composite joints through the thickness where the properties are matrix dominated in comparison to the in-plane, fiber dominated properties. An equation modeling the shear deformation of the adherend is derived in the following

manner. The deflection, w , of the outer adherend which is undergoing elastic bending due to transverse shearing is given by

$$\frac{d^2 w}{dx^2} = B \frac{dQ}{dx} - CM \quad (32)$$

where the constants are given by the following expressions

$$B = \frac{6}{5t_o G_{13}} \quad (33)$$

and

$$C = \frac{1}{D} = \frac{12(1 - \nu_{12}\nu_{21})}{t_o^3 E_1} \quad (34)$$

The peel stress is given by

$$= E_a \frac{w}{t_a} = Aw \quad (35)$$

for a thin adhesive layer. Combining Equations (32) and (35) results in,

$$\frac{d^4 \sigma}{dx^4} = A \left[B \frac{d^3 Q}{dx^3} - C \frac{d^2 M}{dx^2} \right] \quad (36)$$

The equilibrium equations for the outer adherend are

$$\frac{dQ}{dx} = \sigma \quad (37)$$

for vertical equilibrium and

$$\frac{dM}{dx} = Q - \tau \frac{t_o}{2} \quad (38)$$

for moment equilibrium. As in Section 5.1.2, the shear stress in the adhesive layer can be assumed to be perfectly plastic near the ends of the joint where the peel stress is highest. If this assumption is made, then the shear stress is a constant in this region and Equation (38) reduces to

$$\frac{d^2 M}{dx^2} = \frac{dQ}{dx} = \sigma \quad (39)$$

Combining this equation, (39) with Equation (36) yields the governing differential equation of the moment in the adherend,

$$\frac{d^6 M}{dx^6} + E \frac{d^4 M}{dx^4} + F \frac{d^2 M}{dx^2} = 0 \quad (40)$$

where for simplicity $E = -AB$ and $F = AC$. The solution to Equation (40) is found from the following characteristic equation,

$$\lambda^4 + E\lambda^2 + F = 0 \quad (41)$$

For the case of adherends with high through-thickness anisotropy, for which $E^2 > 4F$, the roots of Equation (41) are given by the following equations.

$$\lambda_{1,2} = \pm \left[\frac{-E + \sqrt{E^2 - 4F}}{2} \right]^{\frac{1}{2}} = \pm a \quad (42)$$

$$\lambda_{3,4} = \pm \left[\frac{-E - \sqrt{E^2 - 4F}}{2} \right]^{\frac{1}{2}} = \pm b \quad (43)$$

As in the previous cases, the portion of the joint under investigation is near the end of the joint where $x = 0$ and only the decaying part of the solution is retained.

$$M(x) = C_1 e^{-ax} + C_2 e^{-bx} \quad (44)$$

Using the same boundary conditions as in the previous sections, zero moment and shear at $x = 0$, the solution has the following form

$$M(x) = \frac{\tau_p t_o}{2(a-b)} (e^{-ax} - e^{-bx}). \quad (45)$$

The peel stress can be found from this relation by using Equation (39),

$$\tau_{peel}(x) = \frac{\tau_p t_o}{2(a-b)} (a^2 e^{-ax} - b^2 e^{-bx}). \quad (46)$$

The peak peel stress in the adhesive layer is at $x = 0$ and is given by

$$\tau_{peel, max} = \tau_p \frac{t_o}{2} (a + b) \quad (47)$$

where a and b are defined in Equations (42) and (43), respectively.

The three expressions for the maximum peel stress generated in the adhesive layer, Equations (26), (28) and (47), are compared to finite element results in the following section.

5.1.4 Finite Element Verification

Finite element analyses are used to determine the validity and usefulness of the above equations for the maximum peel stress and the peel stress profiles. Several effects are examined including varying the adherend/overlamine thickness, the applied load, the adhesive plastic cut off shear stress and the materials.

An initial examination of the finite element analyses shows that the computed maximum peel stress varies with the dimension of the elements. As the element size decreases, the peak, peel stress increases, as is typically found in regions with singularities or intense stress concentrations when using displacement formatted FEA. The stress profiles are similar, only the maximum computed peel stress changes. This observation is illustrated in Figure 5.1.2. This illustration shows that, while the peel stress profile remains the same for the more refined meshes, the peak stress varies considerably. Figure 5.1.3, shows the variation of the maximum peel stress as a function of the final element size in the adhesive layer of the various finite element meshes.

As the elements become smaller, the maximum peel stress increases, but the profile is the same over a range of sizes. This can be seen in Figure 5.1.2, where the two profiles with the smallest final mesh size are virtually identical except for the peak peel stress values. This observation implies that an accurate maximum peel stress can be found a set distance away from the termination of the adhesive layer. This can also be seen in Figure 5.1.2 where the amount of increase in peak peel stress between various meshes begins to

decrease. By examining the stress profiles from the more refined meshes, a criterion can be created to help determine the maximum peel stress in each configuration.

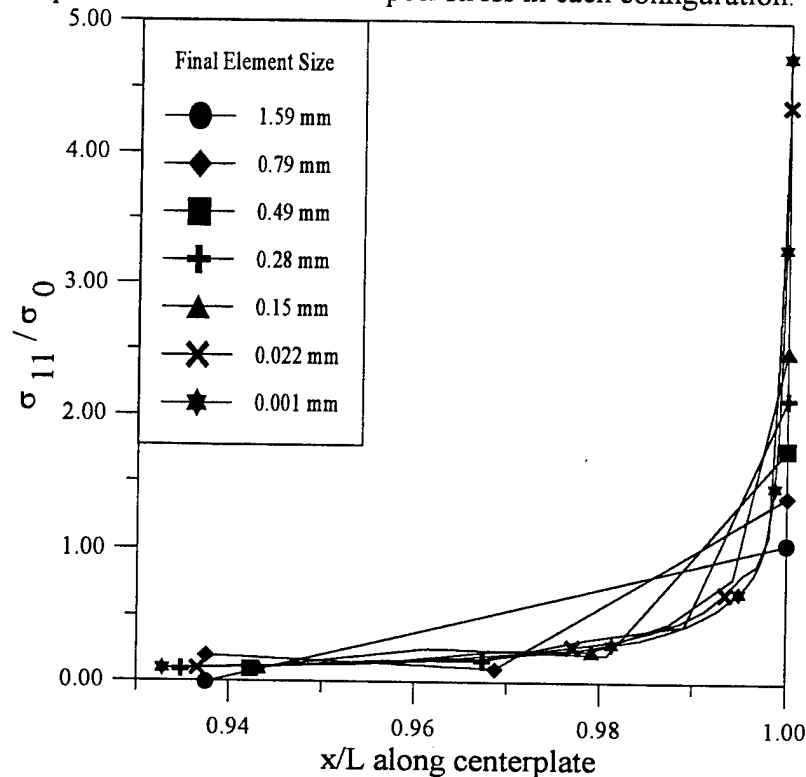


Figure 5.1.2: Peel stress profiles for various finite element meshes with varying element sizes.

Since, the relative change between the calculated, maximum peel stresses decreases as the element size decreases and the main difference between the more refined cases is in the computed maximum peel stress, an accurate assessment of the peak peel stress can be made a small distance from the termination of the overlaminates. See Figures 5.1.2 and 5.1.3. This distance should be small in comparison to the bond line thickness and has been chosen as one tenth of the bond line or .0127 mm. This length is small enough to both capture the quickly increasing peel near the termination of the overlaminates and results in similar peak peel measurements for the more refined models.

The stress profiles predicted by the various models are illustrated in Figure 5.1.4. From this graph, it can be seen that the stress profiles from the analytical and finite element methods are different. The profile predicted by the finite element methods increases sharply at the overlaminates termination while the other analytical approximations predict a more gradual stress increase.

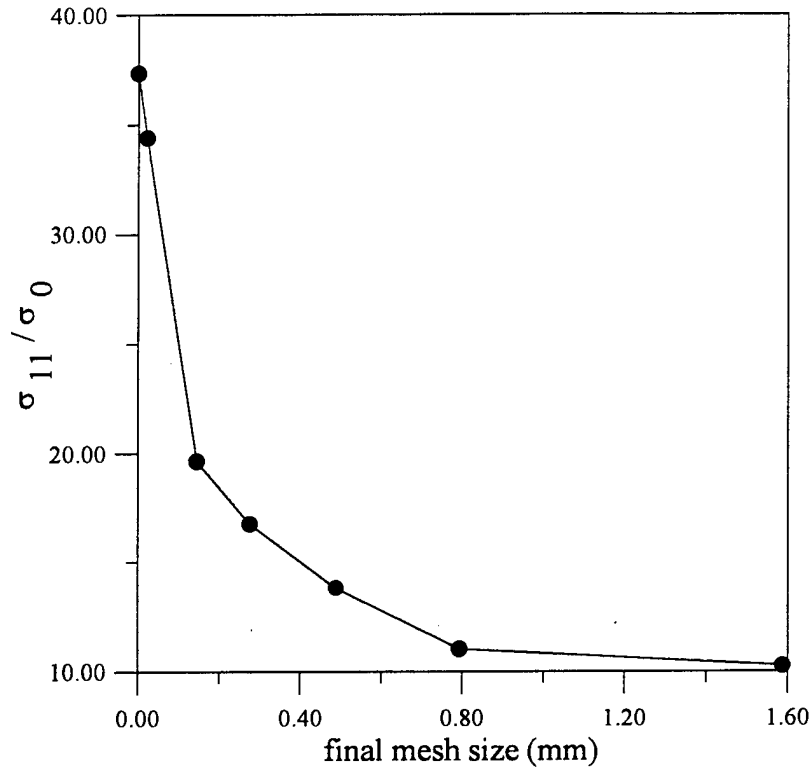


Figure 5.1.3: Peak peel stress as a function of the size of the final element in the adhesive layer from various finite element models.

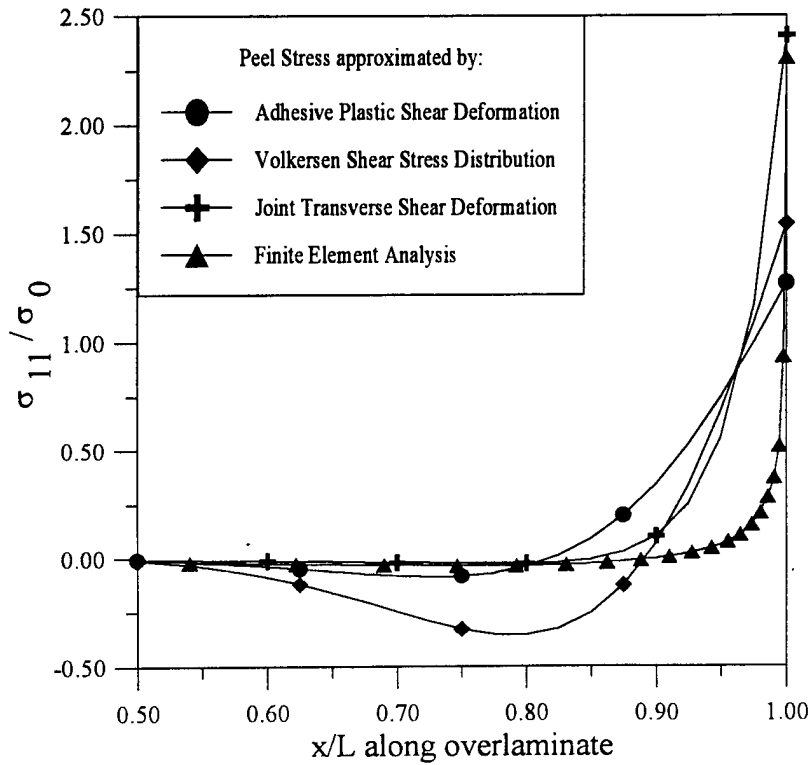


Figure 5.1.4: Analytical and numerical peel stress profiles for the generic tee-joint with a R_m/t of 4 and a load of 1000 N.

Another graph is included illustrating the effects of increasing the anisotropy on the computed stress profiles. See Figure 5.1.5. The material used in this figure is a typical $[0^\circ / 90^\circ]_s$ graphite/epoxy laminate. In this case, the finite element and analytical stress profiles are different, but the profiles are closer than those shown in Figure 5.1.4. The generic tee-joint geometry used in the models shown in Figure 5.1.5 is not designed for graphite/epoxy laminates and greater accuracy should be achieved when using a more realistic design with thinner overlaminates.

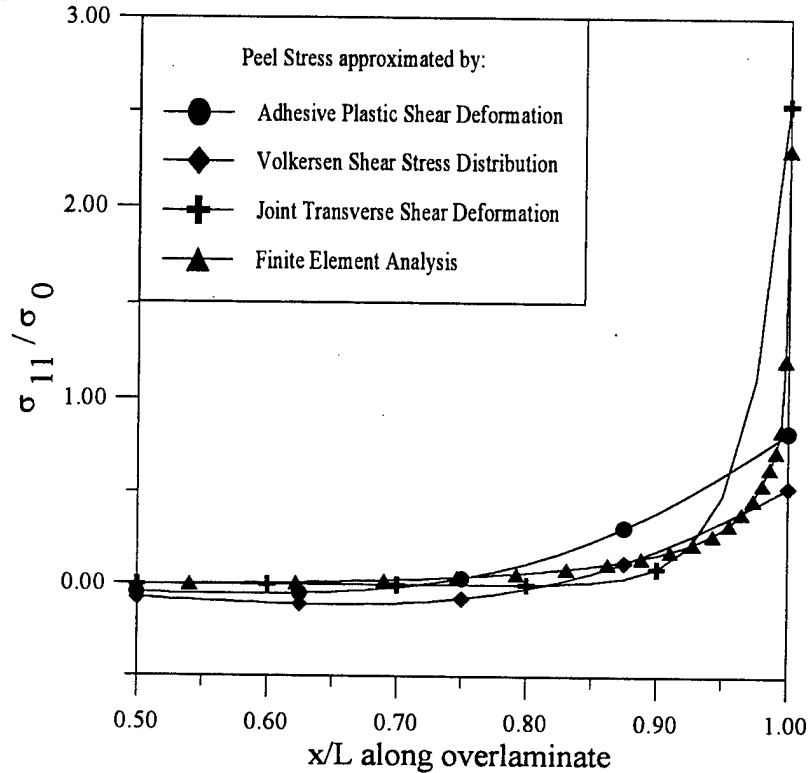


Figure 5.1.5: Peel stress profiles for a tee-joint constructed from a Carbon/epoxy laminate compared to the analytical expressions.

Even though the peel stress profiles between the models are different, the maximum predicted peel stresses from the various analytical models are still of interest. Using the criteria mentioned above, the maximum peel stress, $\sigma_{\text{peel, max}}$, is presented as a function of the overlaminate thickness, see Figure 5.1.6. From this figure, it can be seen that the trend in $\sigma_{\text{peel, max}}$ is most closely modeled by the case using joint transverse shear deformation as discussed in Section 5.1.3.

This model assumes that the outer adherend or overlaminate is undergoing uniform shear deformation. With thin overlaminates/adherends, this is a good assumption. The largest, percentage difference between the finite element profile and the numerical model is approximately 15% for models with overlaminate thickness of less than 6.35 mm or one half the centerplate thickness. However, as the thickness of the outer adherend increases, the shear deformation is localized near the adhesive layer. See Figure 5.1.7. This figure

illustrates the difference in shear stress profiles for tee-joints with thin, 3.175 mm, and thick, 12.7 mm, overlaminates.

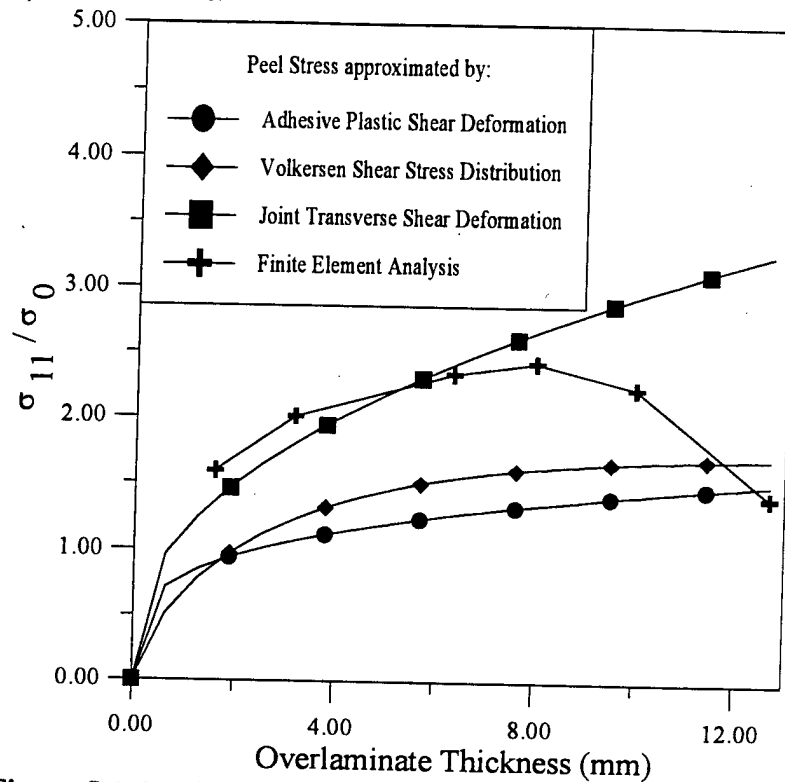


Figure 5.1.6: The maximum peel stress (MPa) as a function of overlamine thickness calculated by both analytical and finite element methods with a load of 1000 N.

It can be seen that in the model with a thick overlamine the shear stress, and therefore shear deformation, is localized near the adhesive/centerplate interface. In the case with a thin overlamine, the shear stress distribution is more linear throughout the overlamine thickness although it is still localized near the adhesive layer. This change in shear deformation profile between these cases results in large errors in the numerical model as compared to the finite element analysis for models with thick overlaminates. The model, as presented in Figure 5.1.6, with an overlamine thickness of 12.7 mm results in a large relative error, $\approx 55\%$, when compared to the FEM predicted value. The material properties of the overlaminates also alters the shear deformation profile in the joint.

This model is also highly dependent upon the adhesive plastic yield stress which is not a well documented material property for many resin systems. The approximation mentioned in Section 5.1.2 is used to find the adhesive plastic yield stress as a function of the tensile yield stress. In this case, τ_p is equal to 46 MPa, 58% of the tensile yield stress based on a simple application of the Von Mises yield criterion. This model is also independent of the applied loading and assumes that the adhesive is undergoing plastic shear deformation. Because of this assumption, this model does not closely approximate the maximum peel stress at low load levels. This observation is illustrated in Figure 5.1.8. This figure indicates that the load is too low to cause plastic shear deformation in the

adhesive layer. Due to this low load, the models that are independent of the applied loading, the adhesive plastic shear deformation and joint transverse shear deformation approximations, overestimate the maximum peel stress in the tee-joint.

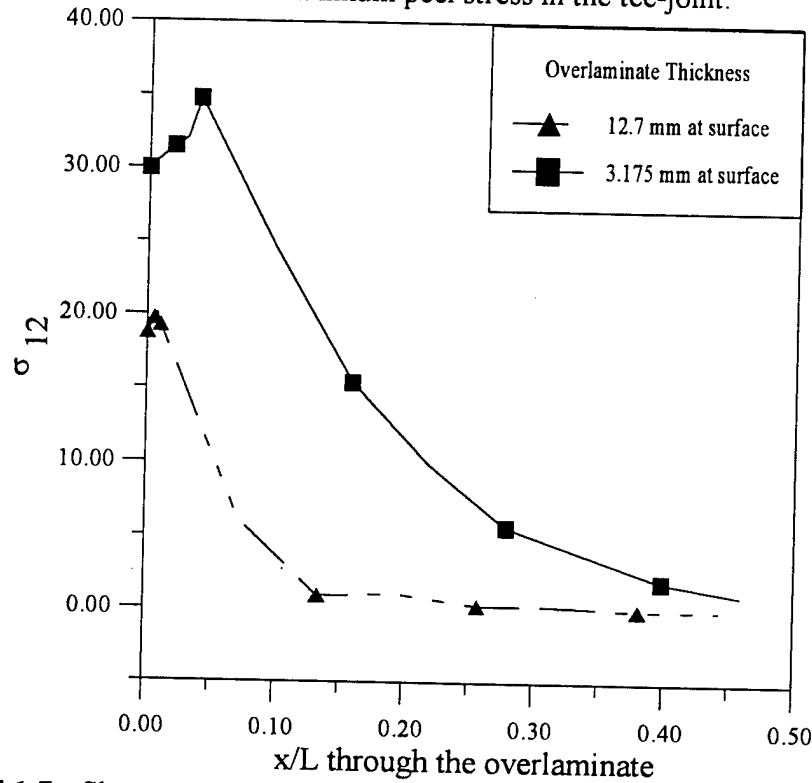


Figure 5.1.7: Shear stress profile in the overlamine measured a short distance, .45 mm, from the surface where L is the total thickness of the overlamine.

At these lower loading levels, the peel stress is more accurately represented by the Volkersen shear stress distribution model which depends on the applied loading in the joint. In Figure 5.1.8, the percentage difference between the finite element analysis and the Volkersen shear stress distribution model is approximately 45%. Although this difference is large, this model is the only one which approximates the loading condition in this section of the tee-joint at lower loading levels. But, this case is not usually of much interest, due to the higher risk of failure of the tee-joint structure at higher loads. Also at load levels where there is a risk of failure, the adhesive should be undergoing perfectly plastic shear deformation for most well balanced tee-joints. Because of these reasons, the Volkersen shear stress distribution approximation should be used for models with lower load levels or linear materials. For other cases with non-linear materials or higher load levels, the joint transverse shear deformation approximation most closely calculates the peak peel stress.

The methods mentioned here for approximating the maximum peel stress in Section A of the divided tee-joint structure, as well as a double lap joints, result in different predictions depending upon loading conditions and geometric parameters. The model which examines the joint transverse shear deformation results in the most accurate predictions assuming an accurate plastic shear yield stress, high loading levels which result

in perfectly plastic shear deformation in the adhesive layer and thin overlaminates where the shear deformation profile is uniform. As long as these conditions are met, the model results in accurate predictions. The other models are less accurate for the range of materials and geometries considered in this study.

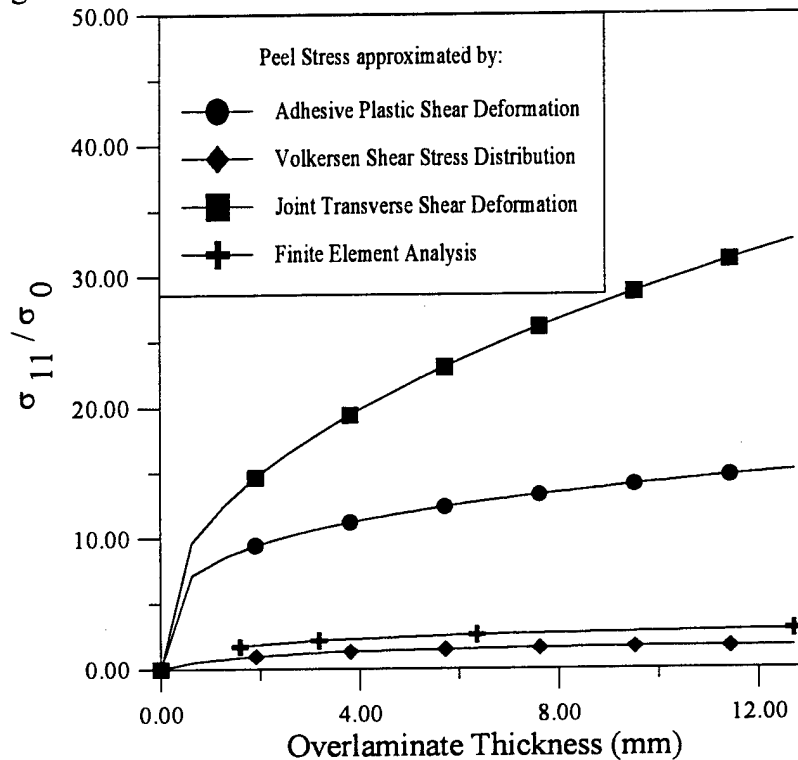


Figure 5.1.8: The maximum peel stress (MPa) as a function of overlamine thickness calculated by both analytical and finite element methods with a load of 100 N.

5.2 Section B: Vertical Doubler

Throughout this study, this section of the tee-joint is not shown to be critical. The stresses in this region are lower than those seen in other sections for all tee-joint configurations studied in this work. Because of this result, Section B, as illustrated in Figure 1.2, has not been examined in depth.

In this section of the tee-joint, the stress transfer from the centerplate to the curved overlaminates continues, but the peak values for the peel and shear stresses are manifest in the double lap section of the tee-joint. This can be seen in various contour plots shown earlier, such as Figures 4.4.6 and 4.5.3. The positioning of this section of the tee-joint is illustrated in Figure 5.2.1 and the area shown in the following figures is highlighted. Stress contour plots of this section of the tee-joint are included in Figures 5.2.2. and 5.2.3. In these figures, the generic tee-joint configuration, shown earlier in Figure 4.1.2, has been segmented to generate contour plots of this area. The stresses in these figures are lower than those seen in other areas and this site will not be critical in the tee-joint design with a pull-off load.

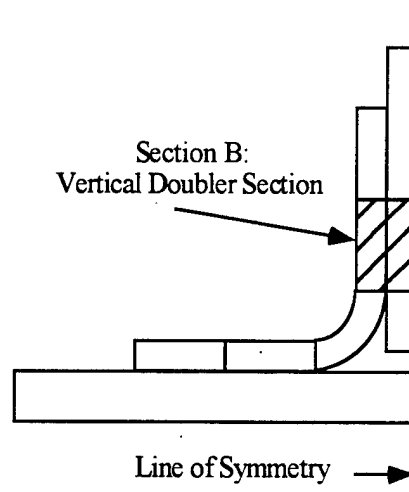


Figure 5.2.1: The shaded area in this figure is the vertical doubler section which is illustrated in the following stress contour plots.

From these contour plots, a few insights can be gained into the mechanics of the tee-joint structure. Examining Figure 5.2.2, shows that the vertical stress profile through the thickness of the overlamine never reaches an equilibrium state where the stress is uniform across the cross section. The stress is still being transferred from the centerplate to the overlaminates in this section with this configuration. This result can change as either the length of the overlamine is increased or the thickness of the overlamine is decreased.

As can be seen from the peel stress profiles presented in Section 5.1, Figures 5.1.4, 5.1.5 etc., the peel stress is slightly compressive near the top of Section B. This result is shown in Figure 5.2.3. As in a double lap joint, the peel stresses begin to increase at the base of this section near the curved region of the structure, but this is due to completely different mechanisms from those in a double lap joint and is of a much lower magnitude than the peel stresses examined in Section A. It can also be seen from this contour plot, Figure 5.2.3, that there are peel stresses at the base of this section attempting to pull the overlamine off of the centerplate. This effect is due to the continuing transfer of stress from the centerplate to the overlaminates and the transition from a vertical doubler to a region with an increasing large fillet region. Also, the peak radial stresses generated in the curved region occur in the portion of the curved section a small distance away from the interface between Sections B and C, see Figure 5.2.1 and Section 5.3. The effect of these stresses generating by the bending moment in the curved section result in a peel stress at the base of this section, as shown in Figure 5.2.3.

ABAQUS

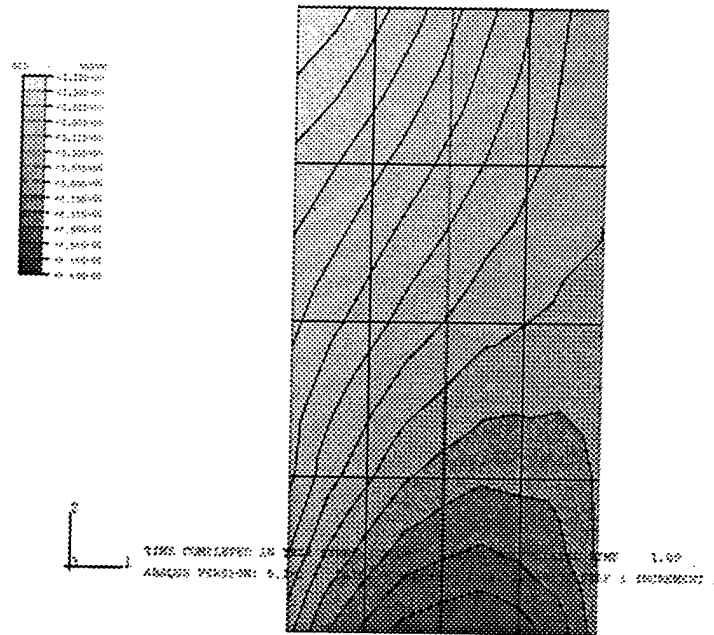


Figure 5.2.2: Vertical stress contour plot detailing Section B of the generic tee-joint, the vertical doubler section.

ABAQUS

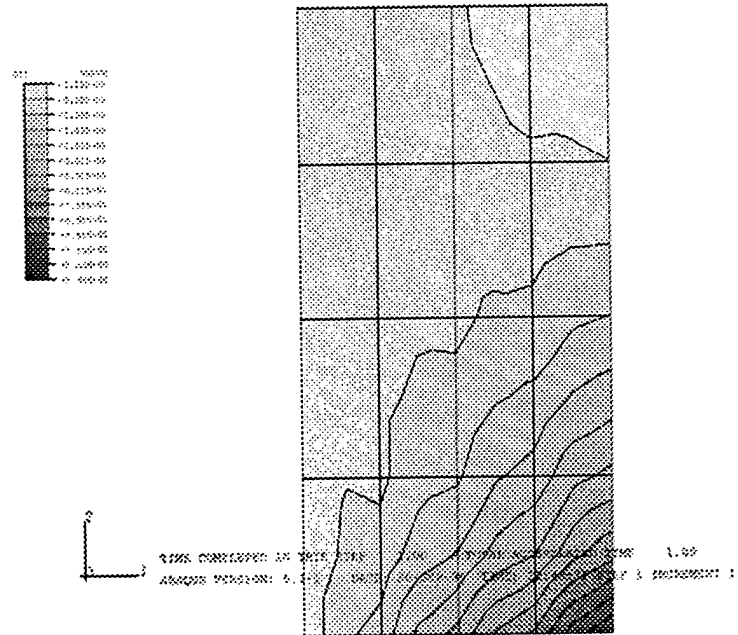


Figure 5.2.3: Horizontal stress contour plot detailing Section B of the generic tee-joint, the vertical doubler section.

5.3 Section C: Curved Region

An important piece of the separated tee-joint is the curved portion of the overlamine. The importance of this section is often critical due to the low relative through-the-thickness strength of polymer matrix composite systems. As the stress is transferred around the bend in this region, the member attempts to straighten out creating tensile stress in the short, transverse direction or, in polar coordinates, the radial direction. The PMC system's strength in this orientation may only be a few percent of the longitudinal strength. Due to this factor, curved regions are a critical factor in the design of composite structures.

This section of the tee-joint is a curved laminate loaded in tension, bending and shear. An examination of this beam will start with classical elasticity solutions for curved beams loaded under pure bending and point loads for both isotropic and anisotropic conditions. The evaluation will continue with the examination of simplified approaches and a demonstration of the relative differences between these approaches. These expressions will also be compared to finite element models conducted with the ABAQUS program both as an isolated curved beam and as a portion of the complete tee-joint structure.

In Section 4, the importance of this segment of the tee-joint was illustrated. In the various tee-joint configurations, the curved region is usually the most critical area of concern. Tee-joints can be designed such that other areas are of primary concern. But, in a balanced design with tapers, the focus returns to the curved region.

5.3.1 Classical Elasticity Methods

The first case to be examined is pure bending of an isotropic curved bar as given by Timoshenko and Goodier [1970]. The geometry and terminology is given in Figure 5.3.1. For this configuration, the stress components are:

$$r = -\frac{4M}{N} \left(\frac{R_i^2 R_o^2}{r^2} \ln \frac{R_o}{R_i} + R_o^2 \ln \frac{r}{R_o} + R_i^2 \ln \frac{R_i}{r} \right) \quad (48)$$

$$\theta = -\frac{4M}{N} \left(-\frac{R_i^2 R_o^2}{r^2} \ln \frac{R_o}{R_i} + R_o^2 \ln \frac{r}{R_o} + R_i^2 \ln \frac{R_i}{r} + R_o^2 - R_i^2 \right) \quad (49)$$

$$r_{\theta} = 0 \quad (50)$$

where for simplicity

$$N = (R_o^2 - R_i^2)^2 - 4R_i^2 R_o^2 \left(\ln \frac{R_o}{R_i} \right)^2 \quad (51)$$

Similar relations, Equations (52) through (58), were created to compute the stresses in a cylindrically anisotropic, homogeneous curved beam with a rectangular cross section under pure bending by Lekhnitskii [1981] following the same terminology as shown in Figure 5.3.1. The assumption of homogeneity in the beam should give reasonable accuracy as long as the laminate is fairly thick and the ply orientations are evenly dispersed, Kedward, et al. [1989].

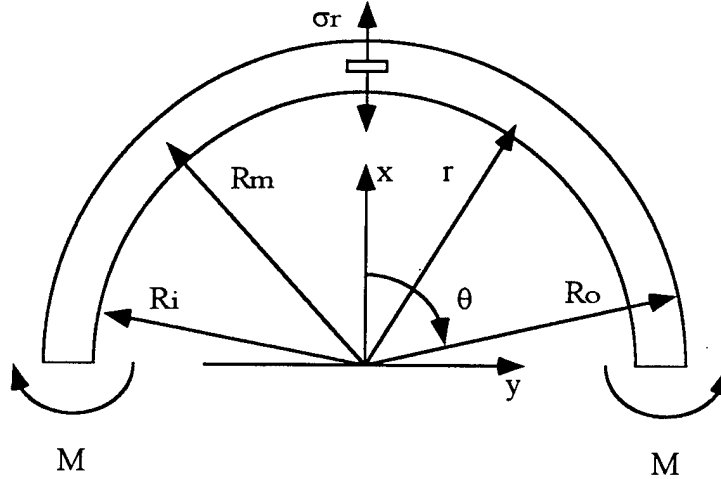


Figure 5.3.1: Geometry and terminology for the classical elasticity equations.

For the case of an applied end load, the moment is replaced by a point load, P , at an angle, ω , as measured from the x -axis.

$$r = -\frac{M}{R_o^2 b g} \left[1 - \frac{1-c^{k+1}}{1-c^{2k}} \left(\frac{r}{R_o} \right)^{k-1} - \frac{1-c^{k-1}}{1-c^{2k}} c^{k+1} \left(\frac{R_o}{r} \right)^{k+1} \right] \quad (52)$$

$$\theta = -\frac{M}{R_o^2 b g} \left[1 - \frac{1-c^{k+1}}{1-c^{2k}} k \left(\frac{r}{R_o} \right)^{k-1} - \frac{1-c^{k-1}}{1-c^{2k}} k c^{k+1} \left(\frac{R_o}{r} \right)^{k+1} \right] \quad (53)$$

$$r_\theta = 0 \quad (54)$$

where

$$c = \frac{R_i}{R_o} \quad (55)$$

$$k = \left(\frac{E_\theta}{E_r} \right)^{\frac{1}{2}} \quad (56)$$

$$g = \frac{1-c^2}{2} - \frac{k}{k+1} \frac{(1-c^{k+1})^2}{1-c^k} + \frac{k c^2}{k-1} \frac{(1-c^{k-1})^2}{1-c^{2k}} \quad (57)$$

The maximum radial stress occurs at the location given by:

$$r = \left[\frac{(k+1)(1-c^{k-1})c(R_i R_o)^k}{(k-1)(1-c^{k+1})} \right]^{\frac{1}{2k}} \quad (58)$$

Lekhnitskii [1981] also examines the case of a curved beam under bending due to an end load with the same terminology as in Figure 5.3.1. In this case, one end of the beam is assumed to be fixed and the forces acting along the other end of the beam can be simplified into a concentrated force, P , acting in the mid-plane of the beam. The stresses in this orientation are:

$$r = \frac{P}{R_o b g_1} \frac{R_o}{r} \left[\left(\frac{r}{R_o} \right)^\beta + c^\beta \left(\frac{R_o}{r} \right)^\beta - 1 - c^\beta \right] \sin(\theta + \omega) \quad (59)$$

$$\sigma_{\theta} = \frac{P}{R_o b g_1} \frac{R_o}{r} \left[(1 + \beta) \left(\frac{r}{R_o} \right)^{\beta} + (1 - \beta) c^{\beta} \left(\frac{R_o}{r} \right)^{\beta} - 1 - c^{\beta} \right] \sin(\theta + \omega) \quad (60)$$

$$\sigma_{r\theta} = -\frac{P}{R_o b g_1} \frac{R_o}{r} \left[\left(\frac{r}{R_o} \right)^{\beta} + c^{\beta} \left(\frac{r}{R_o} \right)^{\beta} - 1 - c^{\beta} \right] \cos(\theta + \omega) \quad (61)$$

where

$$\beta = \left[1 + \frac{E_{\theta}}{E_r} (1 - 2\nu_{r\theta}) + \frac{E_{\theta}}{G_{r\theta}} \right]^{\frac{1}{2}} \quad (62)$$

$$g_1 = \frac{2}{\beta} (1 - c^{\beta}) + (1 + c^{\beta}) \ln(c) \quad (63)$$

In this example, the location of the maximum radial stress when $\beta > 1$ is given by:

$$r = \left(\frac{R_o^{\beta}}{2(1 - \beta)} \left\{ 1 + c^{\beta} - \left[(1 + c^{\beta})^2 + 4c^{\beta} (\beta^2 - 1) \right]^{\frac{1}{2}} \right\} \right)^{\frac{1}{\beta}} \quad (64)$$

This set of classical elasticity equations, Lekhnitskii [1981], provides one means of testing the validity of the simplified equations presented later in this report. Many factors will be examined such as the effects of geometry, the R/t ratio, and the effects of increasing anisotropy when using different materials and laminates.

5.3.2 Simplified Design Orientated Expressions

Using the continuing example of a curved beam under opening end moments, an estimate for the maximum radial stress, σ_r , is derived by Ko [1988] from classical elasticity equations for the condition that the thickness of the beam is small. This equation is

$$r_{\max} = \frac{3M}{2btR_m} \quad (65)$$

where t is the thickness and R_m is the mean radius. Other approximations are also detailed in Kedward et al. [1989], such as:

$$|\sigma_{r,\max}| = \frac{12M}{bt^3} \left\{ \left[R_i (R_i + t) \right]^{\frac{1}{2}} - R_i \frac{t}{2} \right\} \quad (66)$$

This relation was derived by Mabson and Neal [1988]. This expression can be simplified to:

$$r_{\max} = \frac{12M}{bt^3} \left[R_m - (R_i R_o)^{\frac{1}{2}} \right] \quad (67)$$

This simplified relation is derived by using simple bending theory with the assumption of a linear distribution of the circumferential stress. The major change between these expressions is the assumed position for the value of the maximum radial stress. The first expression, Equation (65), assumes the maximum occurs along the central plane where $r = R_m$. The subsequent relations, Equations (66) and (67), assume the correct location of the maximum radial stress, $r = (R_i R_o)^{1/2}$. A correction can be applied to Equation (65), so that $\sigma_{r,\max}$ is calculated at the correct location.

$$r_{\max} = \frac{3M}{2bt(R_i R_o)^{\frac{1}{2}}} \quad (68)$$

The exact values for the radial stress in the case of pure bending, as computed by using Equation (52), are compared to the values determined by the simplified expressions, Equations (65), (67), and (68), in Figure 5.3.2. Of the three expressions, Equation (68) gives the most accurate stress values with a maximum error of approximately 2% at $R_m/t = 1$. At increasing values of R_m/t , all three equations give excellent results and, at $R_m/t > 5$, the error is less than 1% for all the expressions. In this and subsequent graphs, the three methods discussed in this section will be referred to as Methods 1, 2 and 3 corresponding to Equations (65), (67) and (68), respectively. Most design applications would use values of $R_m/t \geq 2.5$, Kedward, et al. [1989], and current literature, Sheno and Hawkins [1992], on tee-joint design for marine applications suggests an even higher range of R_m/t values.

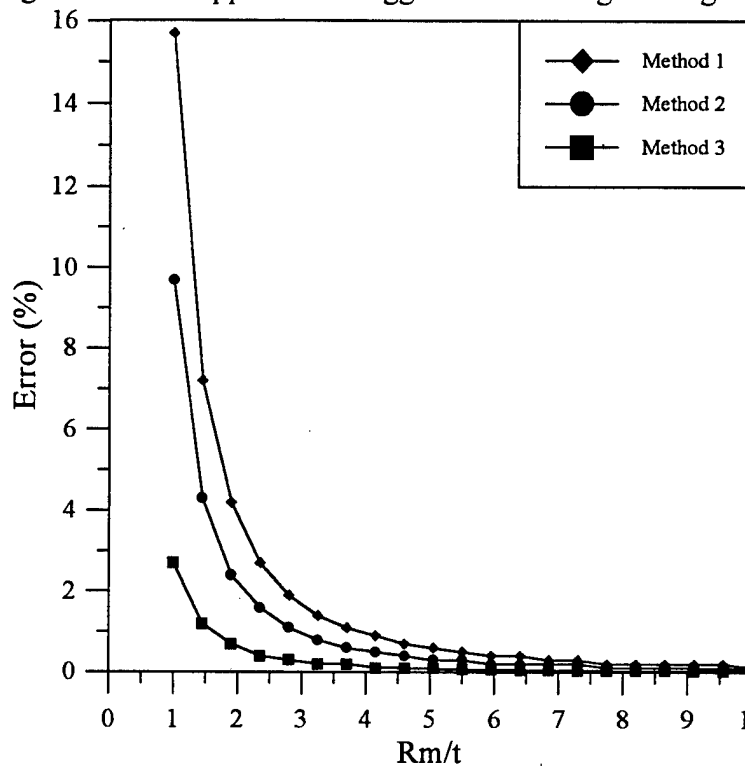


Figure 5.3.2: Comparison of the exact solution for the case of a curved beam under pure bending and the corresponding simplified relations.

At these levels, the accuracy of simplified expressions are excellent, especially Equation (68), for curved sections loaded under pure bending. The applicability of these equations to the more complex loading conditions in actual tee-joints will be examined later through the use of finite element codes.

The effects of anisotropy, again for the case of pure bending, are illustrated in Figure 5.3.3 by plotting the exact results for the radial stress and the results from Equation (68) versus the anisotropy parameter, k . At lower R_m/t levels and higher k , the difference in these two approaches increase. But, at practical ranges for the anisotropy parameter

and R_m/t , Equation (68) gives accurate results. The useful range for the anisotropy parameter is $k < 4$, for reference $k = 3.7$ for uni-directional graphite, T-300, and $k = 2.85$ for uni-directional E-glass, Mallick [1993]. These uni-directional values are upper bounds especially in marine applications where the use of quasi-isotropic or $[0^\circ/90^\circ]$ fiberglass laminates is planned.

The exact values for the maximum radial stress, as computed by Equation (59) using the value of r found by Equation (64), are compared to the results determined by using the simplified relations for the case of an applied end load. These equations are modified by replacing the applied moment by the magnitude of the point load multiplied by the mean radius. Unlike the pure bending case, where the maximum radial stress occurs along the entire beam, in the case of an applied end load, $\sigma_{r, \max}$ occurs only at the mid point of the span where $\theta = 0$ as shown in Figure 5.3.4. Also, it should be noted that the maximum shear stress is developed at $\theta = \pm \pi/2$ and has the same value as the maximum radial stress to a first approximation.

Figure 5.3.5 illustrates the percentage error between the exact Lekhnitskii equations, Lekhnitskii [1981], and the simplified relations. At lower R_m/t levels, the accuracy varies depending upon which equation is used, Equation (65) is the most accurate differing by approximately 10% at reasonable R_m/t values, ≥ 2.5 .

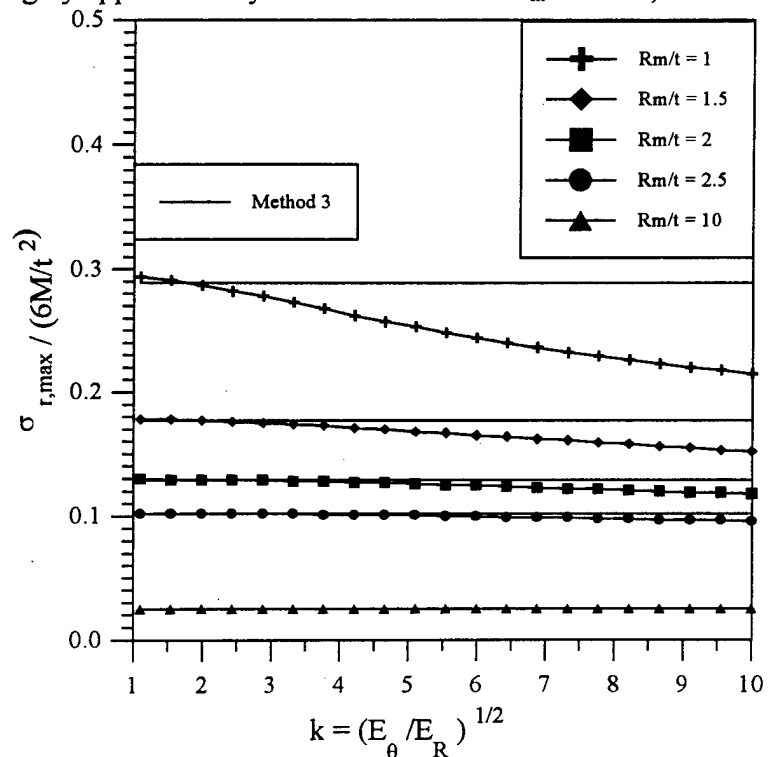


Figure 5.3.3: Comparison between the exact solutions and simplified relations for the case of pure bending as a function of the anisotropic parameter, k .

As R_m/t increases, all three relations approach a percentage difference of approximately 11%. Due to the fairly constant values for all the simplified relations and the asymptotic

behavior at increasing R_m/t , a simple numerical correction factor, a proportionality constant of .9, will give improved results. This type of change is easily incorporated into all of the approximate relations.

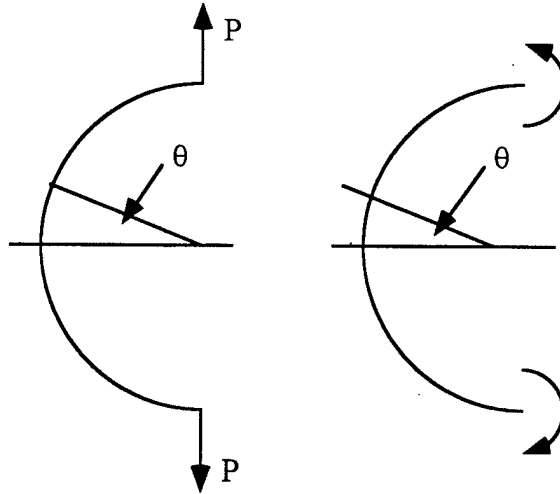


Figure 5.3.4: Illustration of the curved sections under the appropriate loading conditions and the areas of applicability of the simplified relations for the maximum radial stress.

In the case of an applied end load, the level of anisotropy is measured by β as defined in Equation (62), for reference $\beta = 3.7$ for uni-directional E-glass and 5.5 for uni-directional graphite, T-300. The effects of increasing anisotropy are illustrated in Figure 5.3.6, for the simplified expressions, Equations (65), (67), and (68). In this case, at larger values of R_m/t , the exact solution becomes constant for the entire range of β and the simplified expressions all give approximately the same result with a relative error of 11%. As in the previous case, where the R_m/t factor was varied, a correction factor of .9 would improve the accuracy of the approximate equations. With this constant, all three relations give results within 2% of the exact equations for $R_m/t = 4$ and $\beta = 3.77$.

Various finite element models were carried out in order to examine the accuracy of these simplified relations. The first approximations are for the cases of curved beams under pure bending and a point end load. In these cases, the model consisted of 8 noded, plane strain elements in a 90 degree section of a curved beam with one side fixed and the other side loaded appropriately. The finite element mesh is shown in Figure 5.3.7. The resulting stress contour plots in the radial direction under pure bending and an applied end load are illustrated in Figs. 5.3.8 and 5.3.9, respectively. For these models, the material used was uni-directional E-glass, a subsequent model will be run using a $0^\circ / 90^\circ$ E-glass laminate. The properties for these materials are included in Table 3.1. The results from the FE models are compared to the exact and simplified solutions in Table 5.1.

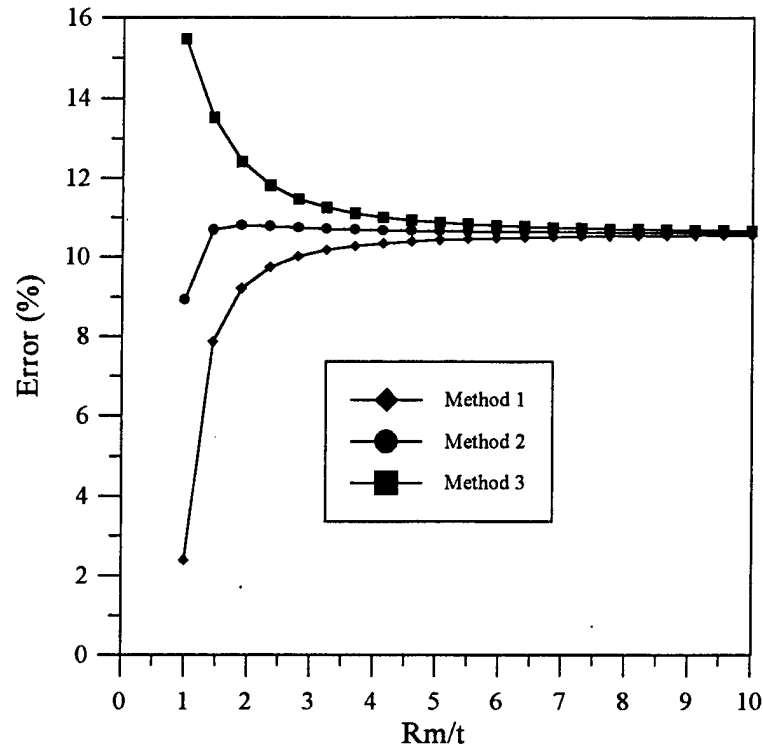


Figure 5.3.5: Comparison of the exact solution for the case of a curved beam under an applied end load and the corresponding simplified relations.

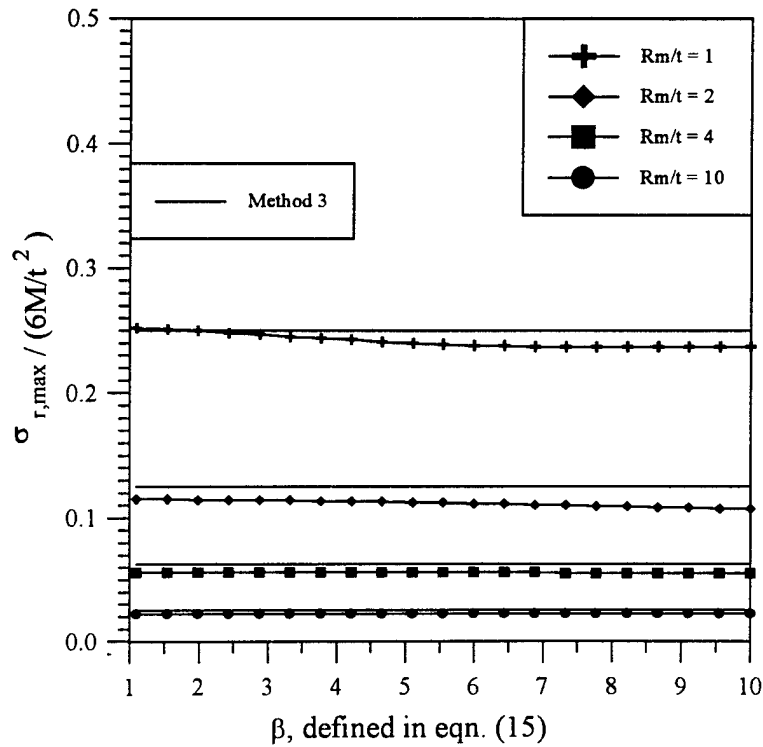


Figure 5.3.6: Comparison between the exact solutions and simplified relations for the case of an applied end load as a function of the anisotropic parameter, β .

ABAQUS

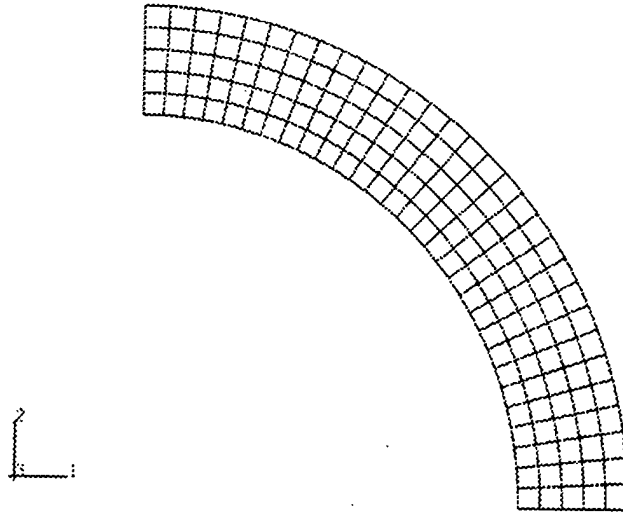


Figure 5.3.7: Finite element mesh used in testing the validity of simplified relations in simply curved beams.

Table 5.1: Comparison of the results of various methods with uni-directional E-glass, a R_m/t ratio of 4 and a moment of 10672 Nm.

Method	Pure Bending	Applied End Load
Simplified Expressions	100 MPa	100 MPa
Finite Element Model	103.7 MPa	103.7 MPa
Exact Equations	100 MPa	89 MPa

As mentioned earlier, the simplified expression, for the case of an applied end load only, results in an answer which has a relative error of approximately 11%. Table 5.2 is included to illustrate the results of the various methods when using a $0^\circ/90^\circ$ E-glass laminate. These values show that the simplified relations and finite element models closely approximate the stresses computed by the exact relations, except for the case of an applied end load.

Table 5.2: Comparison of the results of various methods with a $0^\circ/90^\circ$ E-glass laminate, a R_m/t ratio of 4 and a moment of 10672 Nm.

Method	Pure Bending	Applied End Load
Simplified Expressions	100 MPa	100 MPa
Finite Element Model	103.4 MPa	103.5 MPa
Exact Equations	100 MPa	89 MPa

It can be seen from Figures 4.4.2, 4.4.8, and 4.4.9, that, although the simplified expressions introduced here closely approximate the exact equations for the cases of curved beams under end loads and applied moments, these simplified relations do not accurately approximate the stress levels present in the actual tee-joint structure. The stress profiles shown in the figures mentioned above are much different from the profiles in Figures 5.3.8 and 5.3.9. This difference is caused by various factors, including the complex loading conditions and the effects of the addition of an elastic backing, the resin fillet. The fillet shifts the maximum, radial stress from the center portion of the beam to the exterior edge of the member, see Figure 4.4.2. Various methods have been attempted to modify the simplified methods to more closely approximate the conditions seen in a tee-joint, but these have been unsuccessful. Because of these results, the simplified expressions presented should not be used to model the stresses in the curved portion of the tee-joint structure. These expressions are of use and accurate in other joint types which do not use a resin fillet, such as hat stiffeners and even tee-joints without a resin filler.

In an attempt to more accurately predict the radial stress in the curved region, the loading conditions examined above are combined to approximate the conditions seen in the actual tee-joint. Finite element models of this configuration do not resemble the in-situ curved region. The stress in this case is more evenly distributed over the thickness of

ABAQUS

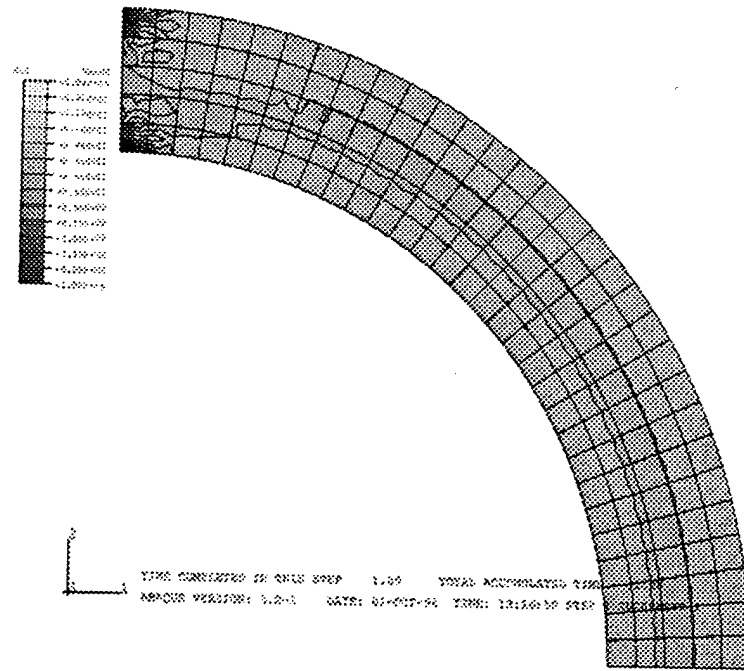
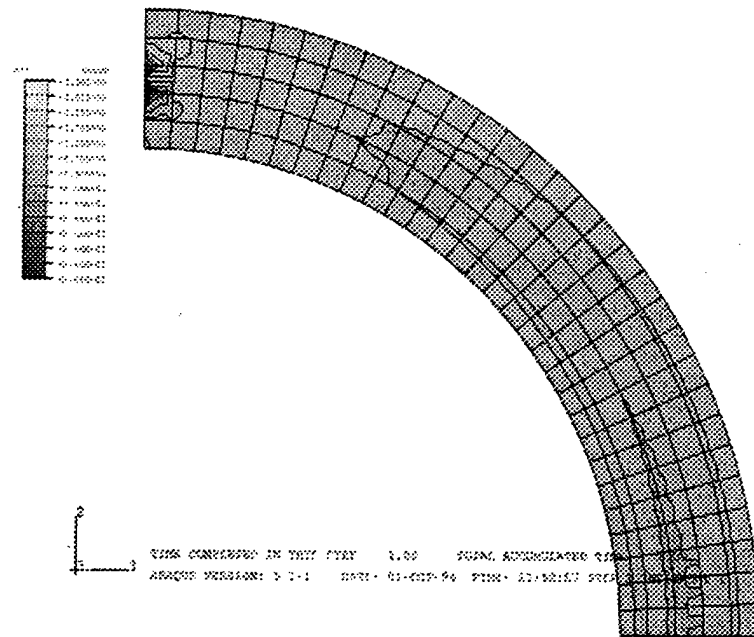


Figure 5.3.8: Radial stress contour plot for the case of pure bending.



75

the region unlike in the actual tee-joint. This modification does not improve the results from the simplified expressions as compared to the in-situ tee-joint.

Additional Considerations

The peak radial stress in the curved region can be obtained by using a modified beam on elastic foundation formulation as described in Hetenyi [1946]. This derivation is similar to those illustrated in Section 5.1 detailing the analysis of a double lap joint. The foundation forces in this analysis are assumed to always be perpendicular to the curved surface in the direction of the center of curvature. The derivation begins with the equilibrium equations for the system shown in Figure 5.3.10. As illustrated in this figure, an infinitesimal portion of the beam is acted on by a shearing force, Q , a normal force, N , a bending moment, M , and the reaction of the foundation, pdx . From this formulation, the equilibrium equations are

$$pdx - Nd\theta = dQ \quad (69)$$

in the radial direction,

$$Qd\theta = dN \quad (70)$$

in the tangential direction, and

$$dM = Qrd\theta \quad (71)$$

for the moment equilibrium equation. Substituting $p = ky$, where k is the stiffness of the elastic foundation, and $rd\theta = dx$ into the above equations and eliminating N and Q , results in the following expression,

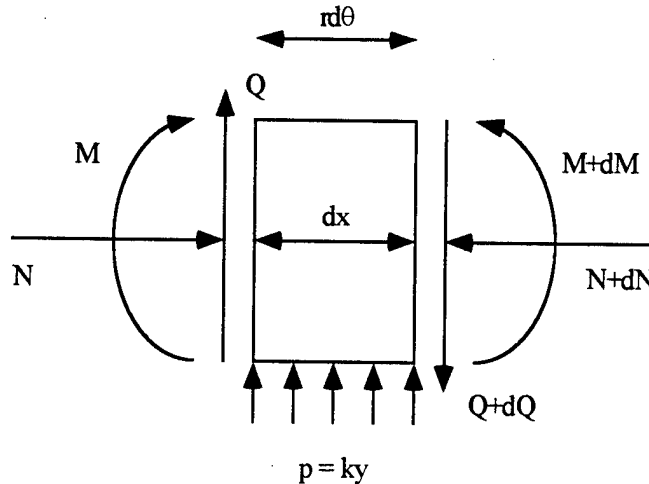


Figure 5.3.10: Free body diagram of a segment of a curved beam on an elastic foundation.

$$k \frac{dy}{dx} - \frac{1}{r^2} \frac{dM}{dx} = \frac{d^3 M}{dx^3} \quad (72)$$

This expression is modified by the differential equation of bending of a circular arch of radius of curvature r and flexural rigidity EI which with neglecting the axial deformation due to the normal force N is

$$EI \left(\frac{d^2 y}{dx^2} + \frac{y}{r^2} \right) = -M \quad (73)$$

Differentiating this expression and inserting into Equation (72) with $x = r\theta$, results in the differential equation for this system,

$$\frac{d^5 y}{d\theta^5} + 2 \frac{d^3 y}{d\theta^3} + \eta^2 \frac{dy}{d\theta} = 0 \quad (74)$$

where

$$= \sqrt{\frac{r^4 k}{EI} + 1}. \quad (75)$$

Equation (74) can be solved by substituting e^{mx} for y which results in the following characteristic equation,

$$m^5 + 2m^3 + \eta^2 m = 0. \quad (76)$$

The general solution of this equation is

$$y = C_0 + (C_1 \cosh \alpha\theta + C_2 \sinh \alpha\theta) \cos \beta\theta + (C_3 \cosh \alpha\theta + C_4 \sinh \alpha\theta) \sin \beta\theta \quad (77)$$

where

$$= \sqrt{\frac{\eta - 1}{2}} \quad (78)$$

and

$$\beta = \sqrt{\frac{\eta + 1}{2}}. \quad (79)$$

Equation (77) can be substituted into Equations (70), (71) and (73) to find expressions for N , M , and Q as functions of θ ,

$$N = rkC_0 + 2\alpha\beta \frac{EI}{r^4} [(C_1 \sinh \alpha\theta + C_2 \cosh \alpha\theta) \sin \beta\theta - (C_3 \sinh \alpha\theta + C_4 \cosh \alpha\theta) \cos \beta\theta], \quad (80)$$

$$M = -\frac{EI}{r^2} \{C_0 - 2\alpha\beta [(C_1 \sinh \alpha\theta + C_2 \cosh \alpha\theta) \sin \beta\theta - (C_3 \sinh \alpha\theta + C_4 \cosh \alpha\theta) \cos \beta\theta]\}, \quad (81)$$

$$Q = 2\alpha\beta \frac{EI}{r^3} [(\alpha C_1 + \beta C_4) \cosh \alpha\theta \sin \beta\theta + (\beta C_1 - \alpha C_4) \sinh \alpha\theta \cos \beta\theta + (\alpha C_2 + \beta C_3) \sinh \alpha\theta \sin \beta\theta + (\beta C_2 - \alpha C_3) \cosh \alpha\theta \cos \beta\theta]. \quad (82)$$

With these equations and the boundary conditions from the in-situ tee-joint, this problem can be solved to find the displacement and from that the maximum radial stress along the curved elastic foundation.

The boundary conditions for this problem consist of a curved beam constrained at one end and with applied loads at the other, see Figure 5.3.11. The applied loads can be modified and are chosen to approximate the conditions seen in the in-situ curved portion of a tee-joint. These values are dependent upon the geometry of the tee-joint and will have different values at the same applied load depending upon the thickness of the overlamine. Other geometric and material factors can also affect the load path through the joint, as discussed earlier in Section 4, but the overlamine thickness is the only factor examined in this section.

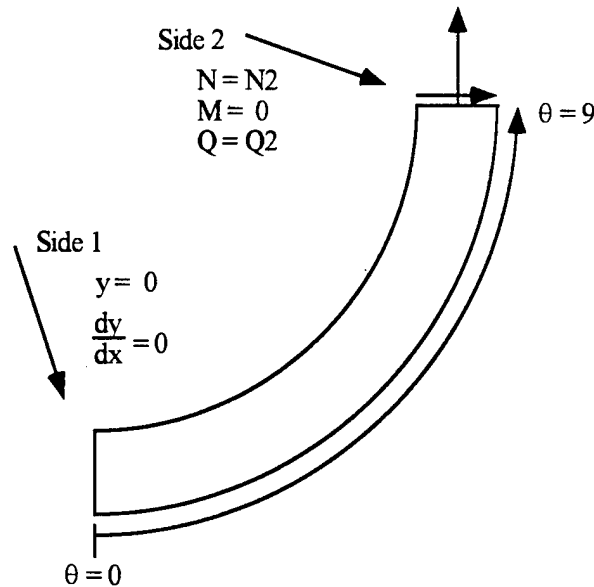


Figure 5.3.11: Boundary conditions for the curved beam on elastic foundation problem.

A difference between this analytical approximation and the actual tee-joint structure is caused by choosing a constant foundation stiffness, k . In the tee-joint, the thickness of the fillet changes depending upon the position along the curved region. This is accomplished by using the following equation,

$$k = E_a t_a. \quad (83)$$

In this expression, the effective thickness of the adhesive layer actually varies along the arc of the curved section. But, the assumption of a constant thickness is used to simplify the problem and the thickness chosen is that of the bond line. At this value the approximation yields more accurate results for the generic tee-joint configuration.

Figure 5.3.12 shows the displacement profiles for the two different methods as a function of position measured along the curve. It can be seen from this figure that, although both methods produce curves with the same general trend, the magnitude of the displacement is very different. The curved beam on an elastic foundation model only illustrates the deflection of the curved section while the FE model also incorporates the deflection of the baseplate and the centerplate. This is seen in Figure 5.3.12. The displacement values in the x and y directions, parallel and perpendicular to the baseplate respectively, from the FE model are combined to give the magnitude of the radial displacement. The largest component of this is the displacement in the y direction which is predominately caused by the deflection of the baseplate. Attempts have been made to separate the displacement solely due to the deflection of the curved section in the tee-joint from the other deflections, but this process is difficult due to the complex geometry of the tee-joint and the combination of several factors in producing the displacement of the curved section of an in situ tee-joint. Modifying the FE displacement by subtracting the baseplate displacement introduces errors in the section of the curved beam near the centerplate because of the added deflection due to the centerplate. Other attempts have

also proven ineffective in isolating the deflection in the curved region solely due to the bending of the curve.

The maximum radial stress predicted by this analytical approximation has been compared to the FE model results for a variety of R_m/t ratios. The curved beam on elastic foundation approach models the general trends in the radial stress such as predicting the location of the maximum radial stress and the change in stress with a corresponding change in the thickness of the curved region.

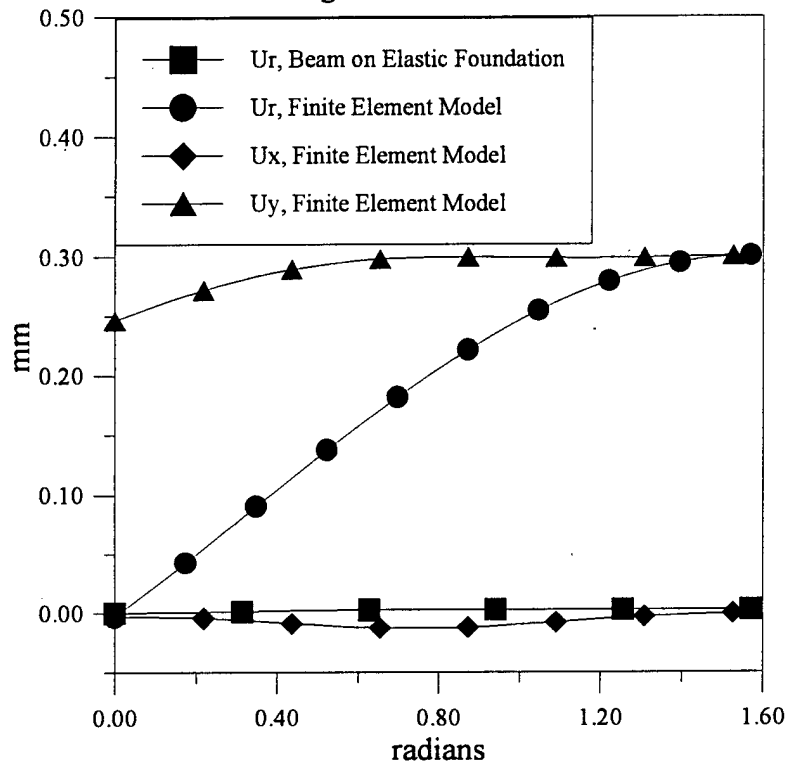


Figure 5.3.12: Radial displacement of the curved section as a function of θ computed by the analytical approximation and finite element methods.

As the thickness of the overlamine decreases, the position of the maximum radial stress moves from near side 2, as shown in Figure 5.3.8, at about 75° to near the middle of the curved section at about 35° . This change is also predicted by the analytical approximation. The approximation also shows the peak radial stress decreasing at smaller overlamine thicknesses, but the values from the two models differ by a factor of three. See Table 5.3.

Although this analytical approximation does model some of the trends that occur in the radial stress and displacement of the curved section of a tee-joint, the model is too complex to be used as a design tool. The purpose of this work is to create a set of design guidelines for the construction of polymer composite tee-joints. These guidelines are to be used in conjunction with FE modeling and other tools to design this type of structure. The current analysis does not conform to this need. The input necessary for the model, especially the boundary conditions, are highly dependent upon many geometric and

material parameters. As discussed in Section 4, the load path through the tee-joint changes with alterations in any of the many studied parameters. Because of this dependence, FE analysis must be conducted to correctly determine the boundary conditions for this model at which point examining this analytical approximation becomes redundant. Due to the departure from the simplified methods desired in this work, this approach has only been examined in a cursory fashion. Further work adding more complexities may result in more accurate results, but this departs from the simplified design oriented approximations required in this work.

Table 5.3: Maximum radial stress values predicted by the two models.

Overlamine Thickness (mm)	$\sigma_{r, \max}$ Beam on Elastic Foundation (MPa)	$\sigma_{r, \max}$ FE Model (MPa)
12.7	≈ 1.9	3.6
6.35	≈ 1.2	3.65
4.233	≈ 1	3.3
3.175	$\approx .97$	3.0

5.3.3 Experimental Verification

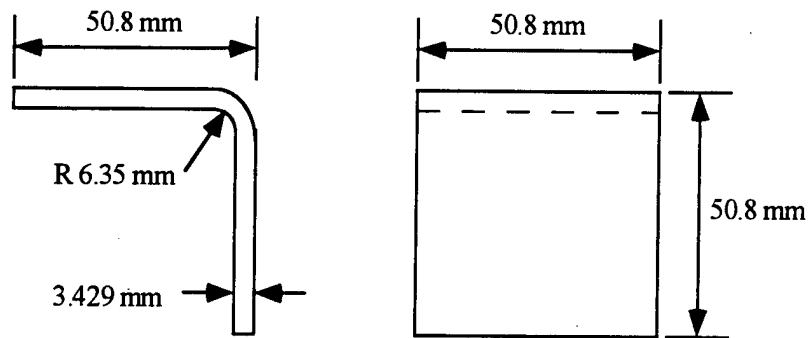
A series of tests conducted at the University of California Santa Barbara (UCSB) Mechanical Test Lab focused on the inter-laminar tensile strength of curved specimens. This material property is critical for the curved sections response to the out-of-plane stress generated during bending or transferring the stress around a bend. These tests were carried out for Pratt and Whitney to characterize materials for use in the Affordable Composites for Propulsion (ACP) program. Various materials were tested in different thermal and moisture regimes. A few of these tests are included to demonstrate the applicability of the simplified relations and the accuracy of the exact relations when used in a practical situation with inclusions such as manufacturing flaws.

The materials used in this study were AS4/PR500 conformable weave in a quasi-isotropic configuration and AS4/CET-4 5 Harness Satin in a $0^\circ / 90^\circ$ configuration. The material properties are shown in Table 5.4. The specimens are constructed using the resin transfer molding, RTM, system. This process creates the parts in a series of steps. First, the dry fabric is tackified with a dry powder form of the PR500 resin. Next, the plies are cut and formed in a preforming tool. The part is then completed by placement into the RTM tool and injection of the resin during the curing process. The completed specimens are then cut into 2 inch segments and ground to the desired width to minimize the cutting damage on the samples.

The geometry of the test specimen and test fixture are shown in Figures 5.3.13 and 5.3.14, respectively. The tests were linear to failure with failure resulting in a large load drop and a substantial decrease in sample stiffness. The load-displacement graphs were similar for all the specimens and the average load maximums are recorded in Table 5.5.

Table 5.4: Material properties for the experimental verification of the various analytical expressions used to find the interlaminar tensile strength.

Property	AS4/PR500 Conformable Weave Quasi-Isotropic	AS4/CET-4 5 Harness Satin 0°/90° Lay-up
E_{11}	67.5 GPa	71 GPa
E_{22}	67.5 GPa	69 GPa
E_{33}	6.9 GPa	6.9 GPa
G_{12}	5.9 GPa	4.75 GPa
ν	.04	.04
k	3.13	3.21

**Figure 5.3.13:** Curved specimen geometry.

Geometric values for use in the analytical expressions are $t = 0.135$ in, $b = 2.006$ in and $R_m = 0.25$ in. The results from the various simplified expressions and the exact, Lekhnitskii solutions are presented in Table 5.5. All of the simplified relations result in excellent approximations for the intra-laminar tensile strength of both specimen types when compared to the exact solution. Equation (65) results in the greatest accumulated error, approximately 2%, when the average from all the tests is compared to the average exact result.

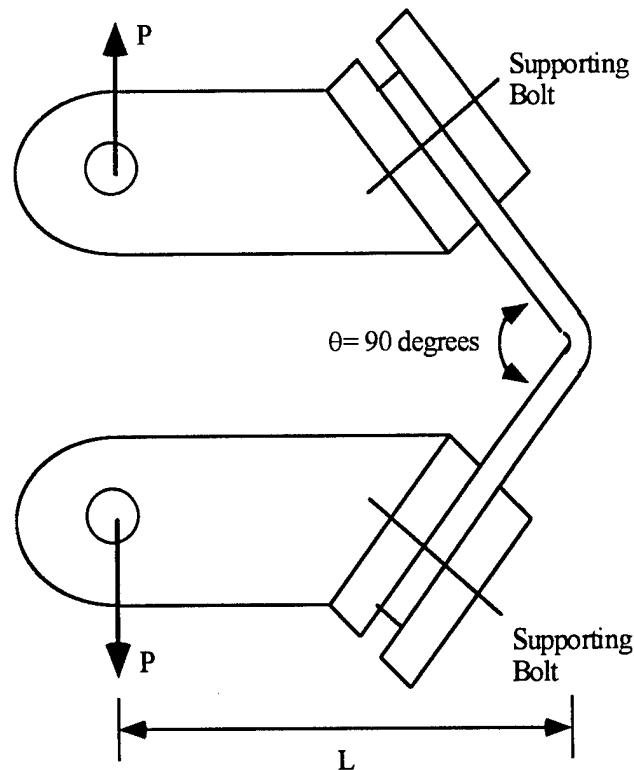


Figure 5.3.14: Test specimen loading fixture configuration.

Table 5.5: Results from the various simplified and exact expressions for the intra-laminar tensile strength of the curved specimens where 5 H.S. is the 5 harness satin material and C.W. is conformable weave material.

Material	Load (N)	Equation (65) (MPa)	Equation (67) (MPa)	Equation (68) (MPa)	Exact (MPa)
5 H.S.	671.6	42.16	42.65	43.15	42.95
5 H.S.	534.6	33.56	33.95	34.35	34.20
5 H.S.	565.3	35.49	35.90	36.32	36.15
5 H.S.	516.9	32.45	32.70	33.20	33.05
5 H.S.	534.6	33.56	33.95	34.35	34.20
C.W.	527.1	33.09	33.47	33.86	33.72
C.W.	600.9	37.72	38.16	38.06	37.95

5.4 Section D: Horizontal Doubler

From earlier figures illustrating contour plots of the various tee-joint configurations, it can be seen that this section of the tee-joint structure (Figure 5.4.1) does develop significant stresses when compared to the far-field stress, as shown in Figure 5.4.2. This is especially apparent in more compliant tee-joints where significant bending stresses are developed in the baseplate and horizontal overlaminates. The peak stress in Figure 5.4.2 is over 3 times the far-field stress as defined above, but still does not pose a significant threat to the tee-joint structure. This is due to the higher stresses which are

generated adjacent to this area in the curved region, as illustrated in Figure 5.4.3. From these figures, it can be seen that, although there are higher stresses generated in this section, the curved region is more critical as a failure site. The stresses generated in this section will also decrease with the use of a thicker baseplate, as discussed in Section 4.

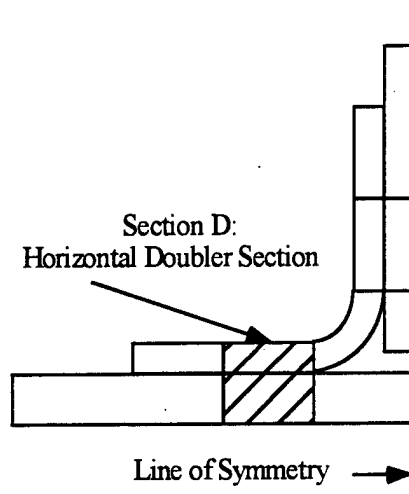


Figure 5.4.1: Horizontal doubler section where the filled area is illustrated in the following stress contour plot.

A method for approximating the geometry and boundary conditions seen in this section is created by a direct application of the Beam on Elastic Foundation methods presented in Hetenyi [1946]. In this case, the overlamine is modeled as a beam bonded to an elastic foundation, the adhesive layer and baseplate. This model is a simple case which neglects the flexure of the baseplate and overlaminates due to the applied load on the centerplate. The flexure of the baseplate and overlaminates is not examined due to the basic formulation of the beam on elastic foundation theory which does not allow flexure or movement of the foundation, in this case the baseplate. As was shown in Section 4, the flexure of the baseplate is an important factor in the overall stress state of the tee-joint and neglecting this factor will cause differences between this model and the in-situ tee-joint. This result will be discussed further below. Figure 5.4.4 illustrates the basic model used.

The derivation of this analytical approximation begins with the beam on elastic foundation approaches discussed in Section 5.1. In this case, the model consists of a beam loaded at one end with a pull-off load and a moment. The solutions for these two cases are superimposed to find the deflection due to the loading,

$$y = \frac{1}{2EI\beta^2} \left\{ \frac{W}{\beta} e^{-\beta x} \cos(\beta x) + Me^{-\beta x} (\cos(\beta x) - \sin(\beta x)) \right\}. \quad (84)$$

where

$$\beta = \left[\frac{k}{4EI} \right]^{\frac{1}{4}}, \quad (85)$$

ABAQUS

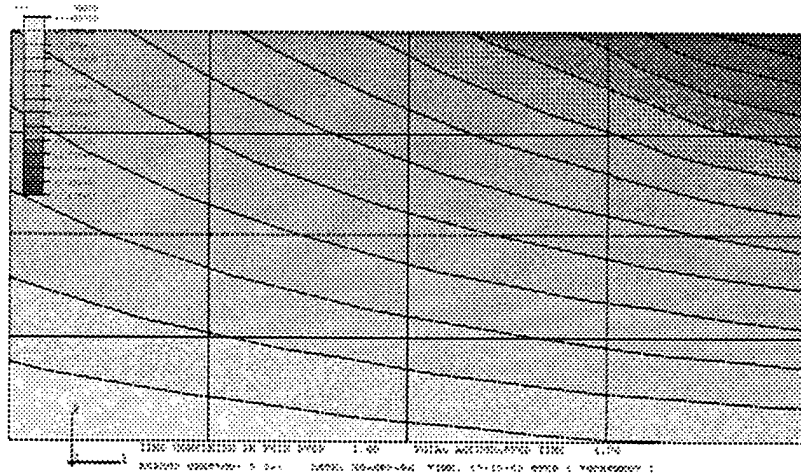


Figure 5.4.2: Horizontal stress contour plot of Section D of the generic tee-joint as shown in Figure 1.2. In this section of the tee-joint the fibers run in the 1 and 3 directions.

ABAQUS

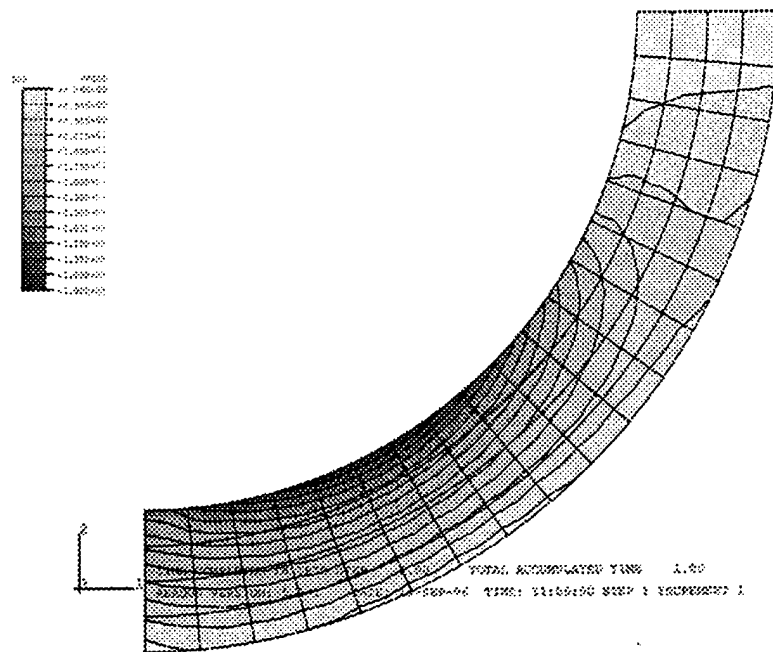


Figure 5.4.3: Circumferential stress contour plot of the curved region of the generic tee-joint structure.

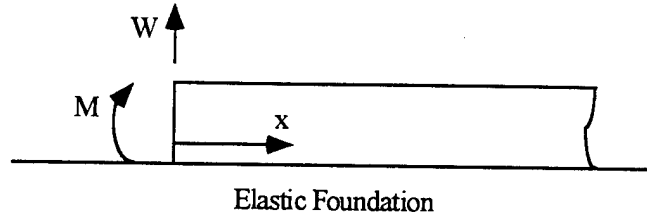


Figure 5.4.4: Beam on Elastic Foundation model for determining the peel stress at the termination of an overlamine or any doubler region.

EI is the bending stiffness of the overlamine, M is the applied moment per unit length and W is the applied pull off load per unit length. As mentioned earlier, the model can be created using a semi-infinite beam due to the exponential decay of the stress from the peak levels. The maximum peel stress is the variable of interest and is found at $x = 0$. As before, the peel stress is given by the following relation,

$$= ky \quad (86)$$

where k is the modulus of the elastic foundation. The expression for the maximum peel stress is given by

$$peel_{max} = \frac{k}{2EI\beta^2} \left\{ \frac{W}{\beta} + M \right\}. \quad (87)$$

This equation can be simplified in terms of basic geometric variables to allow an examination of the trends predicted by this expression,

$$peel_{max} = W \left(\frac{48k}{Ebt_0^3} \right)^{\frac{1}{4}} + M \left(\frac{12k}{Ebt_0^3} \right)^{\frac{1}{2}}. \quad (88)$$

where b is the depth of the beam which is assumed to be a unit depth for the following analysis and comparisons.

Equation (88) predicts that the maximum peel stress will increase with a decreasing overlamine thickness. FE models of the generic tee-joint configuration have been examined and Figure 5.4.5 illustrates the maximum peel stress as a function of the overlamine thickness. It can be seen from this graph that the trends predicted by this model are not the same as those predicted for the tee-joint structure. In the tee-joint case, the magnitude of the peel stress is not related solely to the overlamine thickness. The peel stress is a balance between factors such as the flexure of the baseplate, which is ignored in this model, and the changing load path through the structure as the stiffness is modified by altering the overlamine thickness.

This simplistic model does not accurately predict the peel stresses in this section of the tee-joint structure with the constraints applied to the baseline configuration, but in other cases with less baseplate flexure this method may be more applicable. Figure 5.4.6 illustrates the maximum peel stress as a function of overlamine thickness with the generic configuration modified to include the constraint condition of a fixed baseplate bottom.

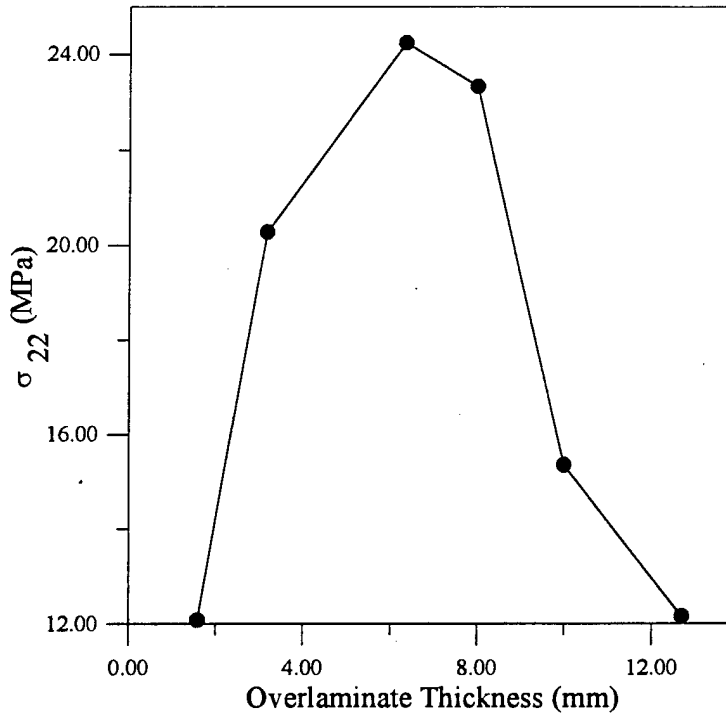


Figure 5.4.5: Maximum peel stress as a function of the overlamine thickness for the generic tee-joint configuration computed by FE methods.

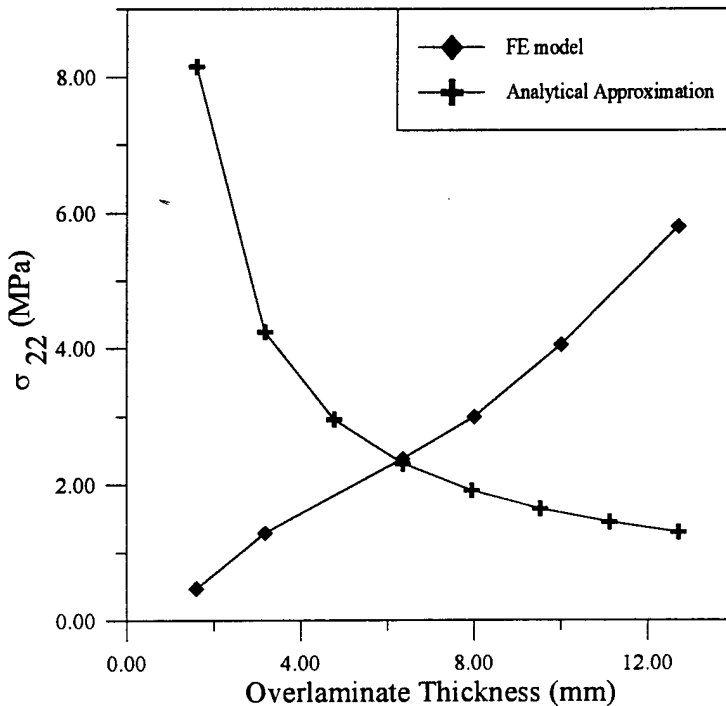


Figure 5.4.6: Maximum peel stress as a function of the overlamine thickness for the generic tee-joint configuration with a fixed baseplate computed by FE methods and an analytical approximation.

The analytically determined values in this figure are constructed to fall in the same range of values as the FE prediction to allow a comparison of the trends determined by the two models and are not dependent upon the boundary conditions found by the FE model. It can be seen from this figure that the simple analytical approximation does not adequately predict the peel stress magnitude or trends in the tee-joint for either type of boundary condition. This result is due to the differences in boundary conditions between the in-situ tee-joint and the model presented here. In the tee-joint structure, the stress is mainly transferred as an axial stress at this section which is not examined in this model. Due to these factors, this analytical approximation is not recommended for analyzing this section of the tee-joint. A short analysis is conducted below to examine the accuracy of this model as compared to a more appropriate configuration.

To determine the accuracy of this approximation, a finite element model was created. The FE model has the same configuration shown in Figure 5.4.4. A simple case is examined with a pull-off load of 10 N and no applied moment. The maximum peel stresses from this case are presented for a range of overlamine thicknesses in Figure 5.4.7 and are compared to the results from the analytical model. The curves presented on this figure are for two cases. The first case consists of a beam bonded to an elastic foundation, another beam. The second case is the same as the first model, but with an adhesive layer between the two beams. The second case is included because this configuration is most often seen in practical problems. The main difference between the two analytical approximations is the stiffness of the elastic foundation which is determined from the modulus and thickness of the foundation. In the first case, the foundation stiffness is the out-of-plane modulus, E_3 , of the fiberglass material multiplied by the thickness of the baseplate. In the second case, the foundation stiffness is the modulus of the adhesive material, E_a , multiplied by the thickness of the adhesive layer, t_a . The foundation stiffness used in the second case does not truly model the foundation stiffness due to the contribution of the material beneath the adhesive layer in the actual and FE cases, but this approximation is examined to determine the effects of the addition of this layer and the affects of changing the simplified model.

From Figure 5.4.7, it can be seen that the simple approximation is within 50% for the first case and 70% for the second case with an adhesive layer. These data points show that the analytical approximation gives results accurate within an order of magnitude for the range of values examined herein and can be used to determine rough values. These two cases with and without an adhesive layer illustrate the extreme cases possible when examining this configuration. Greater accuracy may be possible by using an approximation that combines the effects of the adhesive layer and underlying material. This may be possible by using an effective adhesive layer thickness which is a multiple of the existing adhesive layer thickness. Another improvement may be to increase the modulus of the adhesive material because of the constraints on the adhesive layer due to the geometry of this configuration.

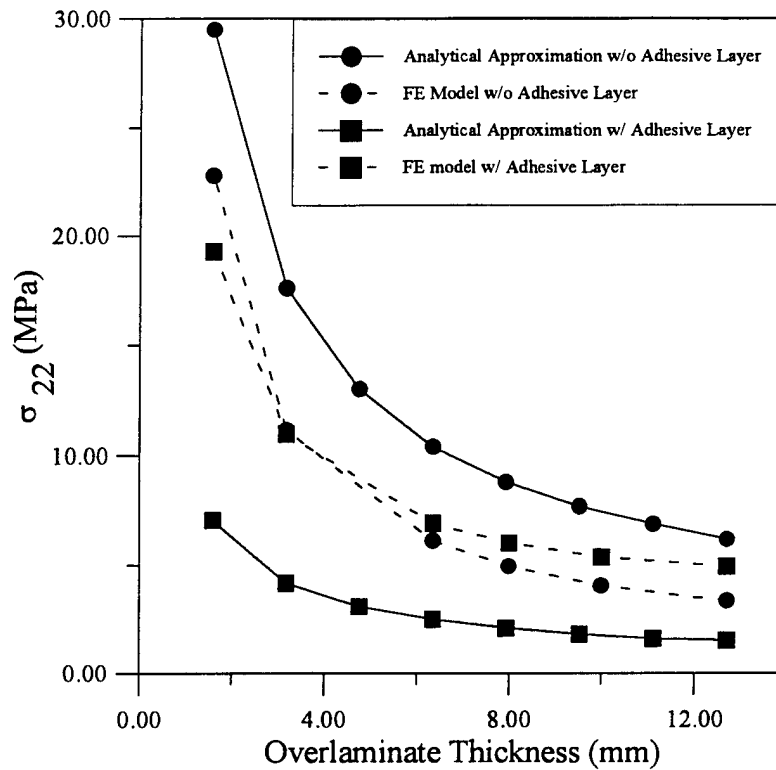


Figure 5.4.7: Maximum peel stress as a function of the overlamine thickness for the simple model computed by FE methods and an analytical approximation.

5.5 Section E: Exterior Horizontal Overlamine

This section of the divided tee-joint structure, Section E in Figure 1.2, is superficially similar to half of a single lap joint, see Figure 2.4. It is also similar to the configuration examined in Section 5.1. The main difference between these two sections is in the bending moment in the baseplate of Section E. In the earlier analysis detailed in Section 5.1, the inner adherend was assumed to be free of any moments due to the applied load and geometry. Here, this is not the case. Figure 4.4.7 illustrates a displaced tee-joint. From this figure, it can be seen that the baseplate undergoes considerable flexure and is, thus, loaded with a moment. Due to the difference between the two cases, different analytical approximations must be used to find the stresses in this section of the divided tee-joint.

Analytical approximations developed to determine the peel stresses in an adhesively bonded single lap joint can not be used to model this section because the boundary conditions seen in a single lap joint are not met in this configuration. In a single lap joint, the load is transferred from the inner adherend to the outer adherend along an eccentric load path and each member consists of one side which is a free surface. See Figure 5.5.1. The boundary conditions for Section E do not follow this pattern. In the tee-joint case, the load is transferred from the overlamine to the baseplate due to the termination of the overlamine. Boundary conditions, as determined for the generic tee-joint configuration, are illustrated in Figure 5.5.2.

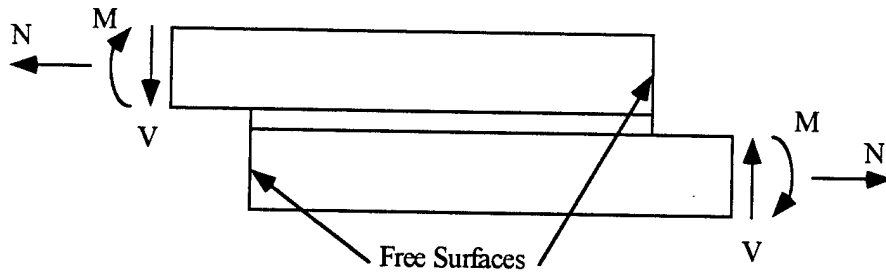


Figure 5.5.1: Typical boundary conditions for a single lap joint.

Due to the differences between the boundary conditions for these two cases the existing methods for examining single lap adhesive joints are not applicable to analyzing this section of the joint.

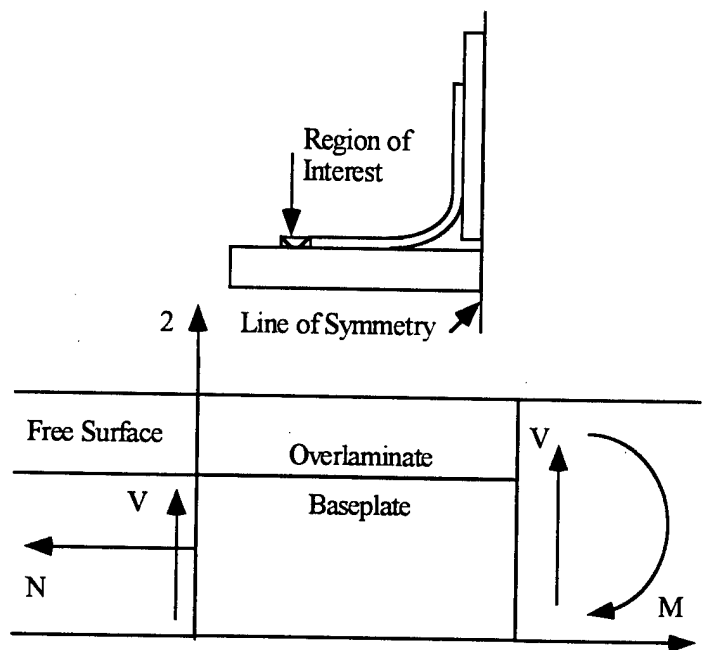


Figure 5.5.2: Typical boundary conditions in this section of the generic tee-joint structure.

The boundary conditions for Section E are also different for tee-joints with different geometries and material parameters. As mentioned in earlier sections, the load path in the tee-joint can vary considerably due to alterations in the various geometric and material parameters. Because of this fact, it is difficult to model the boundary conditions for the various sections in generic terms which will correlate to more than one configuration.

A method for examining the termination of doubler regions, such as seen in this area with large baseplate deflections, is presented. Even though the complexity of the tee-joint precludes the use of these methods for finding the peel stress at the termination of the horizontal overlamine without the use of finite element models for the determination of

appropriate boundary conditions, this analytical approximation is included to demonstrate alternative methods for determining the stress state for this specific geometry.

This method for finding the peel stresses also uses beam on elastic foundation methods presented in Hetenyi [1946]. In this case, the overlamine and baseplate are both modeled as beams separated by an elastic foundation, the adhesive layer, as shown in following figure, Figure 5.5.3.

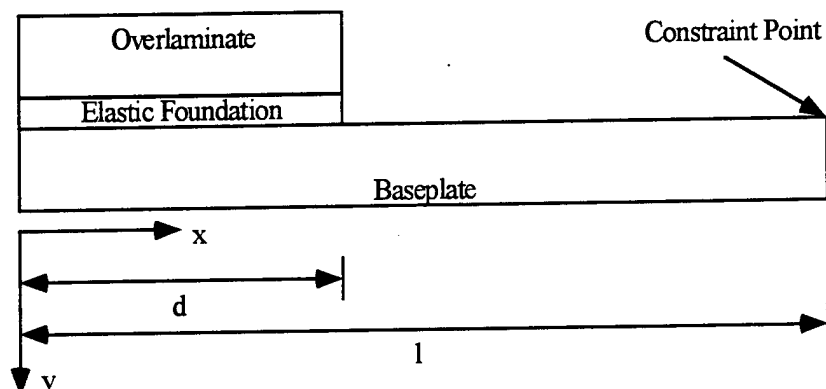


Figure 5.5.3: Illustration of the model where the overlamine and baseplate are modeled as beams separated by an elastic foundation, the adhesive layer.

The derivation of the expressions for the beam on elastic foundation model presented in this section are the same as that presented in Section 5.1 and result in the following equation,

$$D \frac{d^4 w}{dx^4} - \frac{E_a}{t_a} w = 0 \quad (89)$$

where, as before, D is the flexural stiffness of the beam, E_a is the modulus of the adhesive layer, t_a is the thickness of the adhesive layer and w is the deflection of the beam. This equation is for the case of a beam on an elastic foundation and has to be modified in this case to couple the displacements in the adhesive layer. This results in two coupled differential equations in terms on the deflection due to the overlamine with subscript 0 and the baseplate with subscript i ,

$$D_0 \frac{d^4 w_0}{dx^4} - \frac{E_a}{t_a} (w_0 - w_i) = 0, \quad (90)$$

$$D_i \frac{d^4 w_i}{dx^4} - \frac{E_a}{t_a} (w_0 - w_i) = 0 \quad (91)$$

and for the section of the baseplate beyond the termination of the overlamine,

$$D_i \frac{d^4 w_i}{dx^4} = 0. \quad (92)$$

Equation (90) can be solved for the baseplate deflection, w_i , in terms of the overlamine deflection, w_0 ,

$$w_i = \frac{D_0 t_a}{E_a} \frac{d^4 w_0}{dx^4} + w_0. \quad (93)$$

This expression can be substituted into Equation (91) resulting in an eighth order differential equation for the deflection in the overlamine,

$$\frac{d^8 w_0}{dx^8} + \frac{E_a(D_i + D_0)}{t_a D_i D_0} \frac{d^4 w_0}{dx^4} = 0. \quad (94)$$

This equation can be integrated four times resulting in

$$\frac{d^4 w_0}{dx^4} + \frac{E_a(D_i + D_0)}{t_a D_i D_0} w_0 = c_0 + c_1 x + c_2 x^2 + c_3 x^3. \quad (95)$$

The solution to Equation (95) is

$$w_0 = e^{\beta x} [A_1 \cos \beta x + A_2 \sin \beta x] + e^{-\beta x} [A_3 \cos \beta x + A_4 \sin \beta x] + c_0 + c_1 x + c_2 x^2 + c_3 x^3 \quad (96)$$

where in this equation

$$\beta = \left(\frac{E(D_i + D_0)}{4t_a D_i D_0} \right)^{\frac{1}{4}}. \quad (97)$$

Substituting the solution to the differential equation, Equation (96), into Equation (93) results in an expression for the deflection of the baseplate,

$$w_i = -\frac{D_0}{D_i} \left(e^{\beta x} [A_1 \cos \beta x + A_2 \sin \beta x] + e^{-\beta x} [A_3 \cos \beta x + A_4 \sin \beta x] + c_0 + c_1 x + c_2 x^2 + c_3 x^3 \right) \quad (98)$$

With an appropriate set of eight boundary conditions, these expressions can be solved to determine the deflection and subsequently the peel stress between the members. This is accomplished by using the following relation,

$$_{peel} = k(w_0 - w_i). \quad (99)$$

This approximation is not appropriate for use in a design orientated study due to the complexity in determining the boundary conditions for each tee-joint configuration and solving the system of eight equations with eight unknowns which result from this method.

6.0 Experimental Evaluation

Existing work in literature detailing experimental studies on fiberglass tee-joint is limited, Shenoi and Violette [1990], Shenoi and Hawkins [1992], and Shenoi et al. [1995]. In these studies, experimental test series were conducted and compared to finite element, FE, models. These papers are reviewed in the literature review section and only the portions of these papers discussing correlation between the test programs and the FE models are mentioned here.

As mentioned in Section 2.1, Shenoi and Hawkins [1992] detail an experimental test series and a corresponding finite element analysis of a group of tee-joints. The FE models were fairly coarse when compared to the models considered in this work. These models consisted of one element through the overlaminates, the center and baseplates and two rows of elements in the adhesive filler. The various models were run using four combinations of linear and non-linear material properties and small and large deflection analyses. The FE analysis was carried out using the ANSYS finite element analysis package.

It was found in this work, Shenoi and Hawkins [1992], that for traditional marine tee-joints, the FE load/deflection results were of the same order as the experimental results. Also, the results of altering the material response and the deflection model had very little effect on the FE model. For the other configurations composed of tee-joints similar to those studied in this work, the fillet properties had a large impact on the behavior and the results for the linear and non-linear material properties diverged considerably at higher loads due to yielding of the material when subjected to higher loads. Also, the large and small deflection solutions diverged considerably. It was noted in these cases that the FE results underestimated the stiffness of the joint by approximately 50% due to differences in the material properties, as discussed below.

The difference between the linear and non-linear adhesive material property models at higher loads has been discussed in Sections 5.1 and 5.5. As the applied load increases, the adhesive undergoes plastic shear deformation near the termination of the overlaminates. This purely plastic response affects the peak peel stress in these areas and, thus, affects the failure mechanism determined by the FE analysis. At loads nearing the failure values, other areas of the resin fillet can also undergoes plastic deformation increasing the relative difference between the linear and non-linear models.

The authors, Shenoi and Hawkins [1992], mention that the large deflection analysis does not appear to model the load/deflection response of the test specimens. Due to the nature of the differences between the various models, the authors concluded that this difference is caused by inaccurate material properties for the resin fillet. The resin properties were found from an unthickened version of the resin whereas the resin used in the creation of the test specimens was a thickened version of the urethane-acrylate resin. The main difference between the thickened and unthickened versions is in the difficulties in

producing void-free test specimens with the thickened version. Modifying these properties, to account for the difference between the versions of the resin fillet material, resulted in a very good correlation between the experimental series and the FE models. The authors concluded that the FE models provide good qualitative and quantitative correlation with the experimental values. This conclusion is qualified by the assumption that the material properties used in the FE models are consistent with the actual material properties which can be a problem with some resin systems that are not well quantified in the literature.

Although this report does not detail an experimental test series examining tee-joints, the articles by Sheno and Hawkins [1992] and others suggest that good correlation between experimental and finite element models occurs in tee-joints with geometries and materials similar to those used in this study. An experimental test series to verify the parametric study, analytical expressions and design guidelines presented in this work is highly recommend, but is not included here.

7.0 Design Guidelines

This section of the report details a group of design guidelines based upon the analysis presented in the previous sections. Here, the insights gained in Section 4 are used to create a set of graphs to aid in the construction of tee-joint structures. The design parameters examined and commented upon here are similar to those used earlier, but the presentation has been streamlined. Graphical representations of the affects of altering various parameters are created to allow the designer to determine the relative effect of changing the tee-joint geometry. The tee-joint modified in this section is the generic tee-joint described in Section 4 and shown in Figure 4.1.2 and is constrained by rollers located 12.7 mm from the termination of the horizontal overlaminates. In each of the following sections, only one variable is modified while the rest of the structure remains fixed. The mesh used in the finite element models is the same as described in Section 4 and shown in Figure 4.0.1.

The effects of changing each tee-joint parameter are examined by focusing on a group of variables which are critical to determining the failure mechanisms of the structure. A graphical representation of these variables is included in Figure 7.1 which corresponds to the notation included in the following list of variables. These variables are as follows:

- i) vertical displacement - Point A on the following figure,
- ii) the peel stress in the adhesive at the termination of the horizontal overlaminate - Point B,
- iii) vertical stress in the baseplate directly under the centerplate - Point C,
- iv) the peak radial stress in the curved region of the tee-joint - Point D,
- v) the peak circumferential stress also in the curved region of the structure - Point E, and

- vi) the peel stress in the adhesive at the termination of the vertical overlamine - Point F.

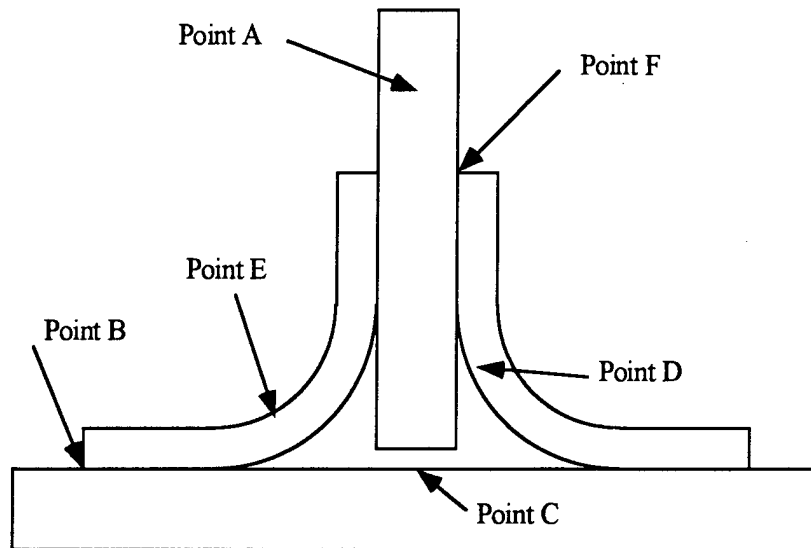


Figure 7.1: The location of the various variables used in this study.

The vertical displacement is measured from a node on the line of symmetry of the tee-joint and 12.7 mm from the load application point, at point A. This distance is far enough from the load application point, so that there is no local displacement due to the load based on the finite element analyses. The peel stress at the termination of the horizontal overlamine is computed at the corner node, Point B, and is assumed to be in an element in the adhesive layer. The same node will have a different peel stress depending upon the material properties of the element chosen. In this case, the node can be in either a baseplate (E-glass/epoxy) or an adhesive (vinylester) element. Also, as mentioned in Section 5, the magnitude of the peel stress will change depending upon the mesh size used in the finite element model, but the relative change remains the same. The vertical stress in the baseplate directly under the centerplate is computed for a node in a baseplate element at Point C. This stress is a compressive stress for most of the cases shown here and will be for joints with thin baseplates. As in the case of the peel in the horizontal overlamine, the peel in the vertical overlamine is measured at Point F and taken from the corner node in an element in the adhesive layer. All of these variables have been examined for each of the tee-joint parameters and the most significant are included in the following figures.

Pull-off Load Case

The first geometric parameter to be examined is the effect of changing the size of the gap between the base and centerplates. This distance, L_{gap} , is referenced with the mean radius of the curved section, R_m , to give the designer a relative size between the gap and the rest of the tee-joint structure. In this graph, Figure 7.2, the two variables most effected by the change in gap length are shown. The other variables are not shown due to the small variation, less than 3%, with the changing gap length. The values shown in this

and subsequent graphs are a relative change in variable. This is accomplished by dividing the values of each parameter, such as vertical displacement, by the smallest value of that same variable. As L_{gap} decreases, the tee-joint approaches a butt-joint as shown earlier and an important failure site is the baseplate directly under the centerplate. Also, as the gap length increases, the stiffness of this region decreases forcing more of the stress to pass through the curved sections of the tee-joint.

The second tee-joint parameter examined is the modulus of the resin filler. From Figure 7.3, the main affects of altering the filler modulus include the peel stresses and the baseplate stress directly under the centerplate. The peel stresses increase due to the increasing stiffness of the tee-joint structure as the filler modulus is increased. The change in baseplate stress is attributed to two factors. First, as the structure becomes stiffer, with increasing filler modulus, the compressive region formed in the gap region becomes larger due to the increased resistance to the curvature of the baseplate. But, this effect is tempered by the second factor, the increased load passing through the gap region from the applied load which is a tensile load. The combination of these two factors results in the curve seen in Figure 7.3 for the case of baseplate stress.

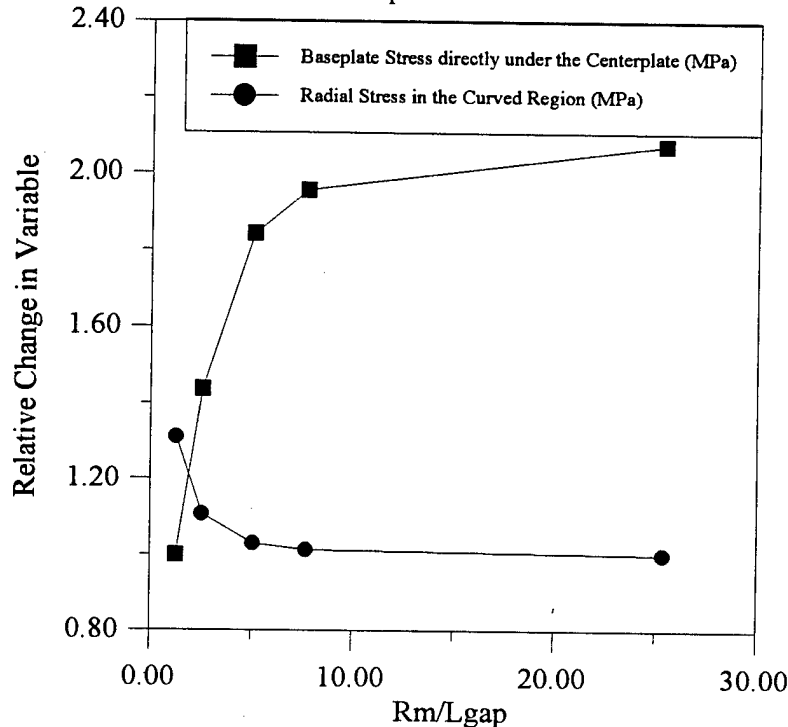


Figure 7.2: Relative change of the included variables as a function of the gap length.

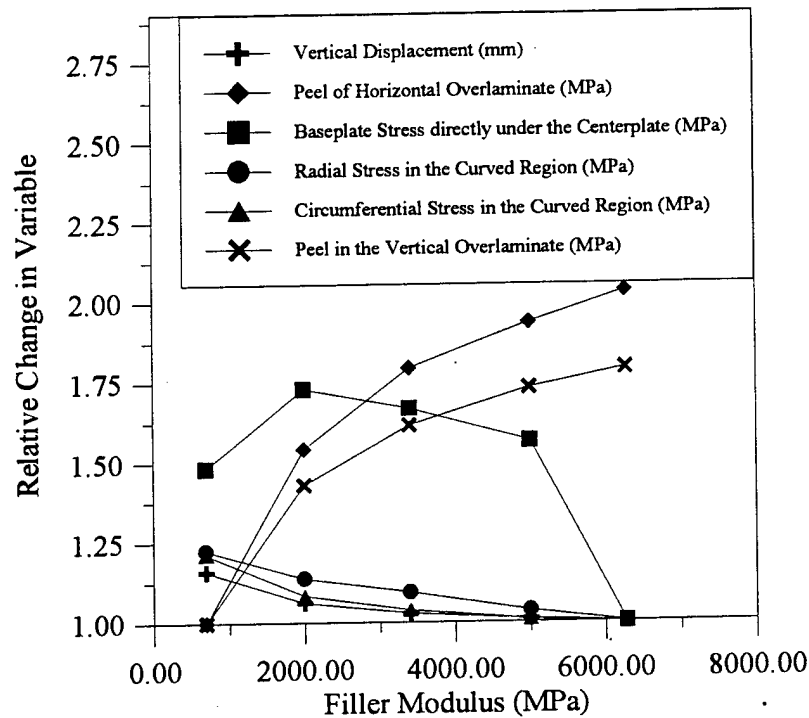


Figure 7.3: Relative change of the included variables as a function of the modulus of the resin filler.

The other variables vary approximately 20% over the range of materials examined, but through the range of most vinylesters, 3000 to 5000 MPa, there is only a small variation in these values.

The R_m/t ratio is the next variable examined. This is a measure of the mean radius of the curved region as a function of the thickness of the overlamine. In this case, the thickness of the overlamine has been altered which directly affects the stresses in the curved region and both the critical peel areas. There are two figures presented in the discussion of this variable due to the large change in the peel stress in the horizontal overlamine which dominates the other variables. This is illustrated in Figure 7.4. Here, the peel decreases as the thickness of the overlamine decreases as was predicted from the models shown in Section 5. The data point shown at $R_m/t = 16$ in Figure 7.4 is negative due to the interaction between the constraints and the peel stress. With a thin overlamine, the peel stress decreases to such a low level that the local compression due to the rollers is large enough to dominate and a compressive stress is generated at an area which previously has been under a tensile stress.

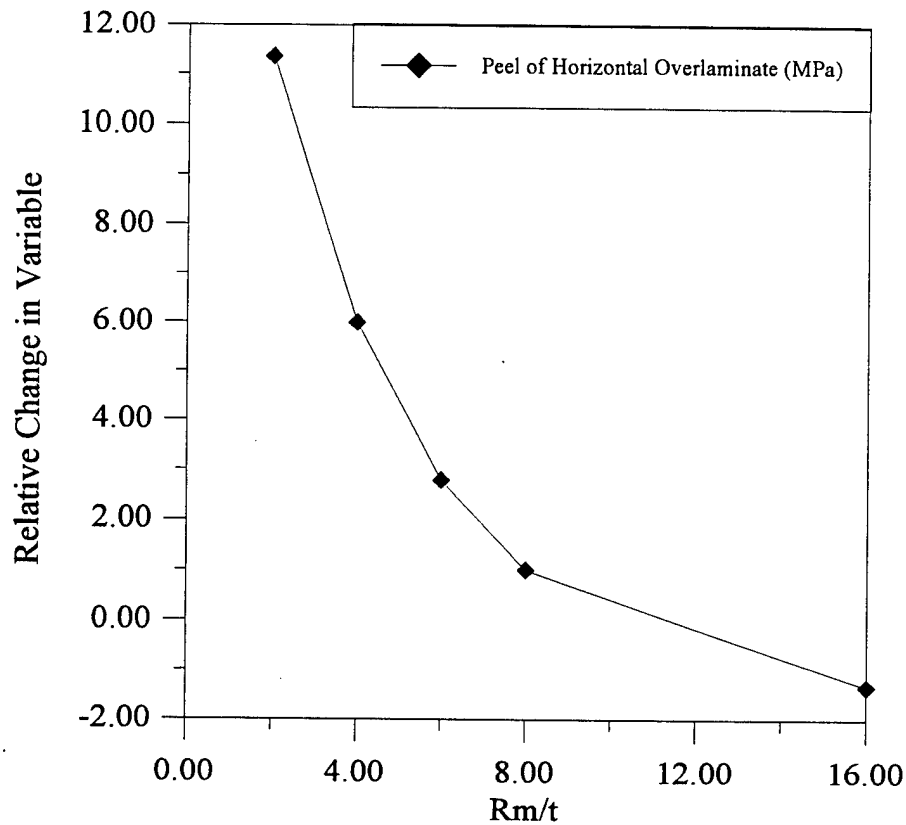


Figure 7.4: Relative change of the peel in the horizontal overlamine as a function of the R_m/t ratio.

The other variables also change as the R_m/t ratio is altered, see Figure 7.5. Here, the smallest change over the range of R_m/t is approximately 50%. The variables in this figure react as previously discussed in this and earlier sections.

The next variable to be studied is the span length of the tee-joint specimen. As stated earlier, the span length is defined as the distance from the termination of the horizontal overlamine to the rollers used to constrain the test specimen. In the generic case, the span length is 12.7 mm. The effects of altering this variable are shown in Figure 7.6.

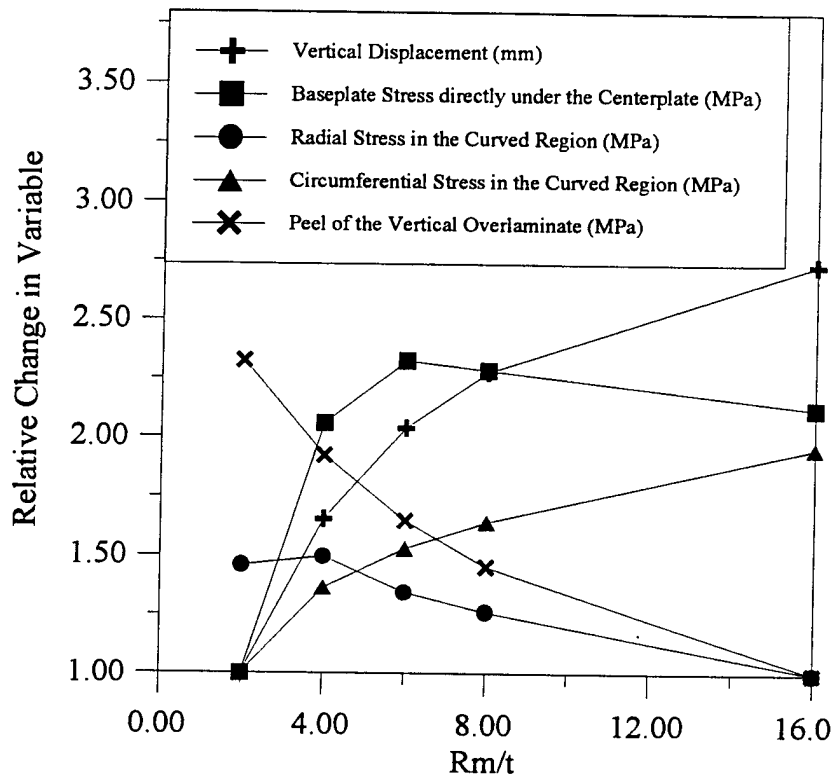


Figure 7.5: Relative change of the included variables as a function of the R_m/t ratio.

Increasing this variable results in larger curvatures in the baseplate which causes higher stresses in most of the critical areas in the tee-joint structure. The peel in the vertical overlaminates is the only variable not greatly effected by altering the span length.

The thickness of the baseplate, t_{bp} , as a function of the thickness of the centerplate, t_{cp} , is the next variable examined. This is shown in Figure 7.7. In this case, the thickness of the baseplate is the altered variable in the finite element models and is compared to the thickness of the centerplate as a means to gauge the relative size of the baseplate and tee-joint structure.

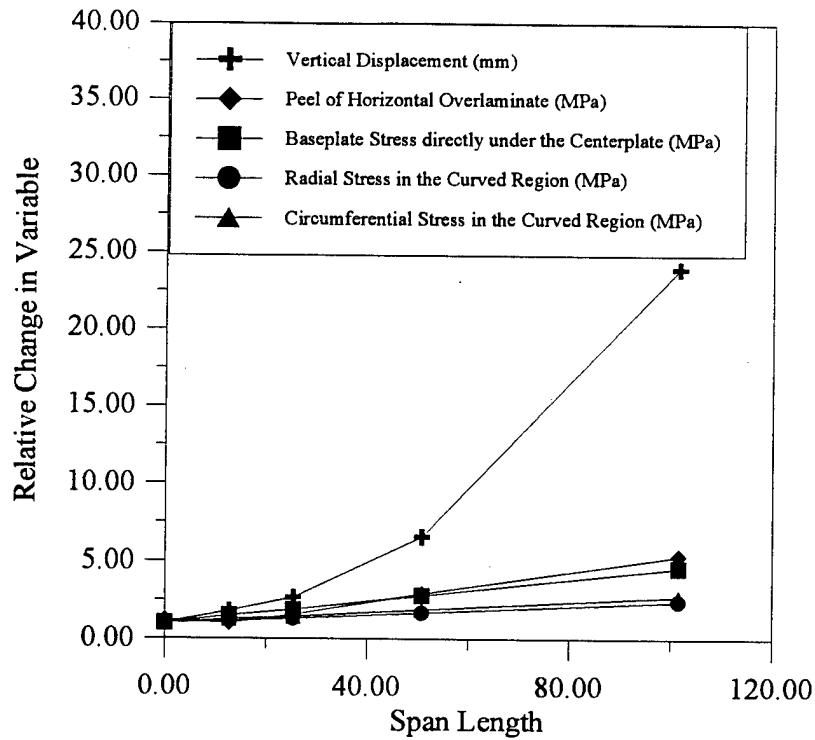


Figure 7.6: Relative change in the variables as a function of the span length.

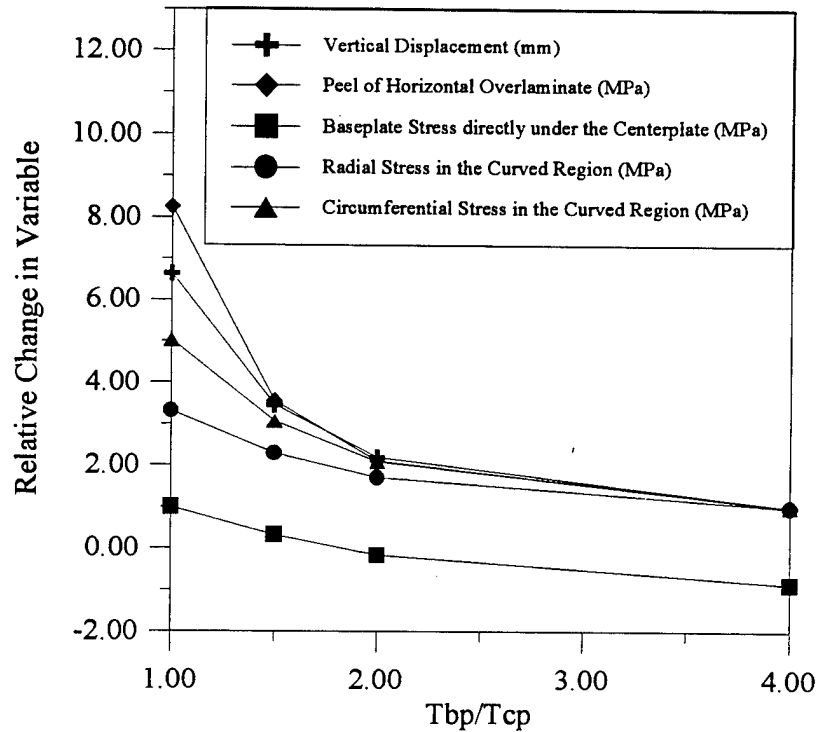


Figure 7.7: Relative change in the variables as a function of the baseplate thickness.

As discussed earlier, as the baseplate thickness increases, the curvature of the baseplate decreases and the stress levels and vertical displacement of the structure decrease. It can

also be seen from this illustration that the stress in the gap region changes from compressive to tensile as the thickness increases.

The final variable examined in this section is the length of the horizontal overlamine, L_{hov} . The effects of this variable are shown in Figure 7.8. The definition of the length of the horizontal overlamine has been detailed earlier and shown in Figure 1.1. In all of these cases, the rollers are 12.7 mm from the termination of the horizontal overlamine. All the variables shown in Figure 7.8 increase with increasing L_{hov} due to the higher curvatures in the baseplate. The exception to this is the peel of the horizontal overlamine. Even though there is an increase in curvature, this variable decreases due to the larger stress transfer area created when this length is increased.

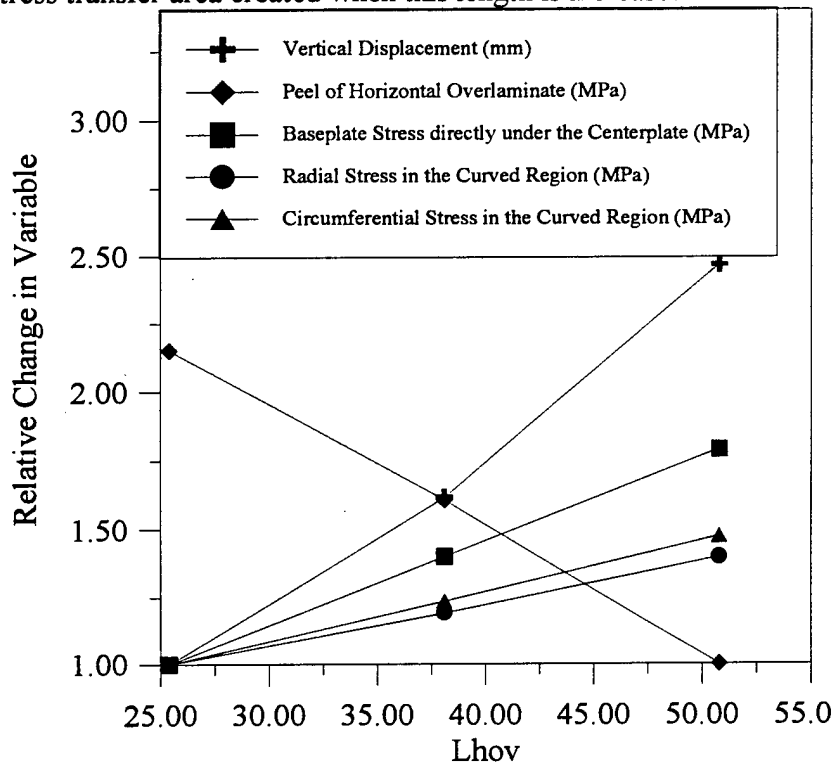


Figure 7.8: Relative change of the included variables as a function of the length of the horizontal overlamine.

These figures allow the designer to see how various changes affect the stresses throughout the tee-joint structure. If a certain failure mode is prevalent in a current design, then, by examining the various figures, a possible correction may be determined. In addition, when creating a new design, the user can see how various parameters affect the stresses in the structure which gives insight into the overall joint design.

45° Loading Case

This report details more design guidelines for the construction of marine tee-joints for the case of an applied load 45° from the horizontal. The loading condition is the same as used in other articles, Shenoi [1992] and others. Failure sites and design variables are

the same with the addition of the horizontal displacement near the top of the tee-joint structure measured at Point A in Figure 7.1.

The first geometric parameter to be examined is the effect of changing the size of the gap between the base and centerplates. This distance, L_{gap} , is referenced with the mean radius of the curved section, R_m , to give the designer a relative size between the gap and the rest of the tee-joint structure. In Figure 7.9, the variable most effected by the change in gap length is shown.

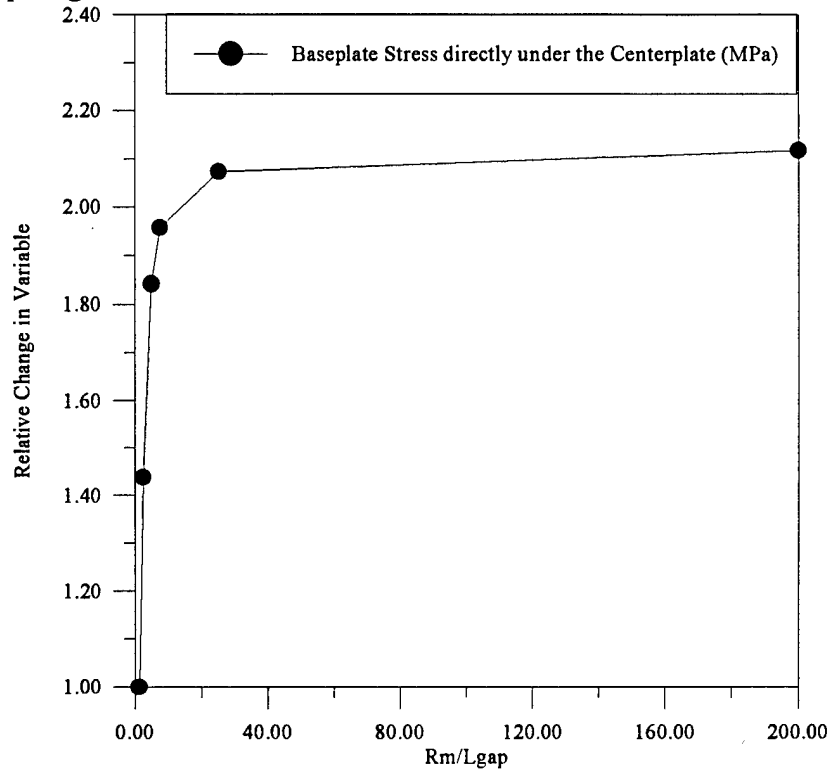


Figure 7.9: Relative change of the included variables as a function of the gap length.

The other variables are not shown due to the small variation of less than 3% with the changing gap length. The values shown in this and subsequent graphs are a relative change in variable. This is accomplished by dividing the values of each parameter, such as vertical displacement, by the smallest value of that same variable. As L_{gap} decreases, the tee-joint approaches a conventional butt-joint as shown earlier and an important failure site is the baseplate directly under the centerplate.

The second tee-joint parameter examined is the modulus of the resin filler. From Figure 7.10, the main affects of altering the filler modulus is seen in the magnitudes of the peel stresses at both the termination of the horizontal and vertical overlaminates.

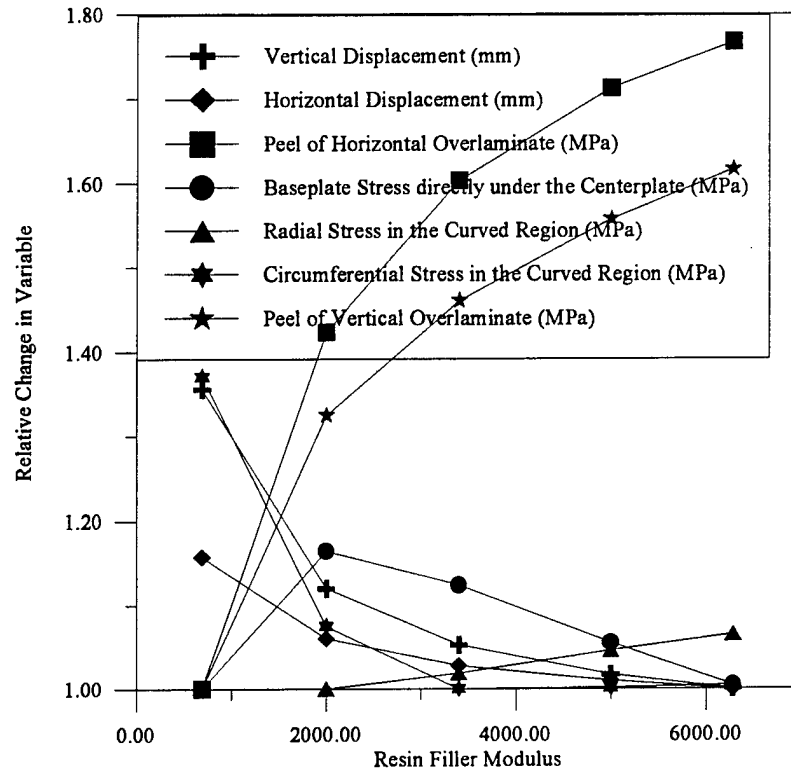


Figure 7.10: Relative change of the included variables as a function of the modulus of the resin filler.

The peel stresses increase due to the increasing stiffness of the tee-joint structure as the filler modulus is enlarged. The other variables vary approximately 40% over the range of materials examined, but through the range of elastic modulus of most vinylesters, 3 to 5 GPa Mallick [1993] there is a smaller variation in these values, approximately 20%.

The R_m/t ratio is the next variable examined. This is a measure of the mean radius of the curved region as a function of the thickness of the overlaminates. In this case, the thickness of the overlaminates has been altered which directly affects the stresses in the curved region and both the critical peel areas. Figure 7.11 illustrates these results.

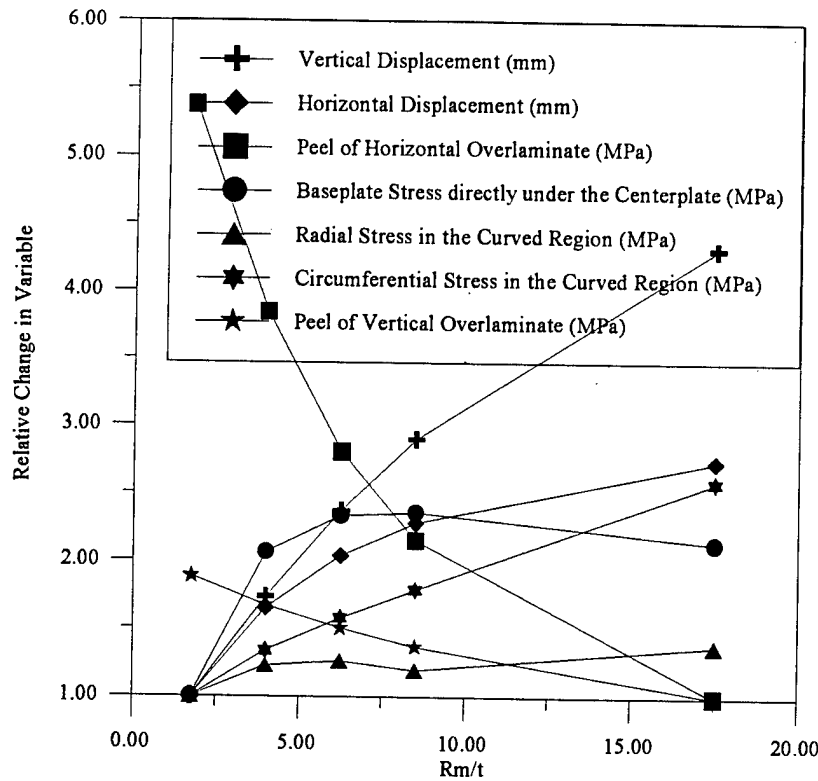


Figure 7.11: Relative change of the included variables as a function of the R_m/t ratio.

The next variable to be studied is the span length of the tee-joint specimen. As stated earlier, the span length is defined as the distance from the termination of the horizontal overlamine to the rollers used to constrain the test specimen. In the generic case, the span length is 12.7 mm. The effects of altering this variable are shown in Figure 7.12. Increasing this variable results in larger curvatures in the baseplate which causes higher stresses in most of the critical areas in the tee-joint structure. The peel in the vertical overlamine is the only variable not greatly effected by altering the span length.

The thickness of the baseplate, t_{bp} , as a function of the thickness of the centerplate, t_{cp} , is the next variable examined. This is shown in Figure 7.13. In this case, the thickness of the baseplate is the altered variable in the finite element models and is compared to the thickness of the centerplate as a means to gauge the relative size of the baseplate and tee-joint structure. As discussed earlier, as the baseplate thickness increases, the curvature of the baseplate decreases and the stress levels and vertical displacement of the structure decrease.

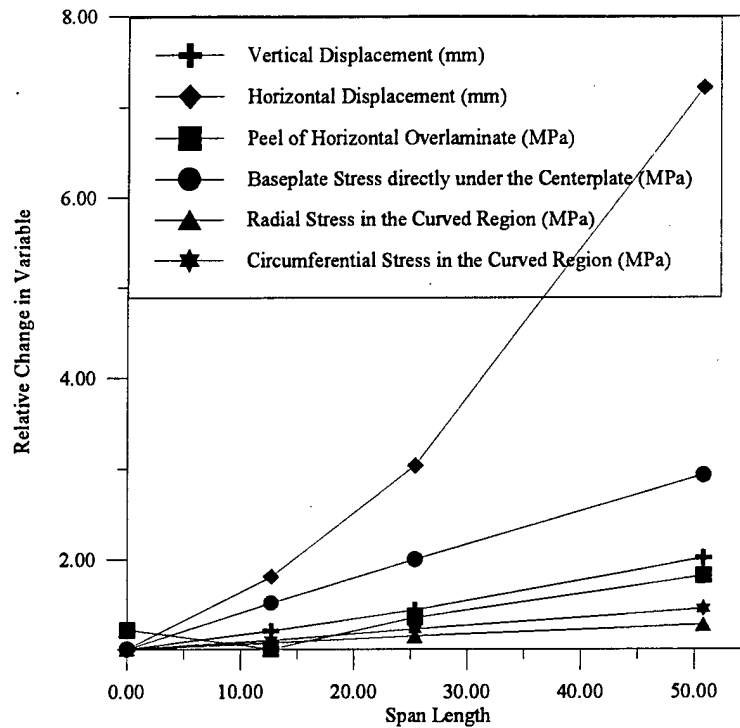


Figure 7.12: Relative change of the variables as a function of the span length.

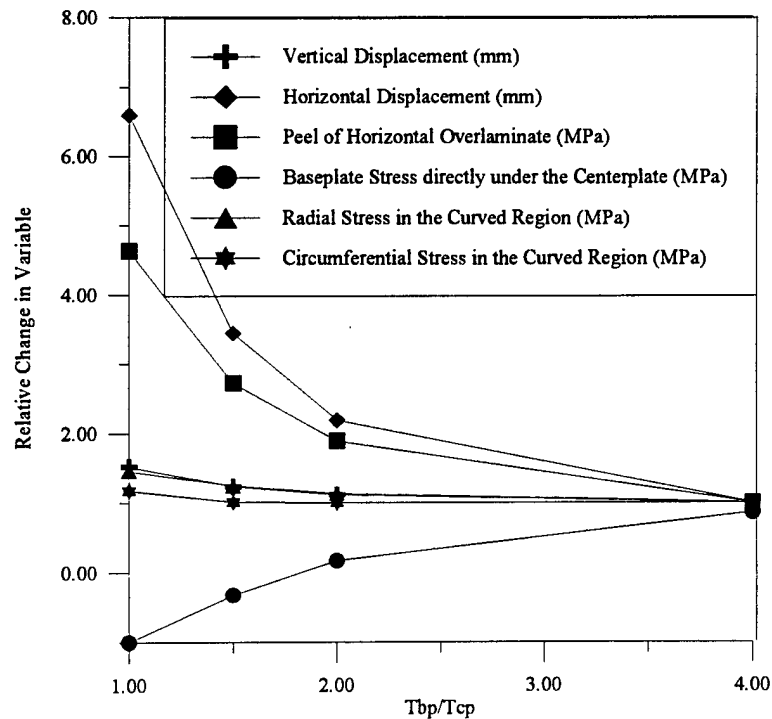


Figure 7.13: Change in the variables as a function of the baseplate thickness.

It can also be seen from this illustration that the stress in the gap region changes from compressive to tensile as the thickness increases.

The final variable examined in this section is the length of the horizontal overlaminate, L_{hov} . The effects of this variable are shown in Figure 7.14. The definition of the length of the horizontal overlaminate has been detailed in earlier reports and is the distance between the tangency point between the curved region and the horizontal overlaminate and the termination of the horizontal overlaminate. In all of these cases, the rollers are 12.7 mm from the termination of the horizontal overlaminate. All the variables shown in Figure 7.14 increase with increasing L_{hov} due to the higher curvatures in the baseplate. The exception to this is the peel of the horizontal overlaminate. Even though there is an increase in curvature, this variable decreases due to the larger stress transfer area created when this length is increased.

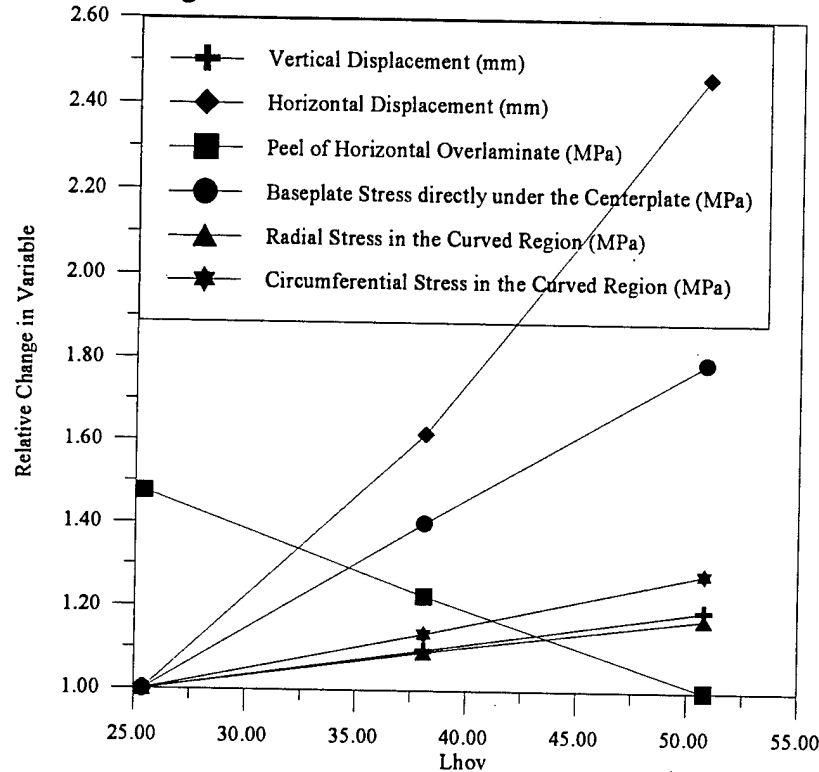


Figure 7.14: Relative change of the included variables as a function of the length of the horizontal overlaminate.

These figures allow the designer to see how various changes affect the stresses throughout the tee-joint structure. If a certain failure mode is prevalent in a current design, then, by examining the various figures, a possible correction may be determined. In addition, when creating a new design, the user can see how various parameters affect the stresses in the structure which gives insight into the overall joint design.

8.0 Conclusions and Recommendations

In order to obtain a better understanding of the parameters affecting the design of resin fillet tee-joints for marine applications, finite element analyses and analytical approximations have been conducted. General conclusions from these models and recommendations for future work are as follows.

The finite element analyses were used as a parametric study to help determine a set of design guidelines for the construction of marine tee-joints. A set of material and geometric parameters were chosen and varied. The effects of these changes are discussed in the Section 5.0, Tee-Joint Sections, and a concise, graphical set of guidelines is shown in Section 7.0, Design Guidelines. Although previous authors have concluded that FE analysis can be accurately used in the determination of design guidelines for this type of structure (see Section 6.0, Experimental Evaluation), verification of the guidelines through mechanically testing would be invaluable.

The design guidelines presented in this work differ greatly from those in earlier articles. A systematic examination of the various variables and the illustration of the results of this study give insight into the mechanics of the structure and allow alterations increasing both the strength and stiffness of the structure as desired.

The analytical approximations of the various tee-joint sections are shown in Section 5.0, Tee-Joint Sections. The analysis of the double lap section of the joint resulted in fairly accurate predictions of the peel stresses for tee-joints with thin overlaminates under an applied loading large enough to cause plastic shear deformation in the adhesive layer. These findings are dependent upon the final mesh size in the FE model, see Section 5.1. The other sections of the joint proved difficult to model through the use of analytical methods. In order to find pertinent boundary conditions in Sections B-E of the divided tee-joint structure, FE analysis was needed which decreased the need for an analytical approximation in a design application. Various methods for finding these through-the-thickness stresses in these areas are discussed, but are generally not useful for a practical, design oriented study of the in-situ tee-joint. The approximations discussed in this section, while not appropriate for the tee-joint configuration, are useful in other design problems both as complete structures and as sub-components.

In both the parametric finite element study and the various analytical approximations, examples of further work have been illustrated. The loading condition examined in this study is the case of an applied load parallel to the centerplate. In practical applications, more complex loading conditions will occur. To help model these configurations, further finite element analyses should be carried out with loads both perpendicular to the centerplate and at 45 degrees. In the case of the 45-degree loading condition, the insights gained in this work would be of direct application. In this loading configuration, failure is predominately seen on the tensile side of the structure, Sheno and Hawkins [1992], where the mechanisms of failure are very similar to those examined in this work.

The use of finite element models to examine stresses near the termination of overlaminates or doublers is impaired due to the mathematical singularity in this region. Both an experimental investigation and an examination of the methods in which finite element codes determine the stresses in this area can be used to help create a length scale at which finite element models give accurate values of the peel stresses in these areas.

This corresponds to important topics in the design of composite structures such as double lap joints, doubler terminations and other generic structural components. A study of this nature would also allow for an experimental verification of the various analytical approximations discussed in Section 5.1.

In the parametric study, the effects of the addition of tapers are examined. Further work both experimental and theoretical is recommended to determine the similarities and differences inherent in using tapers in both glass and carbon fiber materials. The majority of the current literature in the design of composite structures uses carbon\epoxy material systems which have different material properties than glass\epoxy systems. Due to this difference, the usefulness of correlations and guidelines created for carbon\epoxy systems must be re-examined to determine their applicability to other composites. Further work is necessary to build upon the comparisons examined in this work.

9.0 References

- Cui, W., Liu, T., Len, J., and Ruo, R., 1996, "Interlaminar Tensile Strength (ILTS) Measurement of Woven Glass/Polyester Laminates Using Four-Point Curved Beam Specimen," *Composites*, vol. 27, pp. 1097-1105.
- Cui, G.Y., and Ruiz, C., 1995, "Through-Thickness Failure of Laminated Carbon/Epoxy Composites Under Combined Stress," *Composites Science and Technology*, vol. 53, pp. 253-258.
- Ellis, R., 1996, *Finite Element Analyses of Mechanically Fastened Composite to Aluminum Joints; A Comparison of Two- and Three- Dimensional Results*, Master's Thesis, UCSB.
- FAA Design Manual*
- Goland, M., and Reissner, E., 1944, "The Stresses in Cemented Joints," *ASME Journal of Applied Mechanics*, vol. 11, pp. A17-A27.
- Hart-Smith, L.J., 1974, *Analysis and Design of Advanced Composite Bonded Joints*, NASA Contract Report CR-2218.
- Hart-Smith, L.J., 1973, *Adhesive-Bonded Single-Lap Joints*, NASA Contract Report 112236.
- Hawkins, G.L., Holness, J.W., Dodkins, A.R., Shenoi, R.A., 1993, "The Strength of Bonded Tee-Joints in FRP Ships," *Plastics, Rubber and Composites Processing and Applications*, vol. 19, pp. 279-284.
- Hetenyi, M., *Beams on Elastic Foundation*, The University of Michigan Press, An Arbor, 1946.
- Junhou, P. and Shenoi, R.A., 1996, "Examination of Key Aspects Defining the Performance Characteristics of Out-of-Plane Joints in FRP Marine Structures," *Composites*, vol. 27, pp. 89-103.
- Kedward, K.T., Wilson, R.S., and McLean, S.K., 1989, "Flexure of Simply Curved Composite Shapes," *Composites*, vol. 20, pp. 527-536.
- Ko, W.L., 1988, *Delamination Stresses in Semicircular Laminated Curved Bars*, NASA-TM-4026.
- Lekhnitskii, S.G., *Anisotropic Plates*, Gordon and Breach Scientific Publishers, New York, 1968.

Lekhnitskii, S.G., *Theory of Elasticity of an Anisotropic Body*, Mir Publishers, Moscow, 1981.

Lu, T.J., Xia, Z.C., and Hutchinson, J.W., 1994, "Delamination of Beams Under Transverse Shear and Bending," *Material Science and Engineering*, vol. 18, pp. 103-112.

Mabson, G.E. and Neal III, P.M., "Analysis and Testing of Composite Aircraft Frames for Interlaminar Tension Failure," National Specialists Meeting on Rotary Wing Test Technology, March 15-16, 1988.

Mallick, P.K., *Fiber-Reinforced Composites - Materials, Manufacturing and Design*, Marcel Dekker, Inc., New York, 1993

Malvar, L.J. and Bish, J., "Grip Effects in Tensile Testing of FRP Bars," Presented at the 2nd. International Symposium on Non-Metallic (FRP) Reinforcement for Concrete Structures, August 23-25, 1995.

McRobbie, S., Longmuir, A.J., Wilcox, J., Gibson, A.G., and Chandler, H.W., 1995, "Through-Thickness Stress in Curved Laminates of Single and Double-Skinned Construction," *Composites*, vol. 26, pp. 339-345.

Oplinger, D.W., 1994, "Effects of Adherend Deflections in Single Lap Joints," *International Journal of Solids and Structures*, vol. 31, pp. 2565-2587.

Shenoi, R.A. and Hawkins, G.L., 1992, "Influence of Material and Geometry Variations on the Behaviour of Bonded Tee Connections in FRP Ships," *Composites*, vol. 23, pp. 335-345.

Shenoi, R.A., Read, P.J.C.L., and Hawkins, G.L., 1995, "Fatigue Failure Mechanisms in Fibre-Reinforced Plastic Laminated Tee Joints," *International Journal of Fatigue*, vol. 17, pp. 415-426.

Shenoi, R.A. and Violette, F.L.M., 1990, "A Study of Structural Composite Tee Joints in Small Boats," *Journal of Composite Materials*, vol. 24, pp. 644-666.

Timoshenko, S.P., and Goodier, P.M., *Theory of Elasticity*, McGraw-Hill Book Company, New York, 1970.

Tsai, M., and Morton, J., 1994a, "A Note on Peel Stresses in Single-Lap Adhesive Joints," *ASME Journal of Applied Mechanics*, vol. 61, pp. 712-715.

Tsai, M., and Morton, J., 1994b, "An evaluation of Analytical and Numerical Solutions to the Single-Lap Joint," *International Journal of Solids and Structures*, vol 31. pp. 2537-2563.

Volkersen, O., 1938, "Die Nietkraftverteilung in Zugbeanspruchten Nietverbindungen Mit Konstanten Laschenquerschnitten," *Luftfahrtforschung*, vol. 15, pg 41.

Wisnom, M.R., 1996, "3-D Finite Element Analysis of Curved Beams in Bending," *Journal of Composite Materials*, vol. 30, pp. 1179-1190.

Wu, Y.-S., Longmuir, A.J., Chandler, H.W., and Gibson, A.G., 1993, "Delamination of Curved Composite Shells Due to Through-Thickness Tensile Stresses," *Plastics, Rubber and Composites Processing and Applications*, vol. 19, pp. 39-46.